DUCTILE BEAM-COLUMN CONNECTIONS IN PRECAST CONCRETE MOMENT RESISTING FRAMES

by

Onur Ertaş
B.S., C.E. Boğaziçi Universiy, 1998
M.S., C.E. Boğaziçi Universiy, 2000

Submitted to Institute for Graduate Studies in
Science and Engineering in partial fulfillment of
the requirements for the degree of
Doctor of Philosophy

Graduate Program in Civil Engineering
Boğaziçi University
2005

DUCTILE BEAM-COLUMN CONNECTIONS IN
PRECAST CONCRETE MOMENT RESISTING FRAMES

APPROVED BY:

Prof. Turan Özturan ……

(Thesis Supervisor)

Assist. Prof. Şevket Özden ……

(Thesis Co-Supervisor)

Prof. Cengiz Karakoç ……

Assist. Prof. Cem Yalçın ……

Prof. Özal Yüzügüllü ……

DATE OF APPROVAL: 07.07.2005

"Make things as simple as possible but no simpler"

"Simplicity that is based on rationality is the ultimate sophistication."

-attributed to Albert Einstein (1879-1955)

ACKNOWLEDGEMENTS

I owe special thanks to Assist. Prof. Dr. Şevket Özden of Kocaeli University for his endless helps, guidance and encouragements. I am also grateful to Prof. Dr. Turan Özturan of Boğaziçi University to manage TUBİTAK project and to Assist. Prof. Dr. Cem Yalçın for his invaluable recommendations.

I would like to thank to Structures Laboratory research assistants and technicians for their assistance and supports during the experiments. Especially, I gratefully thank to Osman Kaya to share with his time and work at weekends and nights for my project.

Funding provided by TÜBİTAK (İÇTAG I589) and The Turkish Precast Association is gratefully acknowledged. The supply of materials from SİKA Chemicals BETONSA and BEKSA is also gratefully acknowledged.

I am very thankful to GÖK İnşaat A.Ş. and AFA Prefabrik for their supports, suggestions and encouragements.

Finally, I would like to thank to my wife, mom and dad for their continuous support and patience.

ABSTRACT

DUCTILE BEAM-COLUMN CONNECTIONS IN PRECAST CONCRETE MOMENT RESISTING FRAMES

Post-earthquake field investigations on precast concrete structures revealed that the level of damage and the poor performance of the buildings during the 1999 Kocaeli and Düzce Earthquakes in Turkey were closely related to the performance of the precast connections. As a result, a two-phase research program on the performance of precast ductile beam-column connections was developed as a PhD Thesis.

In Phase I, four different types of ductile moment resisting precast frame connections and one counterpart monolithic specimen, designed for high seismic zones, were tested. Precast specimens of Phase I may be subdivided into three subgroups as cast-in-place, composite with welding and bolted connections. Comparisons on the performance parameters, such as energy dissipation and comparisons on ease of fabrication and economy reveals that the modified bolted connection of Phase I may well be used in high seismic zones.

In Phase II, five hybrid connections with unbonded prestressing tendon and partially bonded mild steel were tested. The main variable in Phase II specimens was the percent contribution of mild steel to the flexural moment capacity of the connection. Each hybrid connection was compared with the monolithic reference subassembly in terms of connection strength, stiffness degradation, energy dissipation and permanent displacement. It is observed that the design philosophy of hybrid connections is satisfied when the mild steel moment contribution of the connection is around 30 per cent.

Furthermore, a numerical model was developed for Phase II specimens to highlight the hysteretic behavior under seismic loading.

ÖZET

PREFABRİK YAPILARDA MOMENT AKTARABİLEN SÜNEK KOLON-KİRİŞ BİRLEŞİMLERİ

1999 Kocaeli ve Düzce depremleri sonrası yapılan saha gözlemlerinde, prefabrik yapıların göstermiş olduğu yetersiz performansın nedenlerinden en önemlisinin birleşim bölgelerinin zayıflığı olduğu tespit edilmiştir. Bu amaçla, sünek kolon-kiriş birleşimlerinin inceleneceği iki aşamalı bir araştırma projesi doktora tezi olarak sunulmuştur.

Çalışmanın ilk ayağında, deprem riski yüksek bölgelere göre tasarlanmış olan dört adet sünek ve moment aktarabilen prefabrik kolon-kiriş birleşimi ile şahit deney olarak konvansiyonel eleman testi yapılmıştır. Test edilen bu detaylar yerinde dökümlü, kaynaklı kompozit ve bulonlu birleşim olmak üzere üç alt gruba ayrılabilir. Sonuçta, bulonlu birleşimin konvansiyonel sisteme kıyasla gösterdiği yapısal performansın yanısıra, ucuz ve kolay uygulanabilir bir detay olması nedeniyle deprem bölgelerinde kullanılabileceği görülmüştür.

Çalışmanın ikinci aşamasında beş adet ard-germeli birleşim detayı tersinir tekrarlı yükler altında test edilmiştir. Test değişkeni, birleşim bölgesindeki yumuşak donatının eğilme kapasitesine katkısı olarak seçilmiştir. Tüm birleşim detayları, dayanım, rijitlik kaybı, enerji tüketimi, kalıcı deplasman kiriterleri baz alınarak konvansiyonel sisteme göre kıyaslanmıştır. Deney sonuçları göstermiştir ki, yumuşak donatının eğilme kapasitesine katkısının yüzde 30 olması durumu, ard-germeli sistemlerin tasarım kiriterleri ile uyuşmaktadır.

Bunlara ek olarak, ard-germeli birleşim detayları için herhangi bir deprem etkisi altındaki davranışını aydınlatmak amacıyla nümerik bir model de geliştirilmiştir.

TABLE OF CONTENTS

LIST OF FIGURES

LIST OF TABLES

LIST OF SYMBOLS

A_e	Strain energy
A_h	Dissipated energy
A_p	Area of hystresis loop
A_{pt}	Area of tendon
A_s	Mild steel area (tension side)
$A_{s'}$	Mild steel area (compression side)
C	Compression force
c	Height of the compression block
C_c	Compression force due to concrete block
C_{ms}	Compression force due to the mild steel
$\cot\theta$	Inclination shear angle with horizontal
d	Effective depth of beam
d_b	Bar diameter
d_v	Effective shear depth
E_s	Modulus of elasticity of steel
$E_{1,2}$	Maximum load or moment
F	Instant lateral load at the test
f_c’	150x300 mm concrete cylinder compressive strength
f_{cd}	Design compressive strength of concrete
f_g	Compressive strength of grout
F_h	Lateral force
f_{pi}	Initial post-tensioning stress on tendon
F_{pt}	Post-tensioning force
f_{pt}	Stress on tendon
$f_{pt\text{-}cal}$	Calculated stress on tendon
f_{ptu}	Ultimate strength of tendon
f_s	Stress on mild steel
F_y	Yield lateral force
f_y	Yield strength of mild steel

f_{yd}	Design yield strength of steel
f_u	Ultimate strength of mild steel
h	Height of beam
H_e	Elastic load level
H_u	Ultimate load
k_1	Coefficient of rectangular compression block for TS500
K_i	Initial stiffness on modeling
K_{norm}	Normalized stiffness
K_p	Post yield stiffness on hysteretic modeling
K_r	Reloading stiffness on hysteretic modeling
K_{sec}	Secant stiffness
L_{cant}	Length of cantilever scheme
L_n	Clear span length of beam
l_p	Plastic hinge length
L_{un}	Unbonded length of tendon
l_{un}	Unbonded length of mild steel
M_{beam}	Probable flexural moment capacity of beam
M_c	Probable flexural moment capacity of connection
M_{c1}	Moment capacity at 1^{st} connection on beam
M_{c2}	Moment capacity at 2^{nd} connection on beam
M_{cal-y}	Yield flexure moment
M_{cal-u}	Ultimate flexure moment
M_{col}	Probable flexural moment capacity of column
M_{ms}	Flexural moment due to the mild steel
M_{pt}	Flexural moment due to the tendon
M_u	Positive bending moment at section
N_u	Axial load at section
R	Load reduction factor
T_{ms}	Tension force due to the mild steel
T_{pt}	Tension force due to the tendon
V_D, V_G	Shear force due to the dead load
V_{dy}	Shear force due to the gravity load
V_L, V_Q	Shear force due to the live load

V_u	Probable ultimate shear force at beam or section
α	Mild steel contribution ratio for flexural moment
α_b	Debonding length coefficient
β	Relative energy dissipation ratio
β_1	Coefficient of rectangular compression block for ACI 318
Δ_{bv}	Vertical displacement at beam
Δ_{cb}	Column base displacement
Δ_{cnet}	Net column top displacement
Δ_{ct}	Top displacement of the column
Δ_{deb}	Debonded length
Δ_{ms}	Elongation at steel
Δ_{pt}	Elongation at tendon
δ_r	Residual displacement
Δ_y	Yield displacement of structure
δ_y	Yield displacement of member
ε_c	Strain at concrete
ε_{pi}	Initial strain at tendon
ε_{pt}	Strain at tendon
ε_r	Rupture strain
ε_{sf}	Calculated strain at mild steel
ε_{sh}	Strain hardening level
ε_{si}	Assumed strain at mild steel
ε_{su}	90 per cent of the ultimate strain
ε_u	Ultimate strain
ε_x	Longitudinal strain parameter
ε_y	Yield strain
ϕ	Reduction factor
$\phi_{beam,\ col}$	Curvature at beam or column
ϕ_y	Yield curvature of connection
γ	Coefficient for strength degradation

λ	Coefficient for residual story drift
μ	Displacement ductility
μ_f	Friction coefficient (concrete to concrete)
θ	Story drift
θ_c	Rotation angle at connection
θ_{res}	Residual story drift
θ_y	Yield story drift
ψ	Yield stiffness ratio
ζ_{eq}	Equivalent viscous damping

1. INTRODUCTION

1.1. General

Precast concrete structures are very popular in Europe, North America and Japan because of many advantages such as low construction cost, high member quality and construction speed, better architectural modularity and climate independent project scheduling. To validate these items and expand the market of precast concrete structure, assembling or connection process becomes very important. Therefore, connector concepts need to be identified as [1]:

- Avoiding extensive welding
- Incorporating adequate tolerances
- Avoiding large formed wet joints
- Designing joints that minimize crane time

The percentage of the precast concrete frame type structures, in the field of industrial construction, such as factory buildings and warehousing is dominantly high in Turkey as compared to the cast-in-place reinforced concrete or steel structures. The speed of construction, the quality of plant produced members; precise dimensioning and the low relative cost of such frames are the main piers of the preference for the building owners. On the other hand, two or more story precast concrete shopping malls, school buildings, dormitories, residential buildings, office spaces and parking lots are rare or none.

Performance and damage level of such structures are mainly determined by the capacity and ductile performance of the connections. The premature failure of such connections prevents the ductile behavior of the adjoining members and the overall load carrying frame system.

1.2. 1999 Marmara Earthquakes and Observations for Precast Structures

On August 17, 1999, a magnitude MW=7.4 earthquake struck Kocaeli and Sakarya provinces in northwestern Turkey, a densely populated region in the industrial heartland. The August 17 earthquake is considered to be the largest event to have devastated a modern, industrialized area since the 1923 Tokyo earthquake. Another segment at the eastern end of the same fault has ruptured on November 12 producing the MW=7.2 Düzce earthquake. The region affected by the earthquake is both geographically extensive and economically dynamic. It forms the industrial heartland of Turkey. The four districts, most severely affected, (Kocaeli, Sakarya, Bolu and Yalova) contribute over 7 per cent of the country's GDP and 14 per cent of industrial value added. Per capita income is almost double the national average [2].

In these regions most of the light industrial facilities are precast concrete structures. The 1999 event was a chance to observe the behavior of these precast structures during such a major earthquake since there are few well-documented cases in the literature. Field investigations and analytical evaluations after Kocaeli and Düzce earthquakes revealed that a high percentage of such structures did not have satisfactory earthquake safety [3]. Also, it is reported that most heavily damaged buildings were designed according to the former Turkish earthquake code of 1975 [4].

Single story buildings, with fixed base sockets columns and pin-connected at the roof level, are the most favored system for precast structures in Turkey. Columns are generally fixed at the base by socket type foundations because of quick and easy erection and simplified casting with minimum tolerance problem. This type of connection is able to transmit larger moments to foundation more than the other types [4]. These footings are cross-tied with grave beams. The most common structural system for these facilities is based on a structural configuration that was developed in Western Europe to carry mainly the gravity loads [5]. Turkish engineers modified the connection details so that the precast buildings have the capacity to resist lateral loads to a certain extend. However, each producer of precast elements has developed a unique set of connection and reinforcement details, and the details vary appreciably from producer to producer [6]. Pinned connections in such frames may be constructed either on the column tops with dowels or at points of

contra-flexure under gravity loads over the roof girders by joining two member with one or two bolts. On the other hand, it was observed that moment resisting types of connections are not widely used in Turkey [3].

Generally, precast structures are rectangular in plan with one to four bays in transverse direction and ten to thirty bays in the longitudinal direction. Transverse bay width usually ranges between 10 and 15 m, and the longitudinal bay width ranges between 6 and 8 m. Column height also ranges between 6 and 8 m with 35/35 cm to 50/50 cm varying column dimensions.

The seismic load reduction factor (R) to calculate the design base shear for different types of ductile precast concrete structures ranges from 4 to 6 in the current Turkish earthquake code [7]. The R value of structures which the seismic loads are fully resisted by single story frames, fixed at the base and pin connected at the roof level, is given as 5 in the Turkish earthquake code [7]. On the other hand, the seismic reduction factor of such structures is given as 2.2 in the UBC'97 [8].

For single story precast concrete structures, two main failure types were observed. Namely, the column flexural failure or beam to column connection failure or the both. The main reason of such a column flexural failure may be attribituted to the inadequate strength and stiffness supplied during design and construction. As shown in Figure 1.1, plastic hinging occurred at the column base but the flexural cracks were only in one direction. This means that column could not be loaded under reversal actions. Therefore, no foundation failure was observed. In some cases, plastic hinging occurred at approximately $1/3^{rd}$ height of the column as presented in Figure 1.2. The reason of such a plastic hinge location may well be explained by the abrupt change in the amount of column longitudinal reinforcement at this level.

Figure 1.1. Flexural column failure at the base [9]

Figure 1.2. Flexural column failure at the 1/3rd column height [9]

Figure 1.3 and Figure 1.4 show the common type of beam-column hinge connections where only one or two bolts jointed the precast elements over the corbels. Most of these types of connections were damaged or failed during the 1999 earthquakes. Although these connections were assumed and designed as hinge connection, they had very limited rotation capacity. Furthermore, inadequate rigidity of precast system demanded extra rotation at these connections. As a result, all bolts were ruptured or slipped out.

Figure 1.3. An example of common type beam-column connection [9]

Figure 1.4. Another example of common type beam-column connection [9]

After 1999 Marmara Earthquakes, some researchers [3, 4, 6, 9, 10] studied on the reasons of failures with some case studies. The common results of these researches were that the precast structures had very slender columns and limited stiffness. Therefore, these

earthquakes demanded a large drift and caused extra P-Δ effect. It was also reported that, all the collapsed precast concrete structures were deficient in satisfying the drift limitations. In addition to that, rigid diaphragm detailing at the roof level did not exist in these structures. Finally, soft soil conditions had a dominant effect in the seismic response of precast structures by increasing the drift demand of such structures. Also, these types of deficiencies were presented in Figure 1.5.

1.3. Multi-story Precast Concrete Structures

The high rate of settlement in the big cities, influence the construction practice in Turkey. The so-called “tunnel form” or “box-type” cast in place construction is mostly favored in residential or student housing due to the high construction speed and low cost. Moreover, the good performance during the 1999 Kocaeli Earthquake, promote the growing acceptance of such structures with in the community. On the other hand, the poor modularity of tunnel form of construction still makes it possible to construct precast concrete office buildings and large multi-story condominiums on condition that the seismic resistance and good performance of such structures, especially the connections, should be studied and proven to the public.

The main improvement of precast structures may well be at the beam-column connection region. The 1999 Kocaeli Earthquake showed that behavior of the precast connection had a major impact on the overall performance of such structures. Therefore, a “new generation connection type” should better be implemented into the construction practice, in order to promote the use of the precast systems. Besides, the new Turkish Earthquake Code–1998 [7] punishes the precast design, as compared to the cast-in-place design, mainly due to its connections, which may not behave as ductile as the monolithic construction. The attempts to make the precast connections more ductile, promotes the more complicated detailing, hence resulting in long and expensive on-site construction and quality control process. It was also observed that the connections with corbels or with tapered beams could not lead the structure to the desired performance level; moreover they result in architectural inconvenience. Therefore, the “new generation connection type” should better satisfy the conditions highlighted below:

- Economy and high quality on-site construction
- Quick installation
- Adequate strength
- Adequate energy dissipation capacity
- Less stiffness degradation under reversed cyclic loading
- Architectural advantages

The labor cost and construction expenses have an increasing trend over the time after 1999 Kocaeli Earthquake due to the new quality control regulations starting from the design phase to the construction stage of the structures in high seismic areas. Moreover, the labor cost is expected to increase due to the regulations of the European Community. Therefore, the speed of on-site construction will be an important factor during the decision making process for the building investors. As a result, the plant produced precast systems with lower on-site detail construction may have a better chance to compete on the market. Besides, the quality control of on-site construction is very difficult and costly especially in the case of welded connections.

Briefly, this may be a good opportunity to introduce new generation connection type, which will lead a more ductile and seismically safe structure to the precast industry.

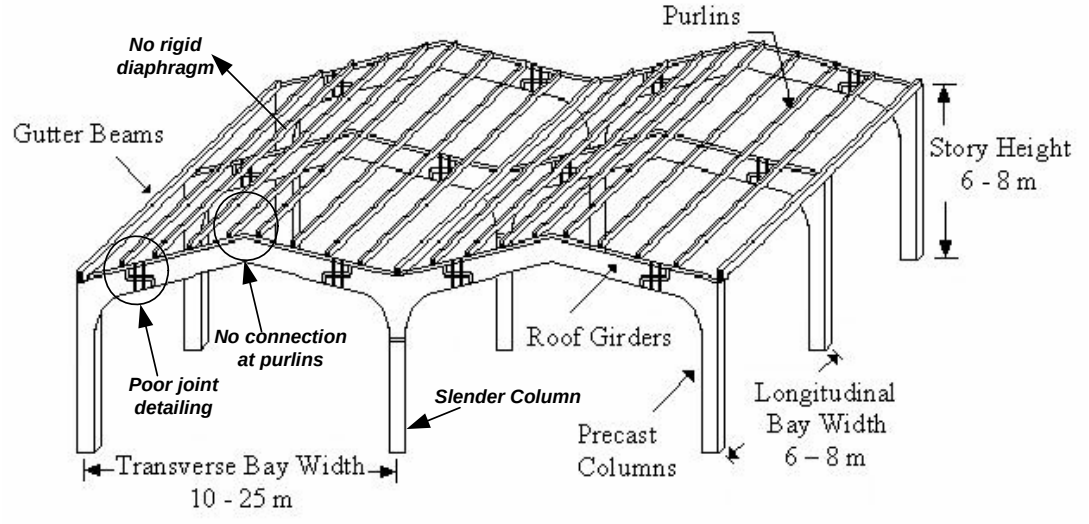

Figure 1.5. Deficiencies in precast structures [9]

2. LITERATURE REVIEW

2.1. General

Precast moment resisting frame connections may be classified in two fundamental groups such as wet and dry connections [11]. Dry connection type can be constructed with bolting, post-tensioning or welding while in wet connections, some part of the concrete can be placed at the construction site. Wet connections may also be called as cast in place (CIP) connections.

The behavior of precast concrete structures is greatly influenced by the performance of its connections. Recent field observations revealed that the joints at precast structures displayed low connection stiffness. This low stiffness implies that a precast frame structure have a greater lateral deflection than a comparable cast-in-place structure. Dolan's [12] tests indicated that the load-deflection behavior of a precast structure exhibited a response different from that obtained by extrapolation of the behavior of a cast in place structure.

Some researches and field observations [13, 14] showed that the reasons of damage at the connection region in the precast structures because of earthquakes may be listed as follows:

- Continuity of bottom reinforcement of beam is not provided since the load reversal is not considered.
- Due to the inadequate reinforcement lap splice length or weld length at the connection region, the stiffness degradation becomes very rapid resulting high story drifts.
- Some problems occur at the welding zone depending on the quality of reinforcement such as high carbon content or workmanship.

The few well-documented cases of failures are related to gross errors in the conceptual design of the structural system and mainly due to poor connections between precast concrete members [15]. The structural system must be laterally stiffer and stronger

than that provided by the rather slender frame members typically used in the buildings under consideration. This can be attained by using more robust columns and beams, but, preferably, by adding stiffening members such as shear walls or braces. Reinforcement detailing in beams, columns and joints must be improved to attain larger ductilities. In particular, the confinement of concrete and longitudinal steel in sections of possible formation of plastic hinges must be achieved using closely spaced transverse reinforcement [16].

When the literature is searched, several types of precast beam-column connection details can be found for moment resisting frames. Widely used joint details may be listed as welded, bolted, cast in place (CIP) and post tensioned connections. These details can be seen in Figure 2.1. In addition to that, location of the connection is observed as another parameter in the design. Connections can be located at column, column face or at the middle of the beam span. Some of the popular connection configurations in the construction sites are given in Figure 2.2.

Gosh *et al*. [17] presented a paper about strong connection concept with 1997 UBC [8] design provisions of precast structures in high seismic zones. A strong connection is designed to remain elastic while inelastic action takes places away from the connection. Because a strong connection must not yield or slip, its design strength in both flexure and shear must be greater than the bending moment and shear force, respectively corresponding to the development of probable flexural or shear strengths of nonlinear action location [18]. In addition to the cost with strong connections, the over strength required in the connectors becomes quite large as the hinge location is moved away from the column face. Also, the hinge relocation approach is that relocating the hinge away from the column face increases the rotational ductility demand to the hinge for a given story drift. Good seismic performance requires that a system be able to sustain a large lateral deformation without significant loss of strength [19].

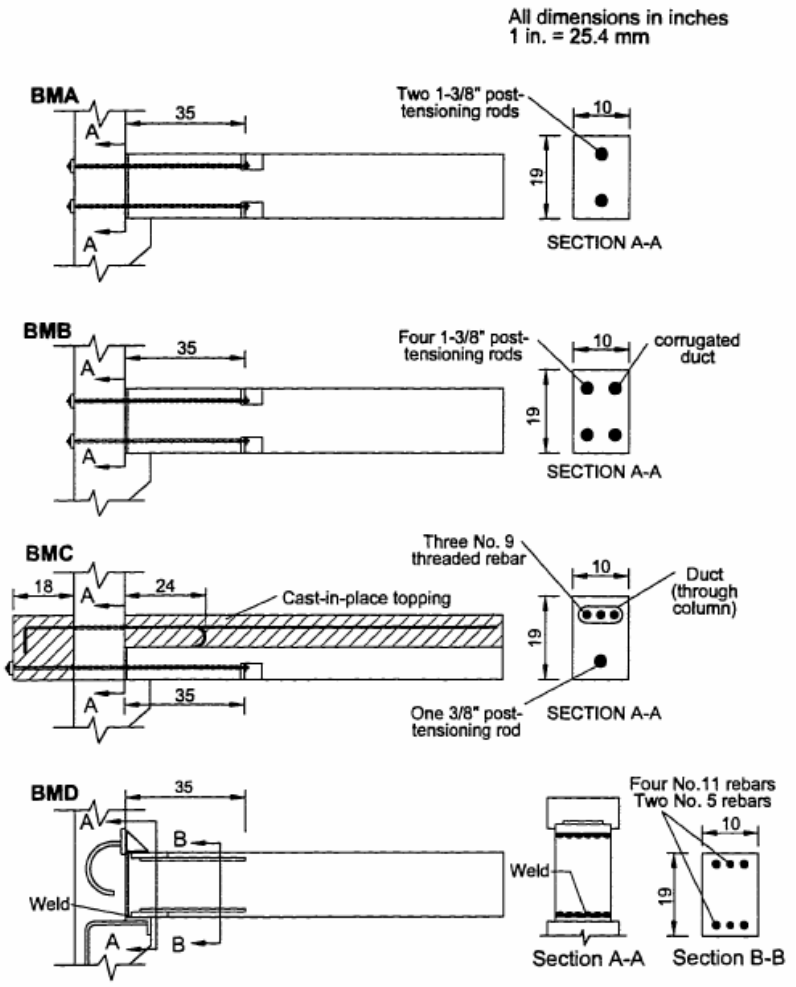

Figure 2.1. Types of connection [20]

2.2. Types of Connection

2.2.1. Welded Connection

Welded connections are widely used because of their easy application and lower cost advantages. Bhatt & Kirk [21] and Pillai & Kirk [22] studies showed that the welded precast concrete member connections tested in these studies, from considerations of strength, stiffness, ductility and energy-dissipating capacity, performed satisfactorily and in a manner comparable to the performance of similar monolithic connections. In this

detailing as presented in Figure 2.3, T section was used in the column and the anchor bars were welded to the horizontal leg of the T.

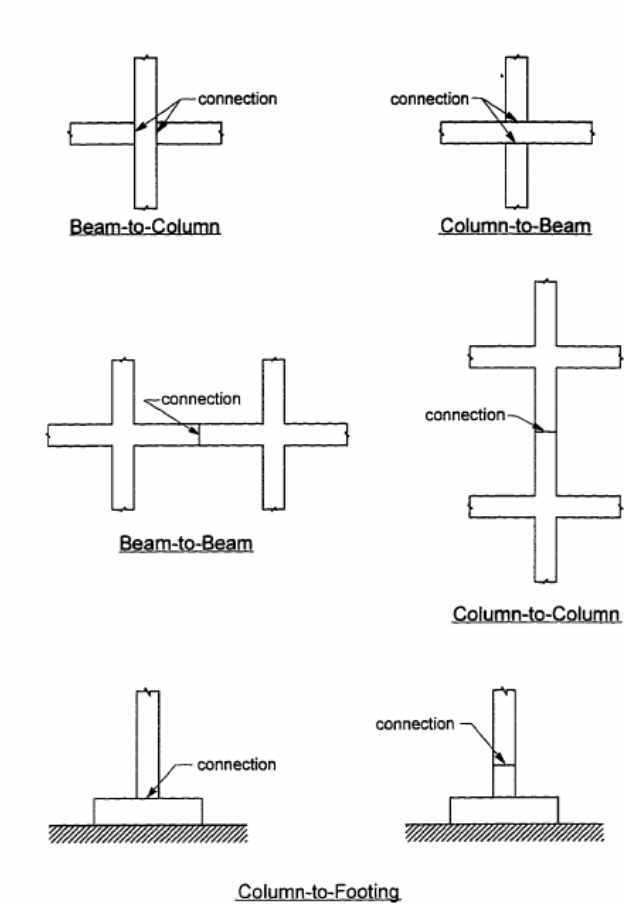

Figure 2.2. Typical connection configurations [17]

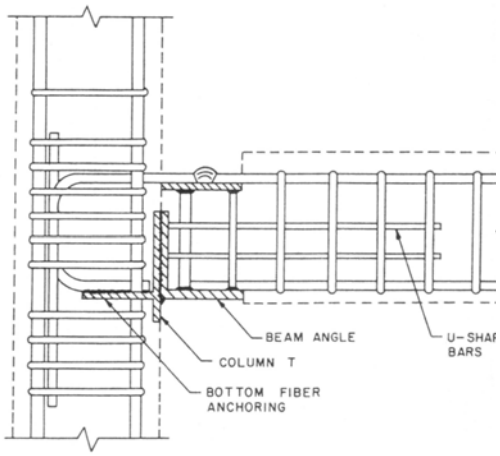

Figure 2.3. Welded connection at column face [21]

Similar results were observed in Ersoy's study [23] with different approaches. In this study, the columns of the structure were extended to the full height of the building and had brackets on each face at each floor level. The beams were connected to these brackets by welded steel plates. The joints were intended to provide monolithic behavior.

Although the behavior of the tested connections was satisfactory, the construction of these specimens requires significant welding of the beam and column reinforcement. The cost and quality control associated with excessive welding diminishes some of inherent advantages of precast concrete construction. For ideal connection, therefore, welding especially field welding must be minimized [24]. In addition to that, welding is labor intensive and time consuming. The heat generated from welding can cause damage to bond in steel bars and cracking in the adjacent precast concrete. Furthermore, high quality welding requires close supervision and inspection [25].

Furthermore, the use of weldable reinforcement and the appropriate weld materials are essential for ductility. Even when weldable reinforcement is used, load eccentricity should be eliminated where possible. Some weld plate designs may be predicted on the plate yielding before the weld fails. Overstrength plate steel could then result in welds failing first, sometimes in a brittle fashion, when a ductile failure was anticipated [26].

2.2.2. Bolted Connection

Bolted connections are preferred because of ease in erection and production. Also performance of the precast connection with threaded rebars is as well as the other type of connections [20]. When this type of connection is designed, shear degradation at the threaded bars, slippage and inadequate anchorage length problems should be considered or need to be eliminated [27].

In April 1991, a series of industry seismic workshops were conducted by the PCI. The primary objective of these workshops was to seek industry input into Concept Development and Connection Classification Projects [28]. In this workshop, spaced-out thread bar frames were discussed. In a spaced-out frame system, longitudinal strength was obtained by making series of separate one-bay moment frames in which connections were

formed by wrench-tight threaded rods. Drop-in beams using simple connections span between the frames. The details of this connection type can be seen in Figure 2.4. This framing system had the advantages that each pair of frames could be regarded as a strength nucleus so that many building configurations could be made up by different arrangements of the same basic nuclei. The main outcome of the workshop was the stressed bar system using a dog-bone type of beam. A dog-bone beam had a deeper section at each end to simplify the connection through the column.

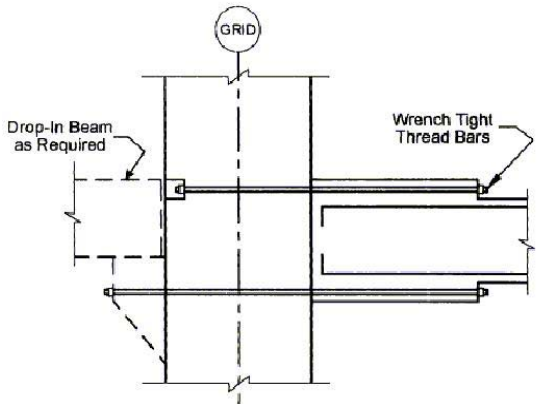

Figure 2.4. Spaced-out thread bar frame [28]

Following the PRESS Workshop results, Nakaki *et al*. [19] designed a ductile link connector for precast beam-column joints. Ductile links took different forms in various systems. In structural steel and monolithic concrete frames, the ductile link was provided by plastic hinges in the ends of the beams.

In a monolithic emulation system, the connections between precast concrete elements were designed to be stronger than the ductile link. Yielding was then forced to occur within the concrete element itself. In addition to that, many of the proposed details required a mixing of trades (i.e., welding, grouting, postensioning or cast-in-place concrete). This slows the progress of the project, and as a consequence, eliminates one of the major benefits of precast concrete: its ability to be erected quickly [19].

In addition to the cost, normally associated with strong connectors, the overstrength required in the connectors becomes quite large as the hinge location is moved away from

the column face. Hinge relocation approach is that relocating the hinge away from the column face increases the rotational ductility demand to the hinge for a given story drift [19].

Under these restrictions, Nakaki *et al*. [19] proposed a ductile bolted connector and it is illustrated in Figure 2.5. This connector allowed the beams and columns to be cast independently and joined at the column face by bolting. The behavior of the ductile connector was acceptable for high seismic regions.

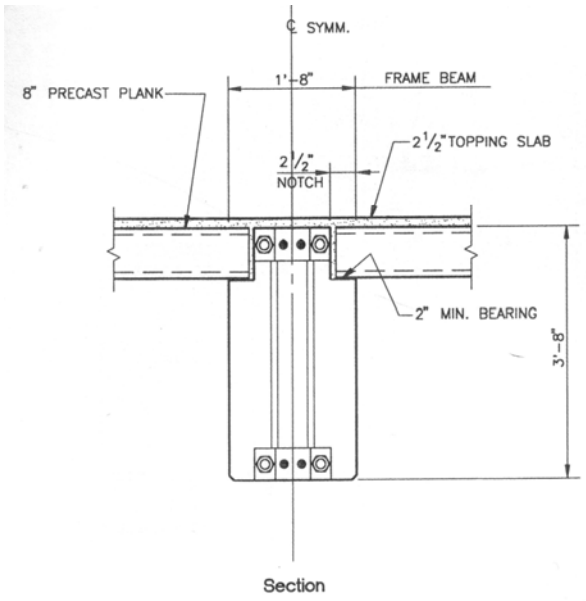

Figure 2.5. Front view of beam-column connection [19]

2.2.3. Post-tensioned Connection

Literature review showed that the studies on prestressed and partially prestressed beam column joints were started in 1970s by Blakely and Park [26] and then continued by Park and Thompson in New Zealand [29].

Tests were conducted on ten concrete interior beam-column frame subassemblies subjected to monotonically increasing cyclic loading. The frame members were near full-

scale and contained a range of proportions of prestressing steel and non-prestressed steel [30].

The behavior of the frames emphasized the need for transverse steel in the plastic hinge zone of flexural members and in the beam-column joint cores to ensure ductile behavior and to avoid diagonal tension failure. The ductility of prestressed beams was enhanced by the presence of non-prestressed reinforcing bars in the compression zone of the members. A central prestressing tendon at mid-depth in the beam passing through the joint was shown to be effective in contributing to joint core shear strength [30].

1971 San Fernando Earthquake observations showed that, failures in precast structures were initiated at the connections. Therefore, studies about hybrid connections started in 1980s. As a result, a series of tests was conducted at the University of Minnesota Structures Laboratory to evaluate the construction feasibility and behavior of different types of moment-resisting connections between beam and column elements. In late 1980s, French *et al*. [20] tested four different connection types. The connection types considered in this study were: post-tensioned (BMA); threaded re-bar connected (BMB); composite-post tensioned in the bottom of the beam with a cast in place top (BMC) and welded (BMD) connections.

All four structures were reported to have exhibited good ductility characteristics. When the beam plastic hinge was concentrated at a single location (BMA), lower ductility in terms of maximum inter story drift was observed compared with cases in which hinging was distributed along the beam (BMB, BMC, BMD). On the other hand, the ratio of energy dissipated to energy absorbed was approximately the same for all the structures [20].

Towards the end of 1980s, NIST (National Institute of Standards and Technology) planned a multi year test program about post-tensioned hybrid connections. The study was initiated to provide data for the development of a rational design procedure for such connections in seismically active regions.

Four one-third scale monolithic concrete beam-to-column connections were tested. In addition, two precast, post-tensioned concrete beam-to-column connections with similar design to the monolithic Zone 4 specimens were tested within the framework of the NIST program [31].

In Phase-I of NIST study, two monolithic specimens were designed according to UBC [8] and ACI352 [32] seismic zone 4 criteria. The criterion used in designing the Zone 4 precast concrete connections was based on the strength of the monolithic Zone 4 specimens. Two one inch diameter post tensioning bars were used to connect the precast beam to precast concrete column, concrete cover being 89 mm. The initial normal stress between column face and the beam, which was due to post-tensioning, was 7 MPa. Also, the post-tensioning ducts were corrugated and filled with a grout having design strength of 41 MPa. The joints were filled with a fiber-reinforced grout. The a/d ratio was 2.47 for Phase-I precast specimens [31].

Based on the results of the NIST Phase-I test program, it appeared that a post-tensioned precast concrete beam-column connection was as strong and ductile as a monolithic connection and was a viable connection for high seismic regions. However, the energy dissipation characteristics, per cycle and cumulative, of the precast concrete connections could be improved [31].

In Phase-II of the NIST study [33], two sets of precast concrete Zone 4 specimens were tested. Post-tensioning bars were used to connect one set of specimens, while prestressing strands were used in the other set. In both sets, the centroid of the longitudinal steel was moved closer to the beam centroid. The first set of specimens were post-tensioned with two post tensioning bars located 140 mm from top/bottom faces of the beams. Post-tensioning with six prestressing strands was used. Steel centroid located 102 mm from beam top/bottom. The Phase-II specimens were designed similarly to Phase-I precast concrete specimens. Similarly, the initial beam prestressing was 7 MPa, and post-tensioning ducts were grouted [33]. The clear span to depth ratio for the specimens (a/d) was 2.4.

The emphasis of Phase-II was to improve the energy dissipation characteristics of the precast concrete connection that was identified in Phase-I. Comparisons were made between the specimens in this phase and also with Phase-I. The comparisons were made based on strength, energy dissipation, and ductility of the connection [33]. Ultimate displacement ductility for the precast specimens was 12. These values were slightly higher than precast specimens in Phase-I. With reference to the connection strength, precast specimens performed satisfactorily, as well as the monolithic specimens. Moreover, improved energy dissipation characteristics due to the changes made in this test phase was evident. The per-cycle energy dissipation was increased by 45 per cent when the post-tensioning bars were moved closer to beam center. An increase of 30 per cent was noted when prestressing strands were used instead of post-tensioning bars.

A concern which arose from Phase-I and II tests was the formation of a slip zone in which the joint exhibited effectively zero stiffness upon load reversals of the precast specimens during the latter stages of the tests as shown in Figure 2.6.

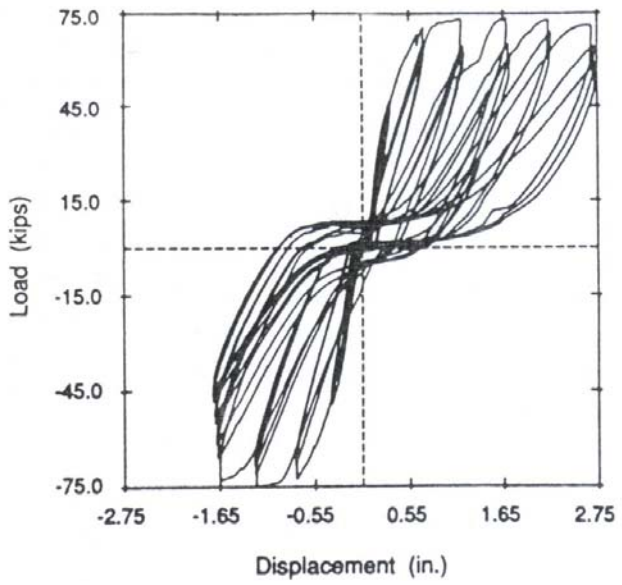

Figure 2.6. Behavior of B-P-Z4 specimen in Phase-I [31]

The slip was felt to be caused by the yielding of the pretension (PT) steel. A suggested method to eliminate this slip was the use of partially bonded tendons. By using partially bonded tendons, a reduction of the tendon strains was expected. As a result,

Phase-III specimens were identical to the Phase-II specimens with exception that the tendons in Phase-III specimens were unbonded through the column and for 381 mm on either side of the column [34].

The experimental data indicated that the envelope curve for the Phase-II specimens could be approximately a bilinear elastic relationship. There was almost no reduction in strength for this set test. The use of partially bonded tendons eliminates the slip zone at zero displacement crossing that was characteristics of the Phase-I and Phase-II specimens. However, the partially bonded precast specimens also dissipated significantly less energy per cycle compared to the fully bonded specimens, approximately 50 per cent less [34].

Two methods were used in the Phase-IV-A specimens to delay yielding of PT steel. One was to place the PT steel in the middle of the beam where it would experience less strain and fully grout it like presented in Figure 2.7. The other was to have unbonded PT steel located at the top and the bottom of the beam (specimens J-P-Z4). In both cases, the mild steel was located at the top and bottom of the beam and was fully bonded. A third type specimen L-P-Z4 was tested three times. The specimen in the first two tests, namely L-P-Z4-A and L-P-Z4-B, contained only unbonded PT steel. The specimen in the third test, L-P-Z4-C, consisted of unbonded mild steel and PT steel located at the top and bottom of the beam [34].

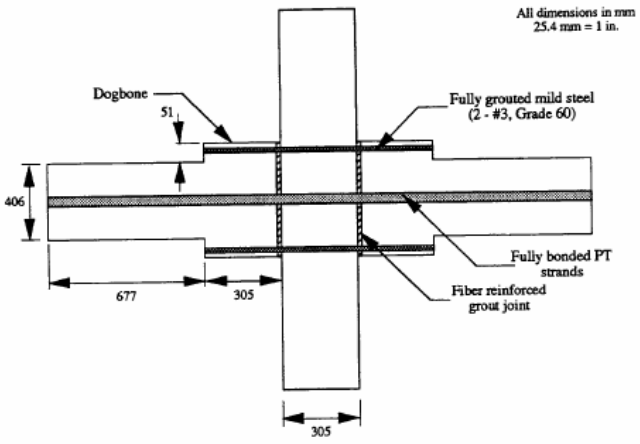

Figure 2.7. Basic details of I-P-Z4 and K-P-Z4 [34]

The results of Phase IV specimens indicated comparable energy dissipation performance with monolithic joint details through approximately 2.00 per cent drift, which was very promising. Also displacement instrumentation indicated no vertical slip of the precast beams with respect to the column at the beam-column joint throughout these tests. This indicated that slip due to the dead load shear was not a factor and that the previous test results were not compromised. However, for the sake of further verification, gravity loads were applied to the specimens in Phase IV B [34].

From the results of these tests (Phases I-IV A), improved energy dissipation per cycle was reported to be achieved by:

- Including low strength mild steel through the joint region near top and bottom of the beams.
- Locating PT steel closer to the beam centroid.
- Having bonded PT steel (If no mild steel is included). However, the latter arrangement risks loss of shear capacity if the PT yields at large story drifts.

The hybrid connections consisted in the NIST research of mild steel used as energy dissipaters and post tensioning steel used to provide the required shear resistance. The variable examined in the next phase of the investigation was the amount and type of mild steel at the connection [35].

The intent at the beginning of Phase IV-B was to proportion the mild steel and PT steels so that the ratios of moment contribution from the mild steel to that from the PT steel would be 10 per cent, 20 per cent and 30 per cent respectively. The Phase IV-B connections were to have central post-tensioning that was partially bonded. The PT steel would consist of pre-stressing strand and steel angles would be included at the corners of the beams at the column face. Initial beam stress on the column connection was kept at 3 MPa [35].

The failure of Phase IV-A specimens was due to the fracture of mild steel bars. Therefore, it was decided to debond the mild steel bars for a length equal to 25 mm on

either side of the beam-column interface [35]. The parameters of Phase-IV study can be seen in Figure 2.8.

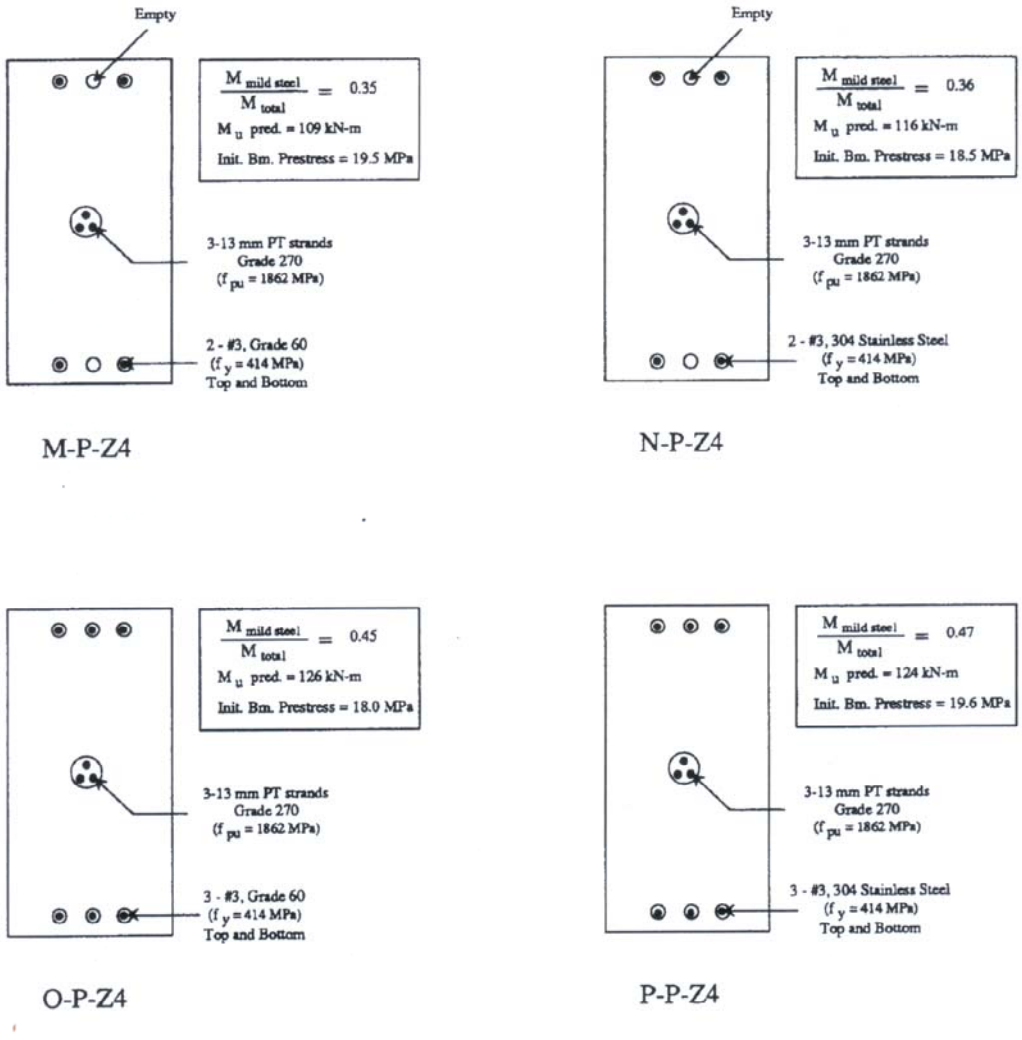

Figure 2.8. Test parameters of Phase-IV-B study [35]

The results showed that a hybrid connection could be designed to match or exceed the performance of a similar monolithic connection in terms of connection strength, drift capacity, energy dissipation, residual drift, and damage to the concrete. The hybrid connection provides a means of connecting the precast members for large forces in severe seismic zones. It takes advantage of the best features of precast construction and combines the hysteric damping of a conventional cast-in place reinforced concrete structure [35].

A similar test that was about hybrid connections with ungrouted post-tensioned strands was performed by Priestly *et al*. [36]. Two ungrouted post-tensioned, precast concrete beam-to-column joint subassemblies were tested under cyclic reversals of inelastic displacement in order to determine the seismic response. One subassembly represented an exterior joint while the other one was an interior joint of a one-way prestressed concrete frame. The large-scale test units were designed with greatly reduced beam and joint shear reinforcement compared with equivalent monolithic joints, but with special spiral confinement of the beam plastic regions [36].

The 813 x 406 mm beams prestressed with two 1200 kN ungrouted 12 x 13 mm tendons post-tensioned to $0.55f_{ptu}$ after looses, providing an axial prestress of 7.2 MPa. For the exterior joint unit, a 500 mm beam stub was provided at the back of the joint for the prestressing anchorages [36].

The interior and exterior joints attained inter-story drifts of 2.80 and 4.00 per cent respectively, without significant strength degradation. On the other hand, very little energy was absorbed in the hysteresis loops during cycles to that displacement level. The structural response was very satisfactory, despite the very low levels of reinforcement provided in the beams, columns and joints. Based on these results, the concept of ungrouted prestressed, precast frames warrants a more detailed research investigation [36].

Finally, at the culmination of the PRESSS research program, a 60 per cent scale five-story precast/prestressed concrete building as shown in Figure 2.9 was tested under simulated seismic loading. The buildings were designed using the direct displacement based approach, which was able to take advantage of the unique properties of precast/prestressed concrete using dry jointed construction. The test building incorporated four different seismic frame systems in one direction, and a jointed shear wall system in the orthogonal direction. Pre-topped double tees were used on three floors; while the other two floors were constructed using topped hollow core slabs. The major objective of the test program was to develop design guidelines for precast/prestressed concrete seismic systems that were appropriate for the use in various seismic zones [37].

Figure 2.9. Prototype five story precast structure [38]

Test building had a two bay by two bay configurations, with a bay size of 4.5 m x 4.5 m. Two different precast frames, one with prestressed beams, and the other using mild steel reinforcing bars across the beam-to-column connections provided lateral resistance at opposite sides of the building in one direction of response with a central structural wall providing lateral resistance in the other direction [39]. The details of hybrid connection are shown in Figure 2.10.

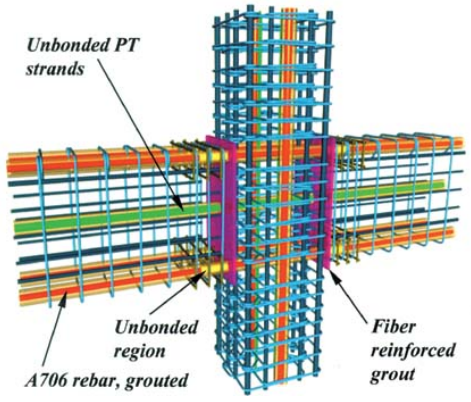

Figure 2.10. Hybrid connection detail [40]

The structural response of the PRESSS five-story precast concrete test building under simulated seismic testing was extremely satisfactory. The following summarizes the response and conclusions available at this stage [39]:

- Damage to the building in the wall direction was minimal, despite being subjected to seismic intensities 50 per cent above design level.
- Damage to the building in the frame direction of response was much less than could be expected for an equivalent reinforced concrete, subjected to the same drift levels. The performance of the prestressed frame was particularly good, with damage being limited to minor spalling of cover concrete in the beams immediately adjacent to the columns and some crushing of the fiber grout pads at the beam-column interfaces.
- At high levels of response displacements, beam rotation about the longitudinal axis was noted, caused by the high torsinal moment induced by the vertical load from eccentrically supported double-tee floor members, and the reduced torsinal resistance in the beam-end plastic hinges.
- The test provided an excellent confirmation of the direct displacement-based design approach used to determine the required strength of the building. The required base-shear strength using direct displacement based was only 5 and 60 per cent of the required by conventional force-based design using UBC provisions for wall and frame directions respectively.

Hybrid precast beam-column connection tests were performed also in METU with the similar approaches [41]. It is reported that four, approximately half scale specimens were designed and tested under simulated earthquake loads. The first specimen (MR1) was the reference specimen for the following precast specimens with a monolithic connection. The second specimen, which was the first original precast specimen (PO1), was designed on the basis of the past practice of the collaborating company, Yapı Merkezi, concerning the properties of the most common types of precast concrete structures designed earlier using some other connection types. Low capacity of PO1 indicated insufficiency in connection reinforcement, especially the prestressed reinforcement. Therefore in the second precast specimen, PM1, the amount of connection reinforcement was increased considerably. However, in this specimen, formation of plastic hinging was

observed at an unexpected section in the beam. As a result, this modified precast specimen could not attain the aimed capacity. The section detail of PM2 is given Figure 2.11.

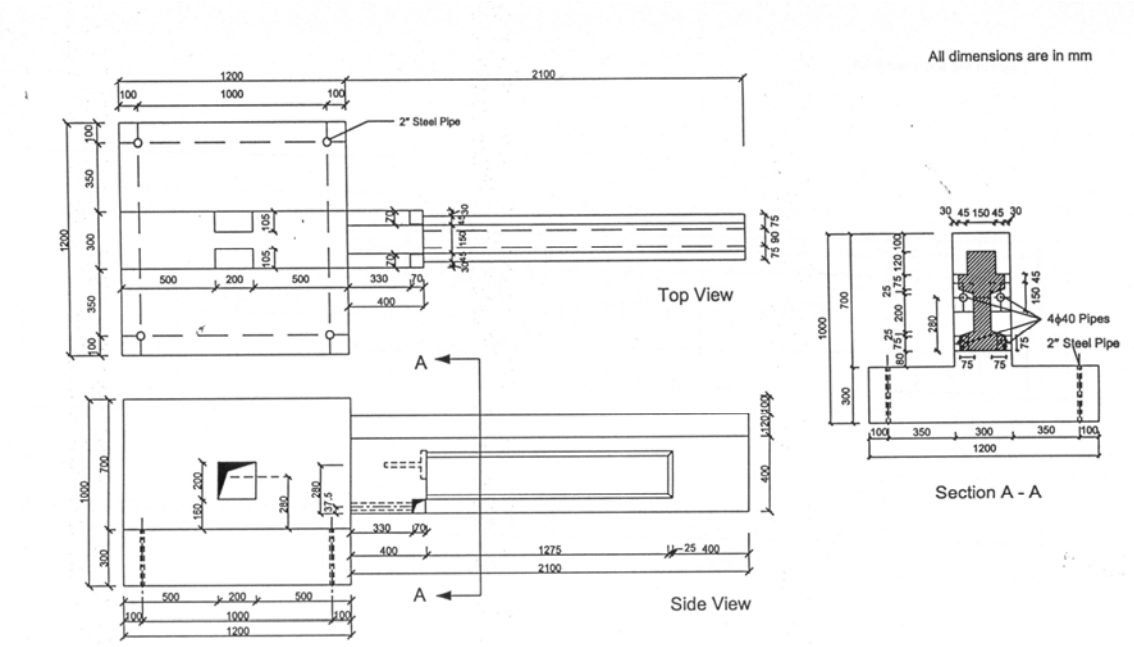

Figure 2.11. Details of PM2 specimen [41]

Consecutive improvements on test specimens consisting of medium size members leaded to satisfactory connection performance, including sufficient strength and ductility and acceptable energy dissipation and stiffness. The relatively low energy dissipation was the natural consequence of the elastic behavior of the unbonded prestressing cable, which provided the major portion of the flexural capacity. Energy dissipation capacity could obviously be increased considerably by providing higher amount non-prestressed connection steel at the top and bottom levels of the section [41].

2.2.4. Cast-in-Place Connection (CIP)

Cast in Place (CIP) connection type is widely used in Japan and New Zealand. If the connections between the precast concrete elements in frames were placed in critical regions, such as potential plastic hinge regions, the approach was to design and construct connections that possess stiffness, strength and ductility similar to that of cast-in-place

concrete monolithic constructions. In other words, monolithic construction was emulated [42].

Arrangements commonly used in New Zealand for strong column-weak beam designs are shown in Figure 2.12. In System1 of Figure 2.12, the precast beam elements were placed between columns, seated on the cover concrete of the previously cast-in-place reinforced concrete column below, and supported under the precast elements. This system leaded to a large reduction in the quantity of site formwork necessary. A difficulty with connection detail that the bottom longitudinal bars of the beams protruding from the precast beam elements was needed to be anchored in the joint cores [42]. The similar technique was presented by Ohkubo *et al.* [43] as a Japanese detailing.

In System 2 arrangement that made more extensive use of precast concrete and avoids placement of cast-in-place concrete in the congested beam-to-column joint core regions is shown in Figure 2.12. The reinforced concrete columns could be either precast or cast-in-place to occupy the clear height between beams. The precast portions of the reinforced concrete beams extended from near midspan to midspan, and, hence, included within precast element over the columns the complex arrangement of joint core hoop reinforcement that was prefabricated at the precasting site. The precast portions of the beams were placed seated on the concrete column beneath, with suitable material between, and supported for construction stability. An advantage of this system was that the potential plastic hinge regions in the beams occurred within the precast elements away from the joining faces between the precast elements. Also, this system made extensive use of precast concrete and eliminated the fabrication of complex reinforcing details during construction. A possible difficulty was the tighter tolerances necessary when assembling the precast concrete systems [42].

A third possible arrangement incorporating T or H shaped precast concrete elements and their site application is shown in Figure 2.12 and Figure 2.13. The vertical column bars in the precast T units were connected using grouted steel sleeves or ducts. At the midspan of the beams, the bottom bars could be connected in a cast-in-place concrete joint. Some details of midspan connections are presented in Figure 2.14. An advantage of System 3 was the extensive use of precast concrete and the elimination of the fabrication of complex

reinforcing details during construction. A possible constraint was that the precast elements were heavy and crane capacity might be an important consideration [42].

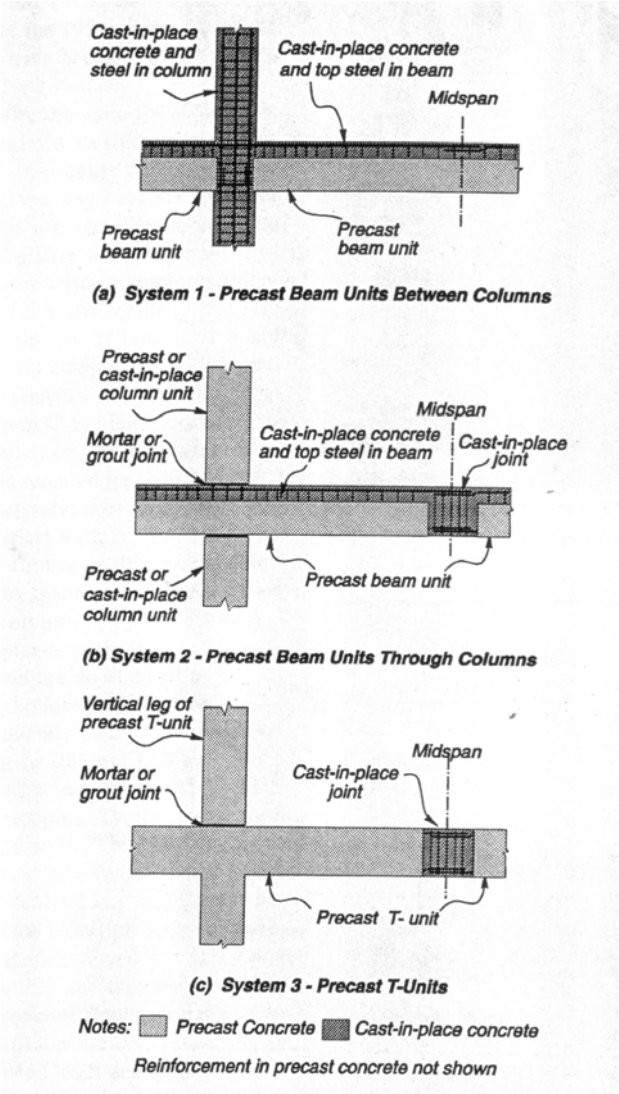

Figure 2.12. Arrangements of precast concrete members [42]

Another building system as illustrated in Figure 2.15 that has become popular in Europe involved the use of precast concrete beam shells as permanent formwork for beams. The precast beam shells were typically pre-tensioned; prestressed concrete U beams were left permanently in position after the cast-in-place reinforced concrete has been cast. The precast U-beams supported the self-weight and construction loads and acted

compositely with the reinforced concrete core when subjected to other loading in the completed structure [42].

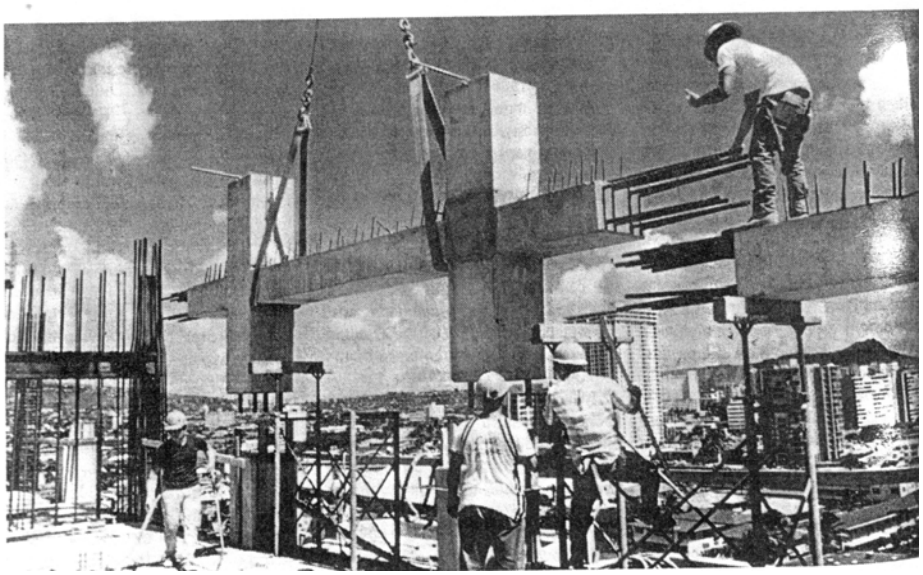

Figure 2.13. H-shaped precast elements [25]

The precast concrete U-beams were generally not connected by reinforcement to the cast-in-place concrete of the beam or column. Reliance was normally placed on the bond between the roughened inner surface of the precast U-beam and cast-in-place concrete core to achieve composite action. Occasionally, protruding stirrups or ties from the U-beams have been used to improve the interface shear strength. During construction, it was very important to ensure that the inside surfaces of the shell beams were clean when the cast in place concrete is cast. Otherwise, sufficient bond between the shell and core cannot develop [42].

Furthermore, Soubra *et al*. [44] studied cast in place connection with steel fibers. The beam-column subassemblages consisted of two precast concrete parts joined by a cast-in-place (CIP) connection as shown in Figure 2.16.

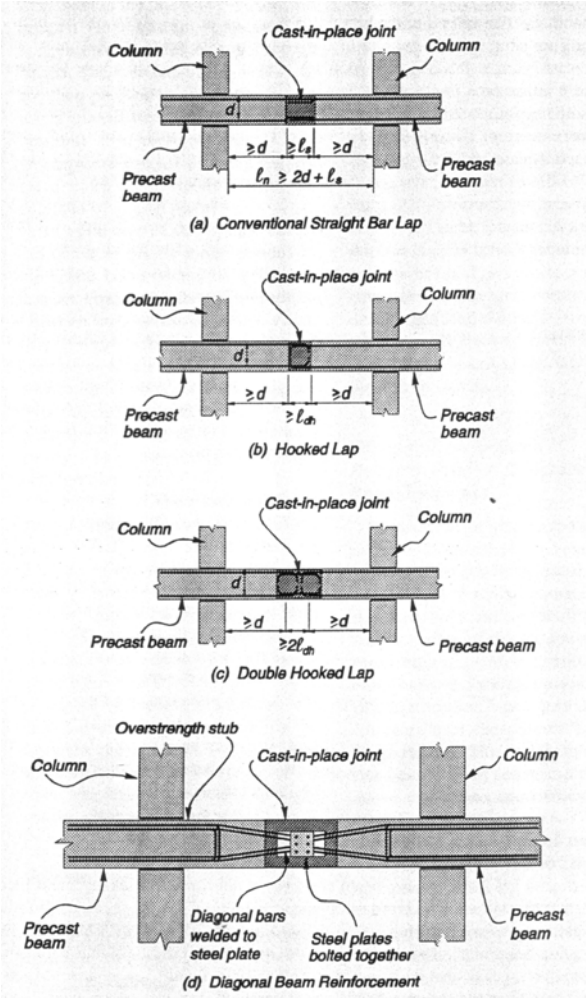

Figure 2.14. Some details of midspan connections [42]

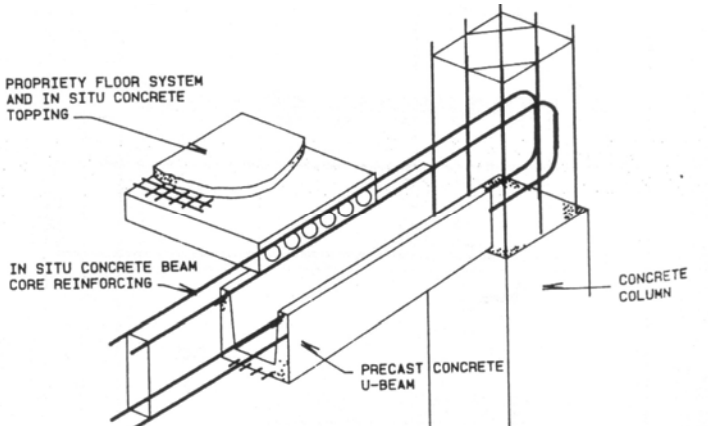

Figure 2.15. Details of U channel system [1]

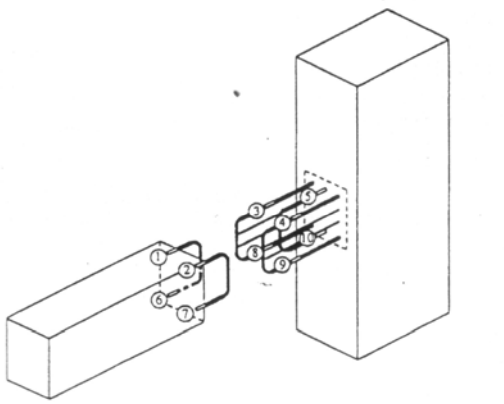

Figure 2.16. Typical CIP connection detail [44]

The specimens were designed to insure plastic hinging action in the CIP connection, away from the column face, where adequate strength ductility and energy dissipation were provided by fiber reinforced concrete. The presence of the moment gradient on the beam part of the specimen required that sections at or near the column face be stronger than those in the CIP connection in order to maintain elastic behavior at the column face and moved the plastic hinge away from the column face.

The advantages of using steel fiber reinforced concrete in CIP connection can be drawn as [44, 45]:

- The FRC-based connection detail was successful in making the connection act as a plastic hinge by spreading yielding from the center to interface.
- The use of fiber reinforced concrete in the CIP connection was very effective in improving the displacement ductility of the specimens.
- The use of fibers in the connection led to slower stiffness degradation during each cycle of loading when compared to the control specimen.
- The energy dissipation of the specimens was dramatically improved by use of fiber reinforced concrete in the CIP connection.

In addition to that, it was possible to use mechanical connector at cast in place region. In Figure 2.17, the connection details between the column units and between the

column and beam units are illustrated. In this scheme a mechanical connection that can develop full continuity between reinforcing bars greatly enhanced the flexibility in the column-to column joint locations. When these connections were combined with adequate grouting in the joint, the vertical precast concrete column unit can be joined at the floor line or at any other convenient location along the height of the column to develop continuity.

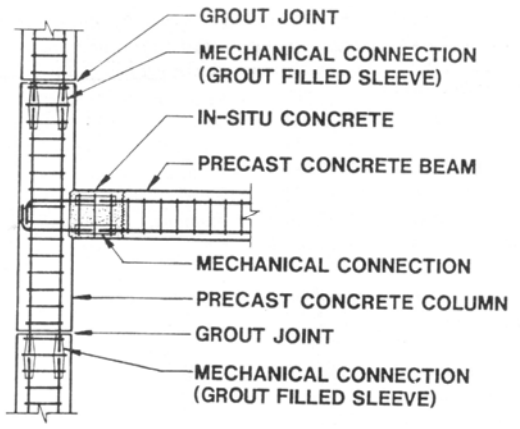

Figure 2.17. Typical precast concrete frame [25]

It should be noted that the mechanical connection between column units can be “blindly” executed; that was, access openings were not needed, thus eliminating the need for patching and grouting after the connection was installed. The grout-filled steel sleeve connection was classified as a “blind” connection that can achieve full continuity in the steel [25].

3. EXPERIMENTAL STUDY

3.1. Objective

The most important ingredient in the design of precast concrete structures may be highlighted as the connection detailing. Connections between precast building elements such as columns, beams, slabs and shear walls must effectively integrate the individual structural components in full continuity with each other so that the overall building structure behaves monolithically. In this manner, the structural analysis and behavior of a building frame would be identical to that of a cast-in-place structure except that the framing system now uses the precast concrete components which are assembled together to act monolithically [25].

A two phase research program on the performance of precast ductile beam-column connections was developed in Boğaziçi and Kocaeli Universities after the 1999 earthquakes. This program is funded by The Scientific and Technical Research Council of Turkey (TÜBİTAK- Project No: İÇTAG I589) and the Turkish Precast Association. In Phase I, cast-in-place, composite and bolted type of connections were investigated and compared with the monolithic counterpart. The Phase I specimens were chosen from the construction practice as the most widely used types in North America, Europe and Japan. In Phase II, post-tensioned hybrid connections with different mild steel reinforcement ratios were examined. All test specimens in this research program were detailed according to the prevailing level of information stated either in the building codes or in the available literature.

3.2. Test Specimens

Test specimens were modeled as an exterior joint of a multi-story office building. A seven-story office building, as a prototype, was analyzed and designed according to high seismic regions. The story height of the prototype moment resisting frame was 3.5 m and the bay width was 7.5 m with 6 bays in each direction. The beam and column dimensions were determined as 450/700 mm and 800/800 mm respectively. Analysis on the prototype

frame revealed that the beam reinforcement ratio at the top was 0.009 and 0.007 at the bottom for joint regions.

All test specimens were designed with strong column and weak beam design philosophy. The test specimens were scaled down to approximately 1/2 of the prototype structure in geometry, hence similar scale factor was observed in flexural moment capacity of the subassembly. The minimum limit for the scaling factor is given as 1/3 in the ACI T1.1-01 [46] document. As a result, the crossectional dimensions of the beam were 300 by 500 mm and clear span of beam was 1600 mm. Hence the shear span to depth ration (a/d) was 3.6. The reason of such a low a/d ratio is to enforce the precast connection to higher shear forces. The height of the precast column was 1920 mm with 400 mm square section without corbel. The dimensional detail of the subassembly is given in Figure 3.1.

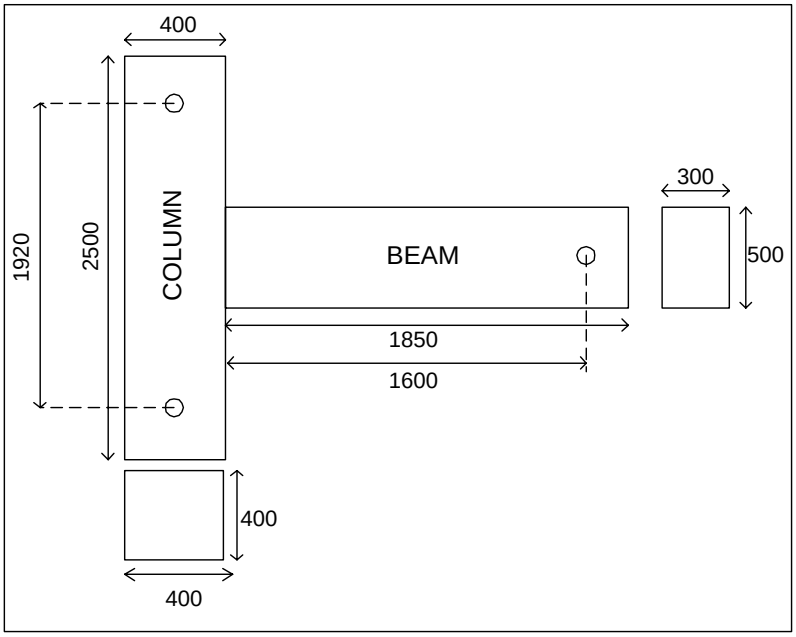

Figure 3.1. Test specimen dimensions

3.3. Material Properties

3.3.1. Concrete

The concrete compressive strength of precast members was kept constant during the production of the test specimens. The nominal 150x300 mm cylinder compressive strength of the concrete was around 40 MPa, since precast concrete member producers generally prefer 40 MPa concrete in their construction practice. In the mix design, maximum aggregate size was 20 mm. Ready mixed concrete supplied by BETONSA, was used for Phase I test specimens except the composite connection GOK-W and the slump value of mix design was around 13-15 cm. The ready mixed and cast-in-place concrete design values were the same as given in Table 3.1. Cast-in-place concrete of Phase I specimens contained hooked end steel fibers that had 40 mm length and 0.6 mm diameter with 0.5 per cent volume fraction. Phase II specimens and specimen GOK-W were produced by GOK Construction company production plant with similar mix design values, with a nominal compressive strength of 40 MPa.

Table 3.1. Concrete mix design values

Ingredients	Amount (kg/m^3)
Cement (PC-42.5)	340
Fly ash	80
Water	270
Super plasticizer	6.30
Crushed stone No I (sandstone)	590
Crushed stone No II (sandstone)	529
Sand (stone powder)	286
Sand (washed sea sand)	376

3.3.2. Reinforcing Steel Bars

For all specimens, except composite connection detail GOK-W, the same grade ϕ20 bars were used as longitudinal and ϕ10 rebars were used as lateral reinforcement that had

20 mm and 10 mm nominal diameters, respectively. The yield and ultimate strength of ϕ20 rebars was 472 MPa and 574 MPa respectively, and the elongation at ultimate strength was 14 per cent. For ϕ10 rebars, these values were 500 MPa and 560 MPa and elongation at ultimate strength was 13 per cent. To determine mechanical properties of reinforcing bars, three sets for each type were tested in Kocaeli University Structures Lab. The summarized test results and their typical stress-strain plots are presented in Table 3.2, Figure 3.2 and Figure 3.3 respectively.

The properties of the prestressing strands met the ASTM Standards. The minimum strength of the stress relieved type prestressing strand was 1860 MPa (Grade 270). The yield strength of the prestressing tendon is defined by the 85 per cent of its ultimate strength. Two different tests were done to clarify mechanical properties of the prestressing tendons. The first one was done in the direct tensile machine with using extensometer in the mid portion of the tendon and measuring the elongation between grips at the same time. For the second one, three strain gages were installed on the wires and tested with post-tensioning grips. Summarized properties and stress-strain plot of prestressing tendons can be seen in Table 3.2 and Figure 3.4.

Table 3.2. Properties of steel

Type	Mild Steel	Mild Steel	Pre.Tendon (with strain gages)	Pre.Tendon (with extensometer)
Diameter (mm)	10	20	13	13
X-area (mm^2)	78.5	314	98.7	98,7
f_y (MPa)	500	472	1530	1530
f_u (MPa)	560	574	1800	1800
E_s (MPa)	200000	200000	200000	200000
ε_y (mm/mm)	0.0025	0.0024	0.0076	0.0297
ε_{sh} (mm/mm)	0.04	0.023	-	-
ε_u (mm/mm)	0.130	0.140	0.011	0.054
ε_r (mm/mm)	0.185	0.200	0.011	0.054

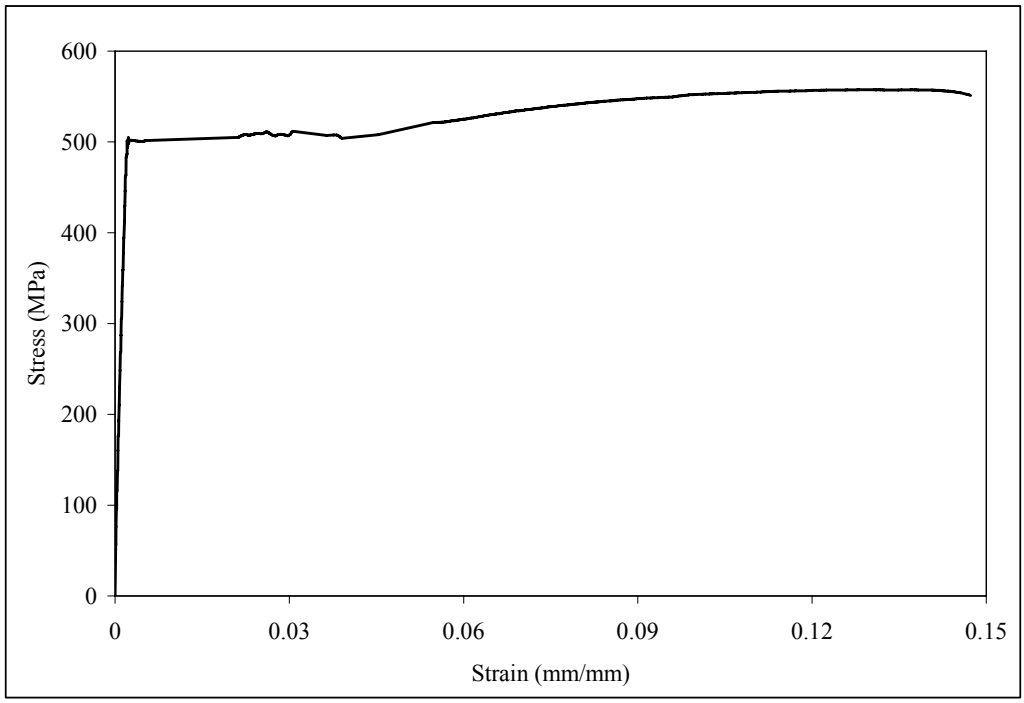

Figure 3.2. Stress-strain plot of 10 mm mild steel

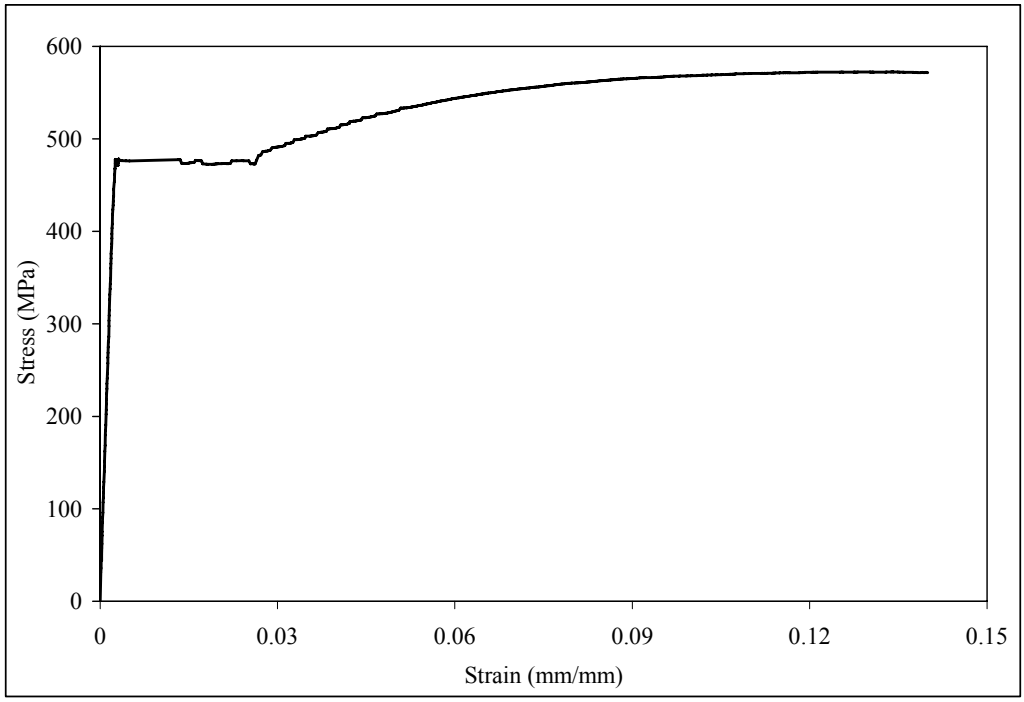

Figure 3.3. Stress-strain plot of 20 mm mild steel

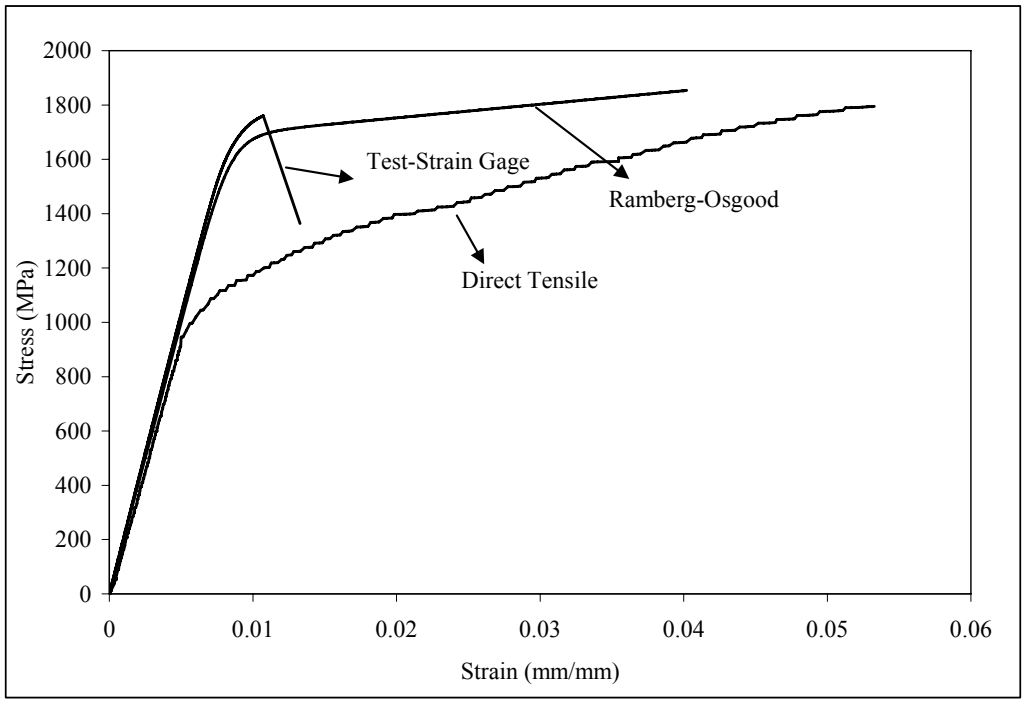

Figure 3.4. Stress-strain plot of prestressing tendon

3.4. Test Setup

All tests were performed at Structures Laboratory in the Civil Engineering Department of Boğaziçi University. Figure 3.5 and Figure 3.6 presents the test set-up and the location of deformation measurements and the test set-up was adapted from the work of ACI.T1.01 [46]. Precast column was supported on a pin connection at the base and the column top was free to move and rotate. A roller supported beam free end was designed; hence the point of contra flexure for both beam and column was achieved within the setup. An axial load of approximately 10 per cent of the column compressive capacity was applied to the columns in all specimens by using a closed frame and a hydraulic ram mounted on top of the column as shown in Figure 3.5. Gradually increased lateral load was applied in order to achieve the predetermined story drifts. Several LVDTs were mounted on the test specimens in order to measure the net story drift, joint rotation, gap openings and shear deformations. The net column top displacement (Δ_{cnet}) was calculated by subtracting the column base lateral displacement and the vertical beam tip rigid body displacement from the lateral displacement measurement obtained at the column top. Top

displacement of the column (Δ_{ct}) was measured by using two 200 mm capacity LVDTs mounted at the level of the hydraulic actuator. Column base displacement (Δ_{cb}) was measured at the pin support level. At this level lateral displacement readings should be zero in the ideal test rig. Also, the vertical displacement (Δ_{bv}) of the beam tip should be zero. Therefore, these displacement readings were monitored continuously and the net column top displacement, which will yield the level of story drift, was calculated according to Equation 3.1 where 1920/1800 ratio is used due to the geometric compatibility. For Phase II specimens, a load cell was installed at the end of the beam to measure the initial effective force for post-tensioning. Also, by using this load cell, average stress changes on the prestressing strands were monitored during cycling loading.

$$\Delta_{cnet} = \Delta_{ct} - \Delta_{cb} - \left(\frac{1920}{1800} \times \Delta_{bv} \right) \tag{3.1}$$

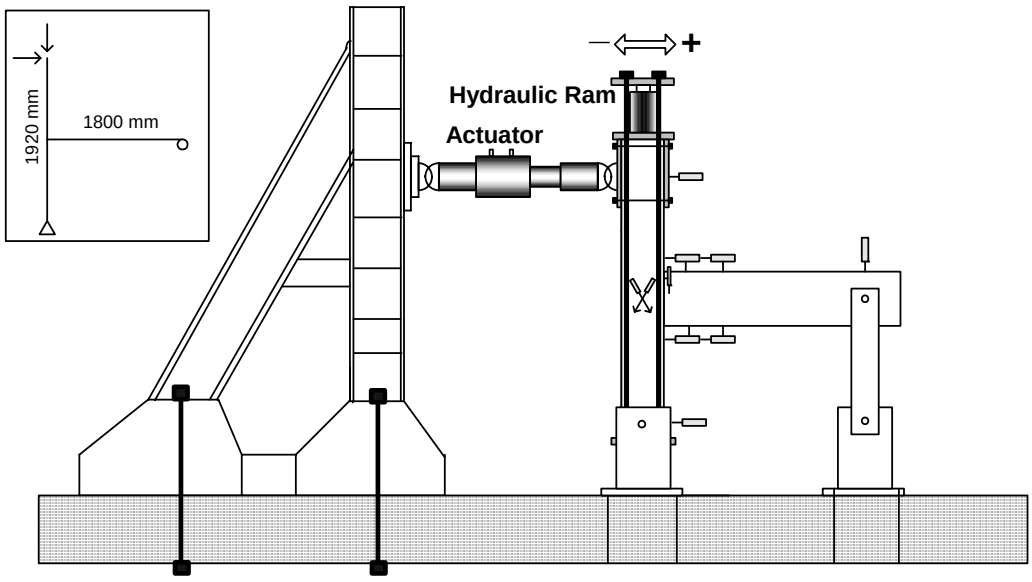

Figure 3.5. Configuration of test setup

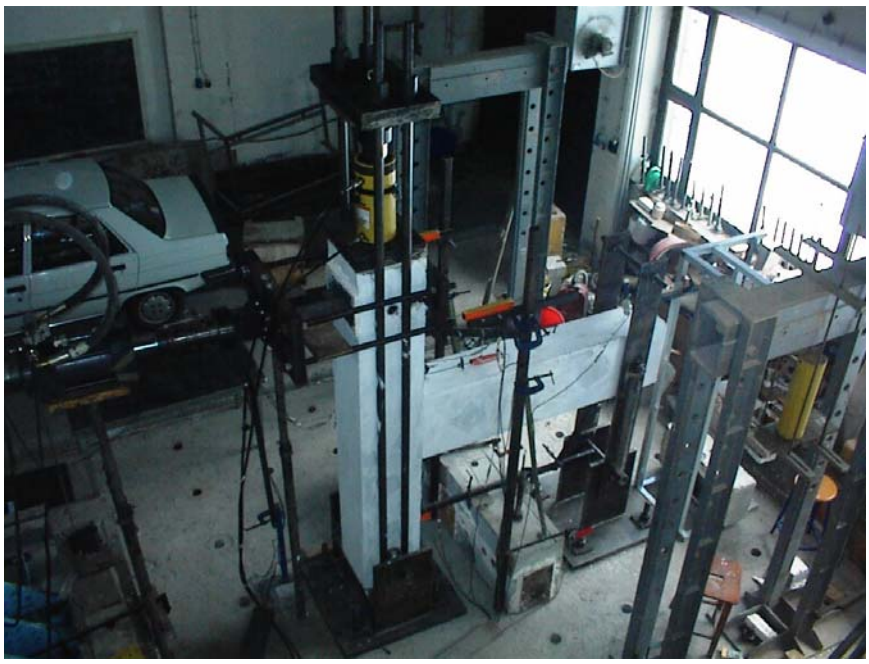

Figure 3.6. A view from test setup

3.5. Test Procedure

Test was performed according to ACI T1.1-01 [46] document. Minimum requirements of the test procedure can be summarized as follows:

- Test modules shall be subjected to a sequence of displacement-controlled cycles representative of the drifts expected under earthquake motions for that portion of the frame represented by the test module. Cycles shall be predetermined drift ratios.
- Three fully reversed cycles shall be applied at each drift ratio.
- The initial drift ratio shall be within the essentially linear elastic response range for the module. Subsequent drift ratios shall be values not less than one and one-quarter times, and not more than one and one-half times the previous drift ratio. If steps are too large, the drift capacity of the system may not be determined with sufficient accuracy. If the steps are too small, the system may be unrealistically softened by loading repetitions, resulting in artificially low maximum lateral resistance and artificially high maximum drifts. Also, when steps are too small, the rate of change of energy stored in the system may be too small compared with the change occurring

during a major event. Results, using such small steps, can mask undesirable brittle failure modes that might occur in the elastic response range during a major event.

- Testing shall continue with gradually increasing drift ratios until drift ratio equals or exceeds 0.035
- Data shall be recorded from the test such that a quantitative, as opposed to qualitative, interpretation can be made of the performance of the module. As continuous recording shall be made of the test module, drift ratio versus column shear force, and photographs shall be taken that show the condition of the test module at the completion of testing for each sequence of three cycles.

There is no requirement for axial load to be applied on the column simultaneously with the application of the lateral load displacements. It is conservative not to apply axial load because, in general, the axial load will be less than the balanced load for frames for which this standard will be used. The lateral load was applied based on the above criteria. Before starting loading cycles, constant axial load was applied. The level of axial load was 10 per cent compressive strength of the column. Figure 3.7 shows the loading pattern that was taken from the ACI T1.1 [46] document. First cycles (0.15 per cent and 0.20 per cent) were generally in the elastic range. Three fully reversed cycles were applied at each drift level.

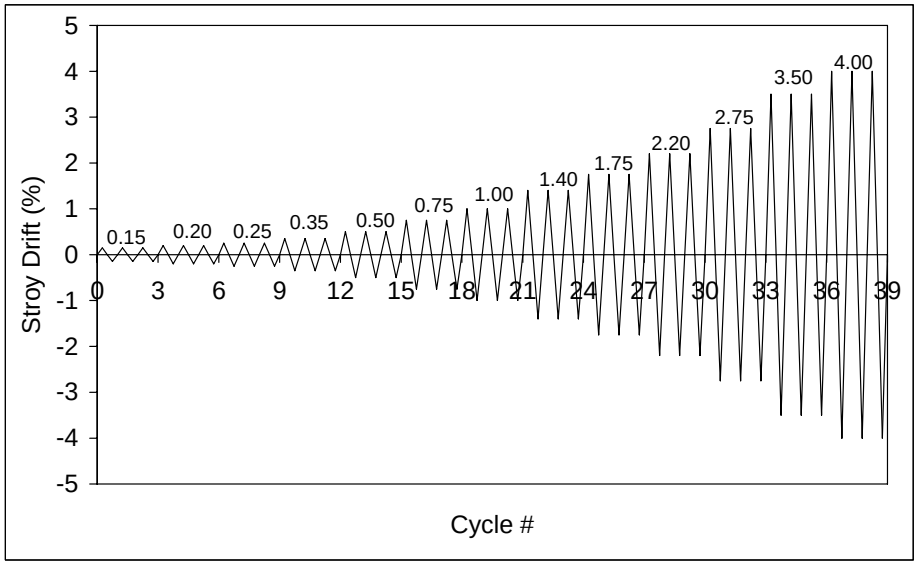

Figure 3.7. Loading history

All data were collected with a 50 Hz. data acquisition system. Cracks, gap openings and failures were monitored in successive three cycle intervals. All test specimens were loaded ultimately until the 4.00 per cent inter-story drift ratio. The test was terminated before the 4.00 per cent drift level in case of a premature failure of the connection, mainly due to the rupture of flexural rebars.

3.6. Specimen Details

Test was performed in two phases as presented in Figure 3.8. In Phase I, four types of ductile moment resisting precast frame connections and one counterpart monolithic connection, designed for high seismic zones were tested.

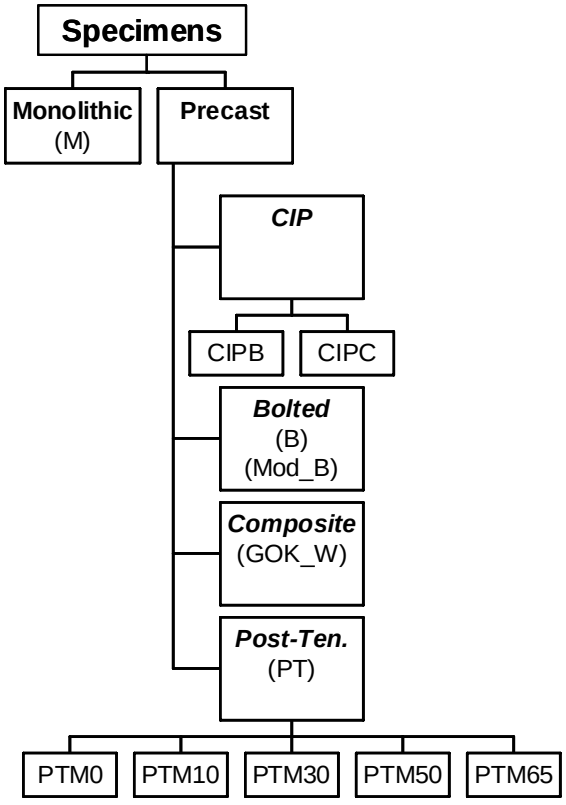

Figure 3.8. Test parameters

Performance of precast connections under reversed cyclic loading was compared with that of the monolithic subassembly (M). Precast specimens of the current presentation may be subdivided into three groups, namely cast-in-place, composite with welding and

bolted connections. The location of cast-in-place connections in precast subassemblies was either in the beam (CIPB) or in the column (CIPC). The composite connection (GOK-W) tested within this study was a common detail in the Turkish precast concrete industry. Two bolted specimens (B and Mod-B) without corbels were also tested. In Phase II, the main variable was the contribution of mild steel for flexural moment capacity of the connection. The range of this contribution was changed from 0 to 65 per cent and these test specimens were called PTM0, PTM10, PTM30, PTM50 and PTM65 depending on the mild steel moment contribution.

3.6.1. Monolithic Specimen (M)

Monolithic reference specimen (M) was designed according to the regulations for high seismic regions. The column longitudinal reinforcement ratio was 2.00 per cent and the spacing of the closed stirrups was approximately 100 mm at the beam-column joint region for the monolithic and the precast specimens. As shown in Figure 3.9, 4ϕ20 and 3ϕ20 rebars were placed at the top and the bottom of the beam respectively, where ϕ designates the rebar diameter in millimeters. The bottom reinforcement of the beam was taken less than the top reinforcement due to the gravity load effect. The compressive strength of the concrete for specimen M was 40 MPa.

3.6.2. Cast-in-Place in Column Connection (CIPC)

In the CIPC detail, there was a gap at the mid-height of the precast column as presented in Figure 3.10. The height of the gap which was 500 mm, was equal to the beam depth. In the precast beam, 3ϕ20 U shaped rebars, due to anchorage considerations, were installed as flexural reinforcement at the connection region. This application was adopted according to Japanese detailing that was developed by *Mikame et al.* [47]. Additionally, there were 3ϕ20 rebars at the top and the bottom of the beam body as main reinforcement. In assembly process, the precast beam was seated through the gap at the precast column. The compressive strength of the concrete for precast members was 52 MPa. In order to eliminate or delay the bond problem in limited joint region where U shaped reinforcing bars were used, concrete with 40 mm hooked steel fibers (volume fraction of fiber = 0.5 per cent) was placed in the joint region. Compressive strength of the cast-in-place concrete

in the wet connection was 53 MPa. Due to the existence of U shaped rebars, closed stirrups could not be installed; instead single leg ties were used in the column joint region.

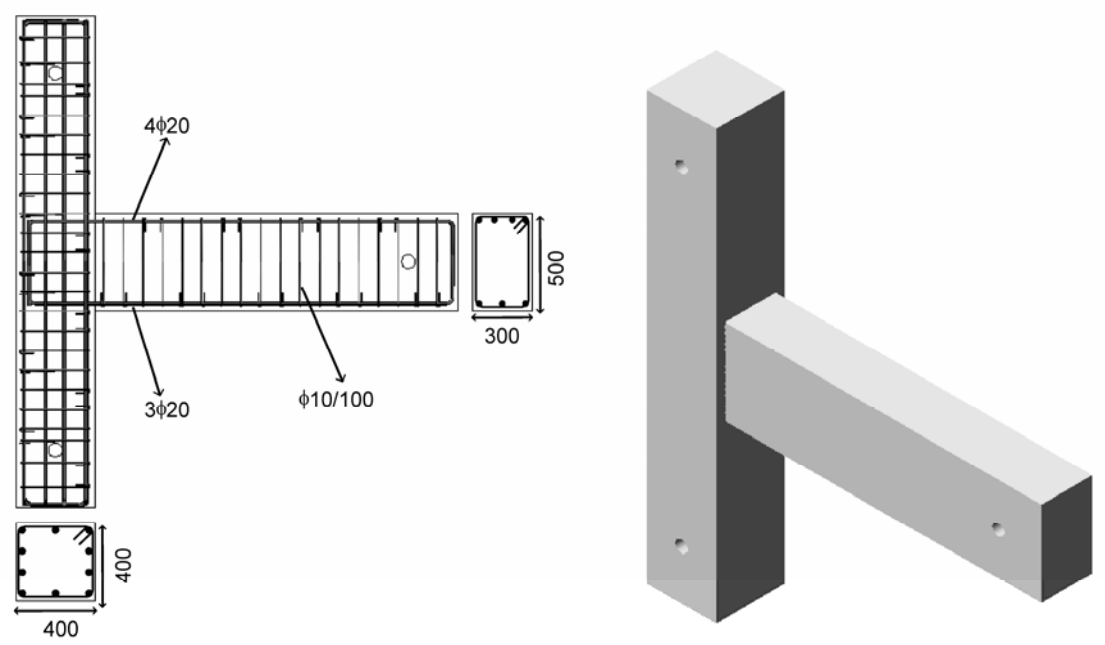

Figure 3.9. Details of the monolithic specimen (M)

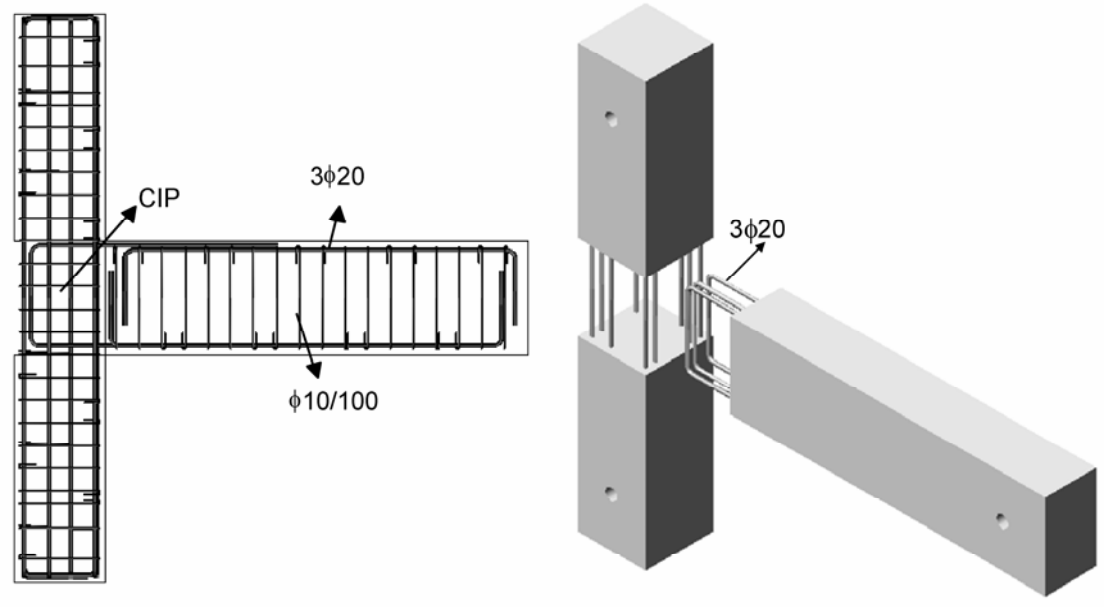

Figure 3.10. Details of the specimen CIPC

3.6.3. Cast-in-Place in Beam Connection (CIPB)

A design concept similar to the CIPC specimen was also applied to the CIPB connection. The difference was the location of the connection region that was 500 mm length and located at the joining end of the precast beam as shown in Figure 3.11. Again U shaped rebars protruding from column (4ϕ20) and from the beam (3ϕ20) for flexure were combined in this region. Compressive strength of precast elements was 40 MPa. During the assembly process, precast beam rebars were located between the bars protruding from the precast column at an interlocking position. Steel fiber concrete with 0.5 per cent volume fraction was placed at the connection region and the compressive strength was 49 MPa. Single leg ties were used in the connection region.

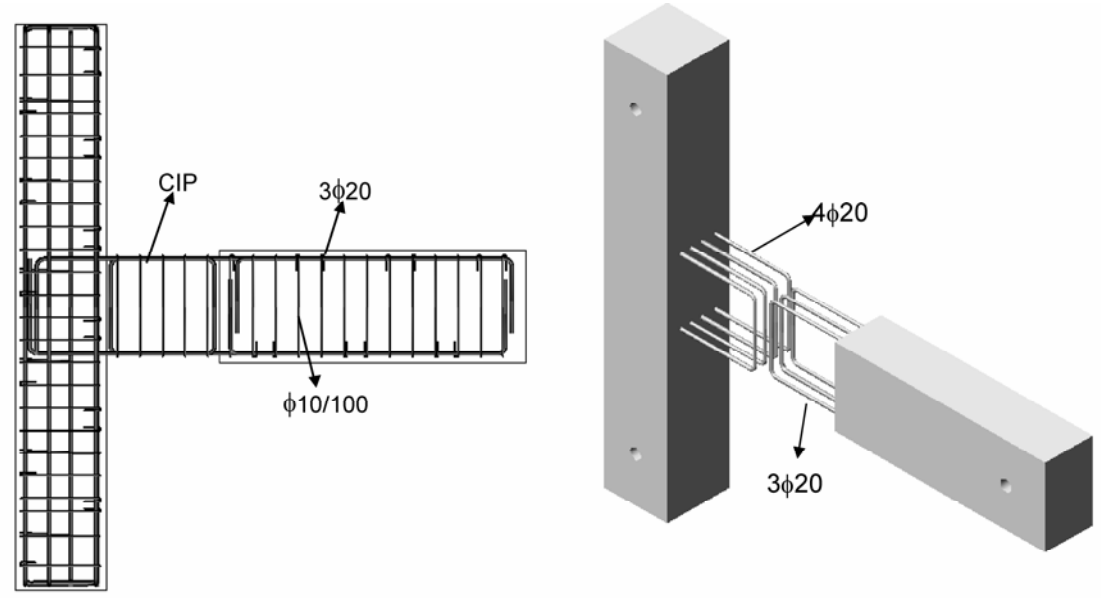

Figure 3.11. Details of the specimen CIPB

3.6.4. Composite Connection (GOK-W)

GOK-W was a composite connection type where the continuity of the beam bottom reinforcement was supplied by welding and the top reinforcement was by cast-in-place concrete through the gap in the column. GOK-W is a common connection type for the Turkish precast producers. This test specimen was designed and produced by GOK

Construction Company. The square crossectional dimension of the precast beam was 300 mm. A region with a height of 200 mm along the precast beam and the gap in the middle of the column was the cast-in-place section of the subassembly as presented in Figure 3.12. There were 3ϕ20 rebars as main reinforcement at the bottom of the beam and these rebars were welded to a steel plate which had 300 x 250 x15 mm dimensions. Additionally 2ϕ20 rebars at 20 degrees angle with horizontal through the beam, were welded to the same plate in order to secure the anchorage of the steel plate to precast beam as shown in Figure 3.12. This detailing also created additional flexural moment capacity. Moreover, two rows of ϕ20 U shaped flexural bars were installed through the gap in the column as top reinforcement of the beam during the assembly process. The distance between these two rows was 36 mm. Main rebars of the precast corbel were welded to a steel plate which will later be welded to the bottom plate of the beam for continuity. Cast-in-place concrete was placed to the upper part of the beam and to the gap of the column. All ϕ20 rebars were weldable steel and the yield and ultimate strengths were 503 MPa and 662 MPa respectively. The elongation of ϕ20 rebars at ultimate strength was 13 per cent. The compressive strength of precast elements was 57 MPa and the compressive strength of the cast-in-place concrete was 55 MPa for specimen GOK-W.

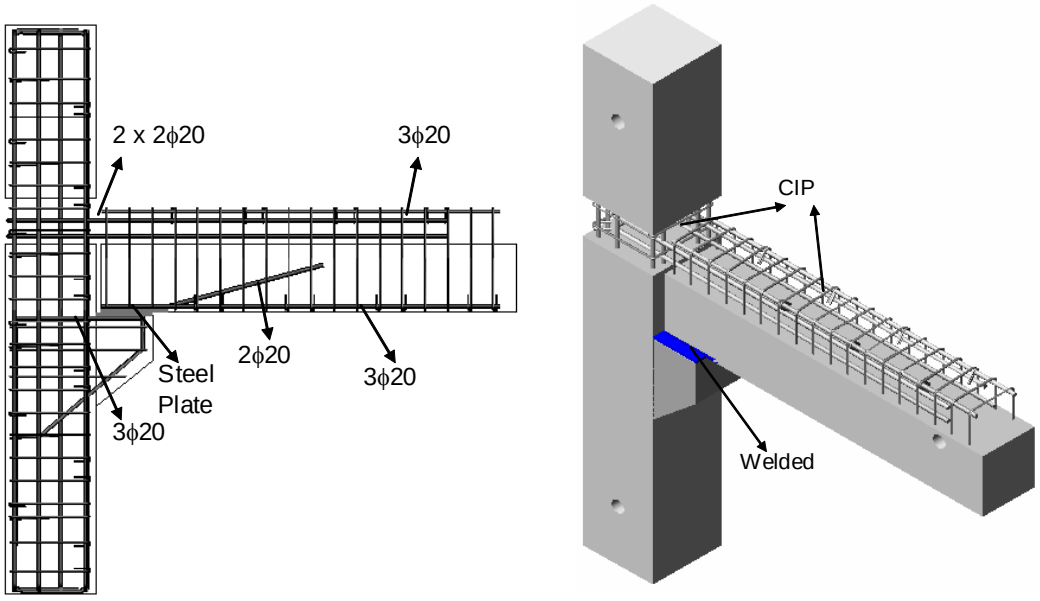

Figure 3.12. Details of the specimen GOK-W

3.6.5. Bolted Connection (specimen B and specimen Mod-B)

The aim of the bolted type of connection was to minimize the field work during the assembly process. In proposed bolted connection detail, rectangular steel boxes were used instead of steel pipes for through holes. As a result of steel boxes more dimensional tolerances for compensating the production errors and more spaces for multiple bolts were obtained. This connection type is more suitable especially for low level gravity induced shear forces, where precast slabs, such as double-T and hollow core slabs, were oriented parallel to the beam axis.

The reinforcement detail and the overall view of the precast members for the bolted connection type is as shown in Figure 3.13. The precast beam had a reservation channel at the top and the bottom of the beam crossection in order to install the connecting bolts during the assembly process. The length of the reservation channel was 1000 mm with a crossectional dimension of 150 x 100 mm. Also, 500 mm long rectangular steel boxes with crossectional dimensions of 120 x 60 mm were located at the joining end of the beam and through the column along the same axis. In this region of the beam, closed stirrups were installed with 70 mm spacing. Moreover, steel plates were placed at the top and the bottom of the beam crossection in order to delay the crushing of beam concrete adjacent to the column face. These steel plates were also connected to each other by two ϕ10 bars welded to either plate.

In the construction process, the precast members were produced with a 28 MPa concrete. During the assembly process, the 15 mm gap between the precast beam and the column was filled with SIKA Grout 210 that was self-leveling, non-shrink grout. The compressive strength of the grout was 58 MPa. After 24 hours, 3ϕ20 rebars were placed into the steel boxes located at the top and the bottom of the connection and a pretensioning force by a torque wrench was applied. Initially 35 Nm torque was applied then this level was increased up to 120 Nm resulting a 1.4 MPa clamping stress at the beam-column interface. The distance of bolts from top and bottom fiber of the beam was around 70 mm. Finally, steel boxes were filled with the same grout.

In the first test, steel boxes were attached directly to the precast beam shear reinforcement and this type of connection was called as Bolted (B). During the test, sliding of the steel boxes with respect to the beam concrete was observed. In order to solve this problem, steel bars were welded around the steel boxes serving as ribs. In addition to that, rods passing through the box crossection were mounted into the steel box in order to eliminate any possible sliding of the infill grout with respect to the steel box itself. The connection type after these modifications is called Modified Bolted (Mod-B). In this detail, compressive strength of concrete in precast members was 30 MPa and the compressive strength of the grout was 36 MPa.

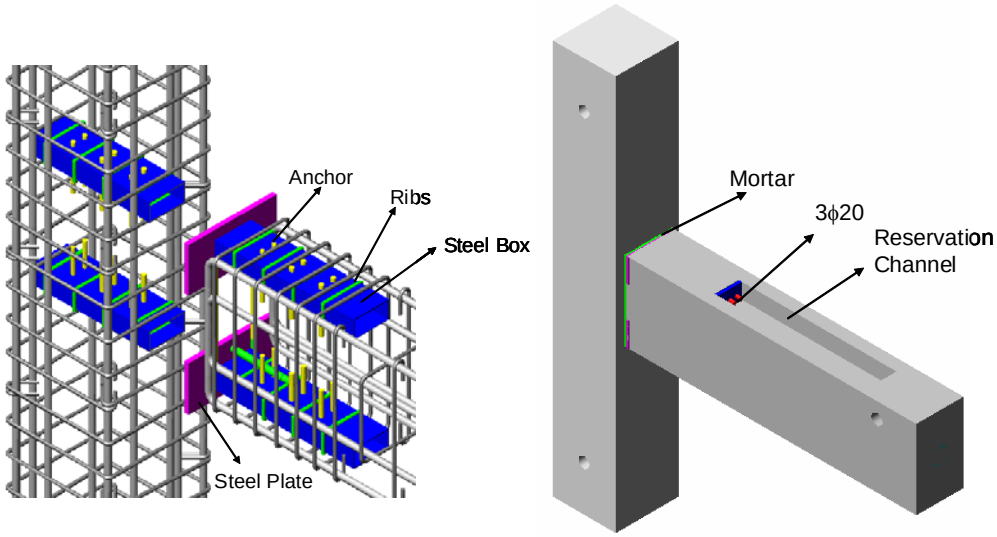

Figure 3.13. Details of the specimen Mod-B

3.6.6. Post-Tensioned Connection (PT)

All the precast beam and columns were produced in a precast concrete member production plant. The main variable investigated in the post-tensioned specimens was the mild steel content at the connection region. In the first specimen of the precast set, no mild steel was used in the connection and the flexural moment was carried solely with the prestressing strands. This specimen was called PTM0. For the second specimen, the contribution of mild steel for the flexural moment capacity was 10 per cent and the specimen was called PTM10. This 10 per cent ratio is the minimum level of mild steel in

precast connections stated in the Turkish Precast/Prestressed Design Standard [48] and the Turkish Earthquake Code [7]. The mild steel contribution to flexure was increased to 30 per cent (specimen PTM30) and 50 per cent (specimen PTM50) as third and fourth design respectively. The fourth specimen had the upper limit for mild steel contribution according to ACI T1.2-03 [49] design code. In the last specimen, the mild steel contribution on the flexural moment capacity of the connection was 65 per cent (specimen PTM65) and this mild steel ratio exceeds the upper limit of ACI T1.2-03 [49] design recommendations.

The geometry and reinforcement details of the precast beams, except PTM0, were the same as shown in Figure 3.14. All precast beams had a reservation channel at the top and the bottom of crossection to install mild steel during the assembly process. The length of the reservation channel was 1000 mm with a crossectional dimension of 150 x 100 mm. Also, there was a plastic (PVC) pipe with 100 mm diameter at the center of the beam crossection for installing prestressing strands. 4 ϕ20 longitudinal rebars were placed at the top and bottom of the precast beam body as main reinforcement and the detail is shown in Figure 3.14.

The crossectional dimension of the precast beams at the connection region was the same as that of the monolithic specimen. For precast members (beams and columns), rectangular steel boxes were installed in the connection region as illustrated in Figure 3.15. The reason of using steel boxes instead of steel pipes was to create more dimensional tolerances to compensate the production errors and reserve spaces for multiple bolts. The 500 mm long rectangular steel boxes installed the connection region had crossectional dimensions of 120 x 60 mm, and they were located along the same axis on the beam and the column. In order to prevent the sliding of steel boxes relative to the beam concrete, steel rods that served as ribs were welded around. Moreover, steel anchors passing through the box crossection were mounted to prevent any possible sliding of the infill grout with respect to the steel box itself as shown in Figure 3.15. Besides, steel plates were placed at the top and bottom of the beam crossection at the connection in order to delay the crushing of concrete in the precast beam. These plates were also connected to each other by two ϕ10 rebars welded to either of the steel plate and steel plates were anchored to beam concrete. In this region, closed stirrups were installed with 70 mm spacing.

In the assembly process, initially, 15 mm gap between the precast beam and the column was filled with SIKA Grout-210 that was self-leveling and non-shrink with 60 MPa compressive strength. As a second step, after 24 hours, mild steels were placed throughout the steel boxes and the threaded ends of the mild steel rebars were fixed. In order to determine the yielding point during the test, strain gages were attached to the mild steel rebars. Steel plates were placed on both sides of the steel boxed as washers and the mild steels were locked with nuts to prevent slip as shown in Figure 3.16. After that, steel boxes were filled with the same self-leveling and non-shrink grout. Finally, prestressing strands that had 13 mm nominal diameter and 1860 MPa ultimate strength were placed at the mid-depth of the beam and post-tensioning was applied. The net effective force was measured by using a load cell located at the tip of the beam and monitored until the test day. The unbonded length of the tendons was approximately 2700 mm.

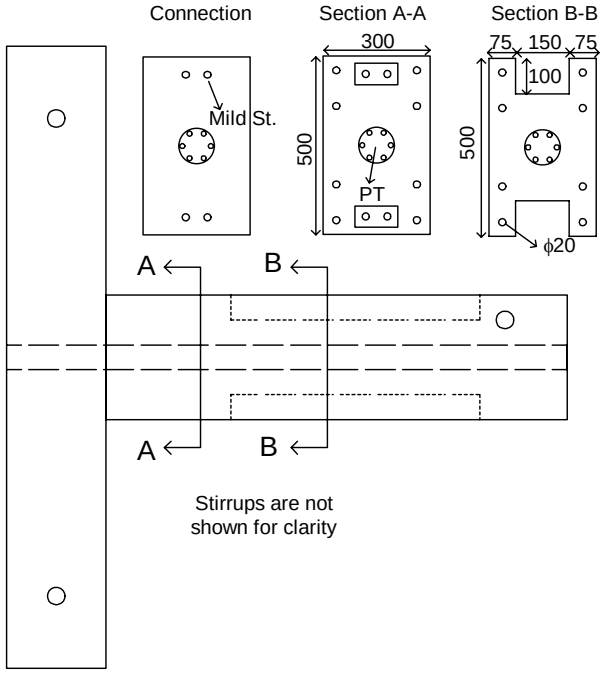

Figure 3.14. Reinforcing details of post-tensioned specimens

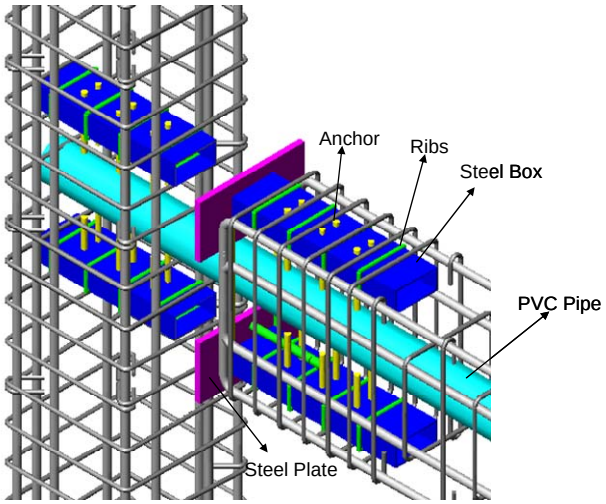

Figure 3.15. Connection details of post-tensioned specimens

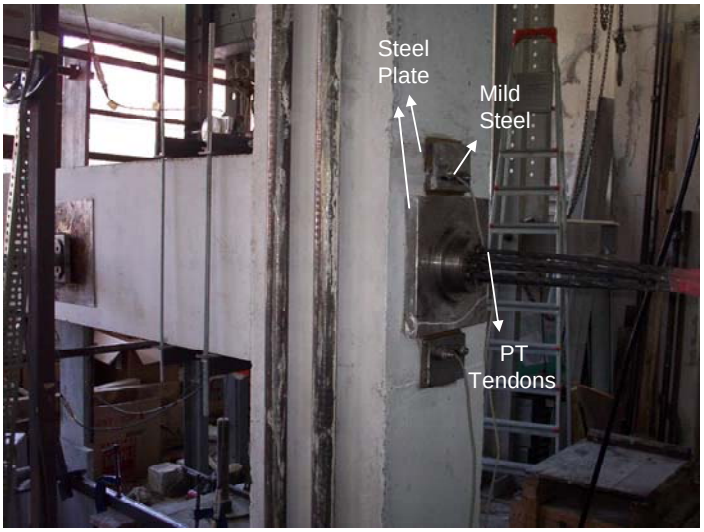

Figure 3.16. Assembled post-tensioned connection

The mild steel reinforcement and prestressing tendons content are illustrated in Figure 3.17 and the specific connection details for each connection were presented as follows:

- *PTM0:* The geometry and reinforcement detailing of PTM0 was a slightly different from the other post-tensioned specimens as illustrated in Figure 3.18. It did not have

reservation channels at the top and the bottom of the beam since no mild steel at the connection region was used. The dimension of the precast beam was the same as the monolithic subassembly. 6 x 13 mm prestressing strands were located at the mid-depth of the beam. The effective post tensioning force level was approximately 40 per cent of the ultimate strength of the strands according to the recommendation given in ACI T1.2-03 [49] document and this force resulted in a 3 MPa normal stress at beam-column interface. Additionally, 2 ϕ20 rebars were placed at the top and bottom of the beam body for flexural reinforcement of the precast beam as main rebars. The compressive strength of the precast elements was 60 MPa.

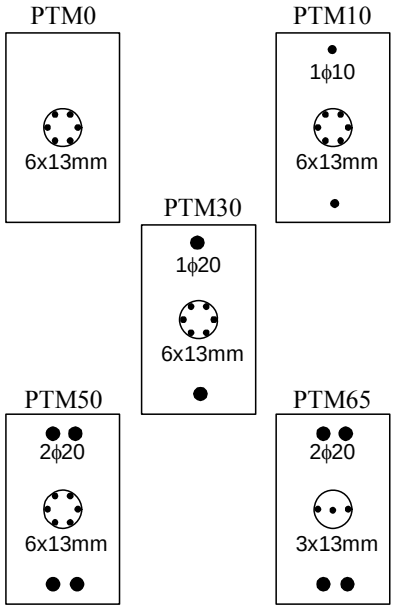

Figure 3.17. Reinforcement content and orientation of Phase II specimens

- *PTM10:* In this specimen detailing, the contribution of mild steel to the flexural moment capacity was kept at 10 per cent. There was one ϕ10 mild steel inserted at the top and the bottom of the connection with a 50 mm unbonded length. The cover thickness for this rebar was 65 mm. Post-tensioning was applied by using 6 x 13 mm tendons and 3 MPa normal stress was created on the beam-column interface. The compressive strength of the concrete in precast members was 67 MPa.

- *PTM30:* The post-tensioning force created by the prestressing strands was the same as PTM0 and PTM10 in this specimen. In order to increase the contribution of mild steel to the flexural capacity of the connection, one ϕ20 rebar was located on the top and the bottom of the crossection through the steel boxes. The cover thickness was 62 mm and the unbonded length of the mild steel at the connection region was 80 mm. The concrete compressive strength of the precast members was measured as 52 MPa.
- *PTM50:* 2 ϕ20 rebars were located to the top and the bottom of the beam crossection to increase the contribution of mild steel to the flexural strength of connection up to 50 per cent. The post-tensioning level in PTM50 was the same as previous specimens. The unbonded length of the mild steel was 80 mm and the compressive strength of concrete was 52 MPa. The cover thickness of the mild steel was around 60 mm.
- *PTM65:* 2 ϕ20 rebars with 80 mm unbonded length were installed in the connection as in specimen PTM50. In contrary 3 x 13 mm strands were placed at mid-depth of the beam and the post-tensioning force was around 40 per cent of ultimate strength of tendons and resulted 1.5 MPa normal stress on the beam- column interface. The cover thickness for the mild steel was 66 mm and the concrete compressive strength for the precast members was measured as 43 MPa

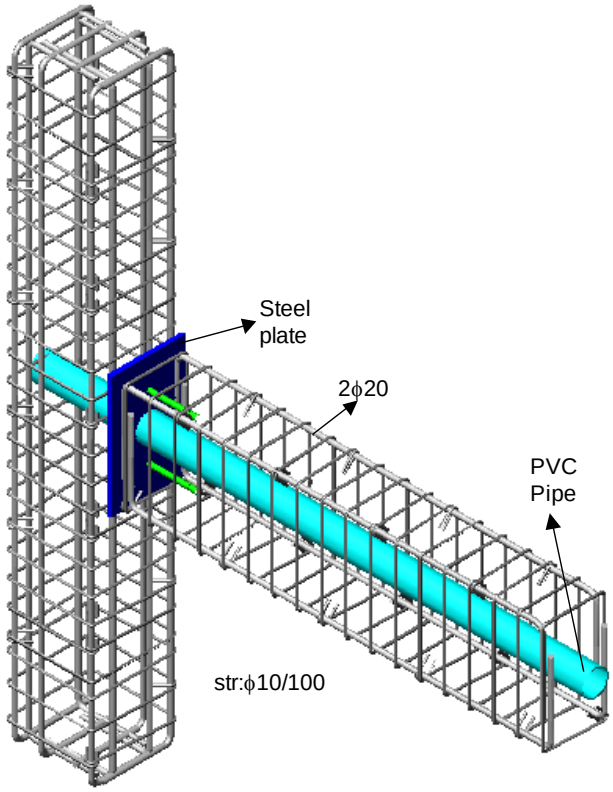

Figure 3.18. Reinforcement and connection details of PTM0

4. TEST RESULTS

4.1. Monolithic Specimen (M)

The response of specimen M was nearly elastic during the first two successive cycles. At 0.25 per cent story drift level, minor flexural cracks were observed on the beam located at a distance of 25 cm from the column face. At 0.75 per cent story drift level, first hairline diagonal crack was observed on the column at the beam-column joint core. The first diagonal cracking in the beam was observed at the 1.40 per cent story drift level and the crack distribution at 1.75 per cent which was approximately design level can be seen in Figure 4.1. The spalling of concrete at the beam joining end started at 3.50 per cent level as shown in Figure 4.2 and the beam top flexural rebars were buckled at 4.00 per cent story drift level. The cracks were well distributed over the beam end region. The lateral load vs. story drift response of specimen M is presented in Figure 4.3. Also, moment vs. curvature and moment vs. rotation relations were presented in Figure 4.4 and Figure 4.5 respectively. Behavior of the monolithic specimen was good in terms of ductility and energy dissipation. No pinching effect was observed on the reversed cyclic response and there was no significant strength degradation until the 4.00 per cent story drift level. The ultimate lateral load capacities of the specimen for forward and backward cycles were 114 kN and -149 kN respectively.

4.2. Cast in Place in Column Connection (CIPC)

First flexural crack in specimen CIPC was observed at 0.25 per cent story drift level at the beam column interface. No diagonal cracking was observed at the joint core throughout the test because of the steel fiber concrete and most of the cracks were concentrated on the beam near the column face. The overall behavior of CIPC was very similar to that of monolithic specimen up to the 2.75 per cent story drift level. The yielding load level in both specimens was reached around at 1.00 per cent drift level. After that level, the strength degradation was more pronounced and accelerated as compared to the monolithic specimen M. Around 1.75 per cent story drift, cracks were well distributed over the precast beam as shown in Figure 4.6. The reason of that rapid degradation was due to

the crushing of concrete at the top and bottom of the beam crossection and due to the buckling of rebars. The reduction in the beam crossection due to the spalling of concrete resulted in sliding of precast beam relative to the precast column. This type of response was first observed at 2.20 per cent story drift level and rapidly increased up to 15 mm at 3.50 per cent drift level as illustrated in Figure 4.7. No bond problem was observed throughout the test. The maximum lateral load attained was 107 kN in forward and -111 kN in backward cycles. Plastic hinging took place on the beam near the column face. The load vs. story drift and moment vs. curvature responses were presented in Figure 4.8 and Figure 4.9 respectively.

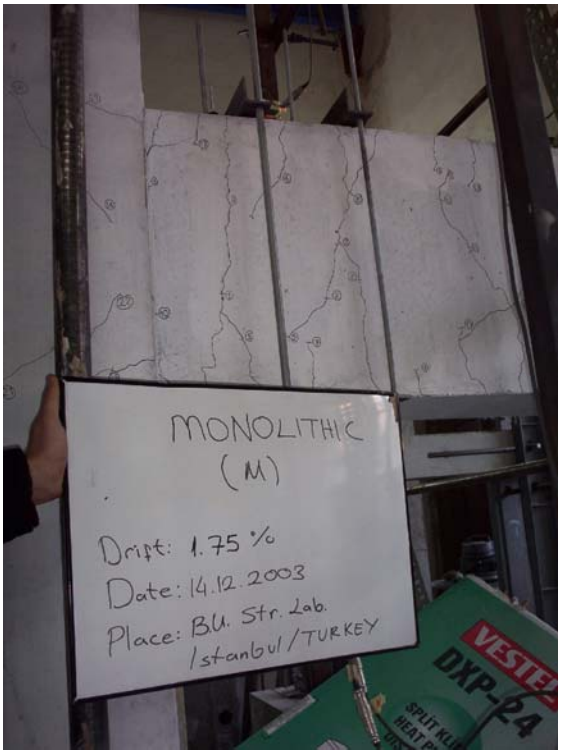

Figure 4.1. Crack distribution of specimen M at 1.75 per cent story drift

Figure 4.2. Crack distribution of specimen M at 3.50 per cent story drift

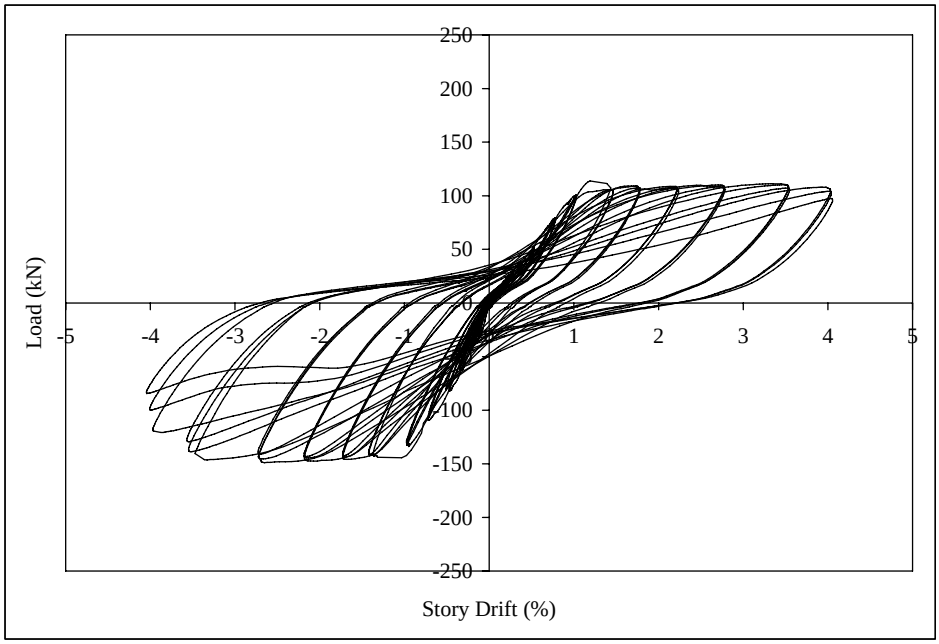

Figure 4.3. Load vs. story drift response of specimen M

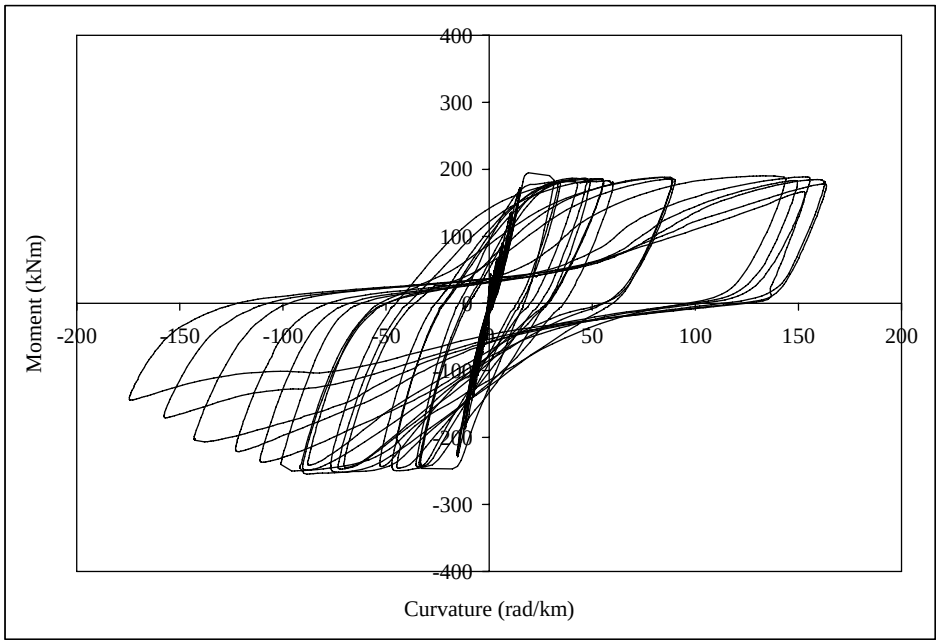

Figure 4.4. Moment vs. curvature response of specimen M

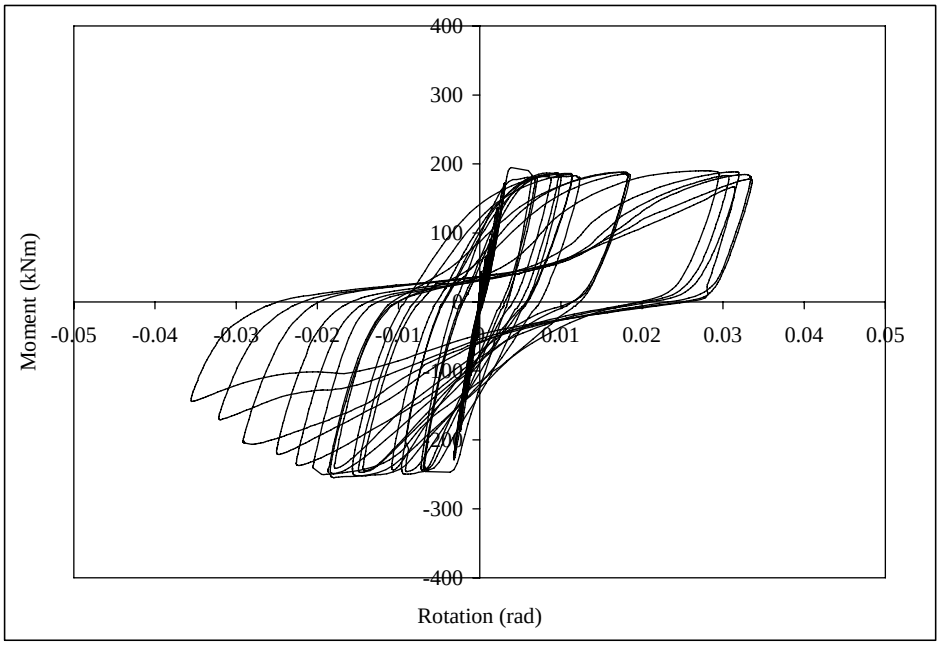

Figure 4.5. Moment vs. rotation response of specimen M

Figure 4.6. Crack distribution of specimen CIPC at 1.75 per cent story drift

Figure 4.7. Crack distribution of specimen CIPC at 3.50 per cent story drift

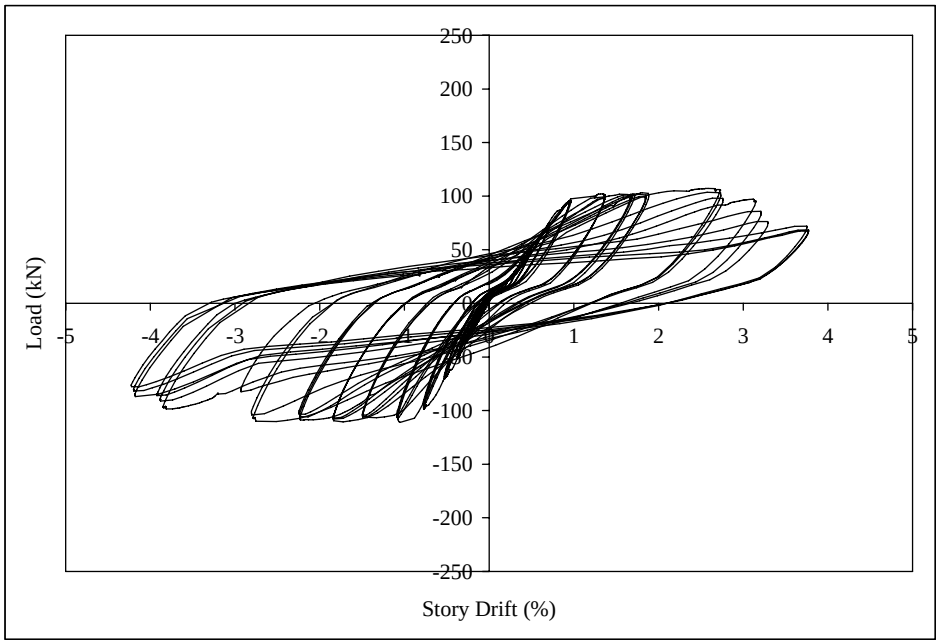

Figure 4.8. Load vs. story drift response of specimen CIPC

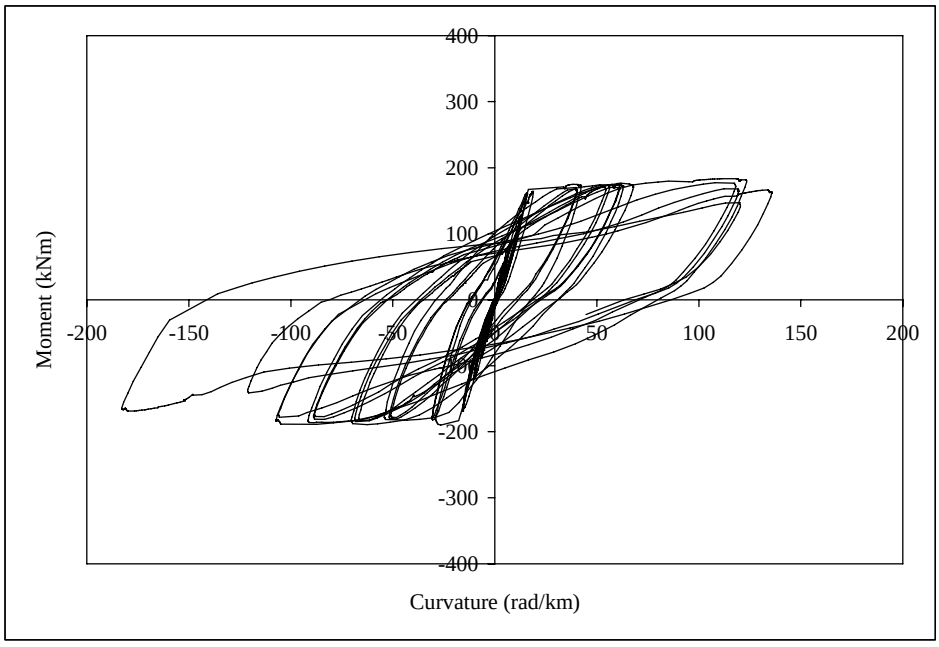

Figure 4.9. Moment vs. curvature response of specimen CIPC

4.3. Cast in Place in Beam Connection (CIPB)

The first visible cracks were observed along the cast-in-place concrete and the precast element interface both in beam and column at 0.25 per cent story drift level. Generally, the flexural cracks were concentrated at these two interfaces. The hairline diagonal crack at beam-column joint core was first observed at 1.75 per cent story drift as shown in Figure 4.10. When the story drift level reached 2.75 per cent, the gap opening between column face and the CIP interface reached approximately at 8 mm. Afterwards, the crack concentration relocated to the beam-to-CIP interface and widening of this crack accelerated at higher drifts leading to the failure of specimen. The CIP part that was 50 cm in length behaved like a linear link element that is presented in Figure 4.11 at 3.50 per cent story drift level throughout the successive load cycles. The lateral load vs. story drift response of specimen CIPB is shown in Figure 4.12 and it was very similar to specimen M. No pinching effect was observed throughout the reversed cyclic response of specimen CIPB. The recorded maximum lateral load was 142 kN and -151 kN for forward and backward cycles respectively. Furthermore, Figure 4.13 illustrated moment-curvature relation under cyclic loading.

Figure 4.10. Crack distribution of specimen CIPB at 1.75 per cent story drift

Figure 4.11. Crack distribution of specimen CIPB at 3.50 per cent story drift

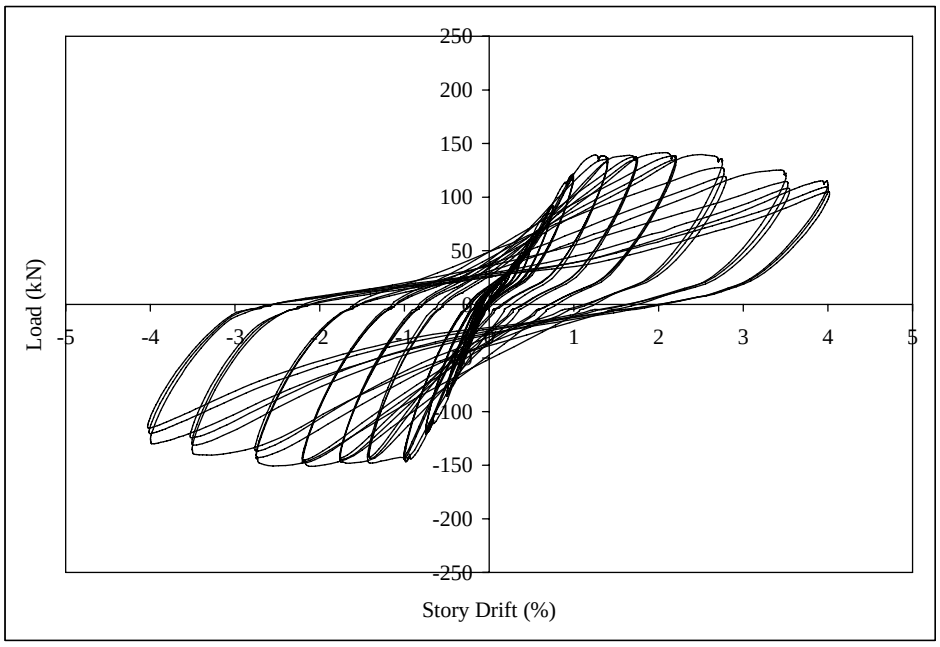

Figure 4.12. Load vs. story drift response of specimen CIPB

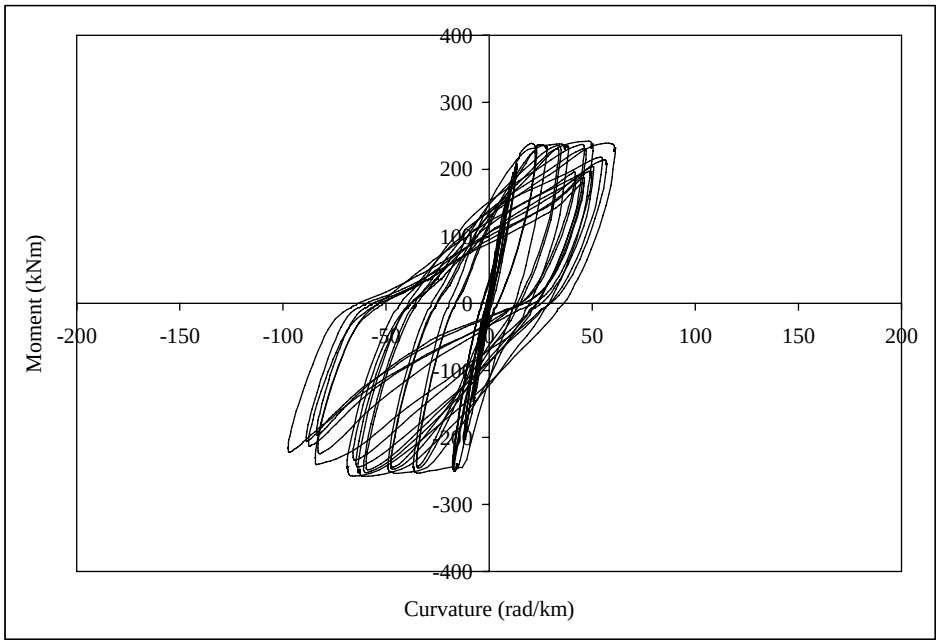

Figure 4.13. Moment vs. curvature response of specimen CIPB

4.4. Composite Connection (GOK-W)

During the assembly process, the cast in steel plates of corbel and beam were welded to each other in order to secure the continuity of the beam bottom reinforcement. It was observed that, the bond of approaching reinforcing bars in the vicinity of the weld location was damaged resulting hairline cracks parallel to bar axes. The first flexural crack on the beam was observed at the 0.50 per cent story drift level located 25 cm away from the precast column. This distance corresponds to the tip of the precast corbel. Flexural cracks on the beam were distributed evenly. At the 1.40 per cent story drift level, a diagonal crack was observed at the corbel-column region and Figure 4.14 presents the crack distribution at 1.75 per cent story drift. Moreover, the diagonal cracking at beam-column joint core was first observed at 2.20 per cent story drift. The failure of specimen GOK-W occurred suddenly with the rupture of beam bottom reinforcement at 3.50 per cent story drift level. The damage level at 2.75 per cent story drift that was prior to failure was illustrated in Figure 4.15. Figure 4.16 and Figure 4.17 shows the lateral load versus story drift and moment-curvature response of GOK-W sub-assembly. The ductility of the specimen GOK-W was smaller than that of the previous test specimens. The early rupture of rebars may well be explained with the changing mechanical properties of the material due to the

welding done during the preparation of steel cages prior to molding. The ultimate load was 226 kN for forward and -209 kN for backward cycles.

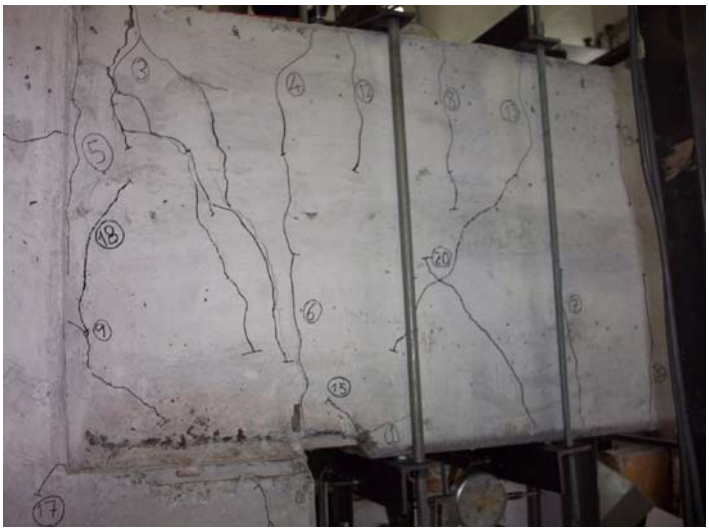

Figure 4.14. Crack distribution of specimen CIPB at 1.75 per cent story drift

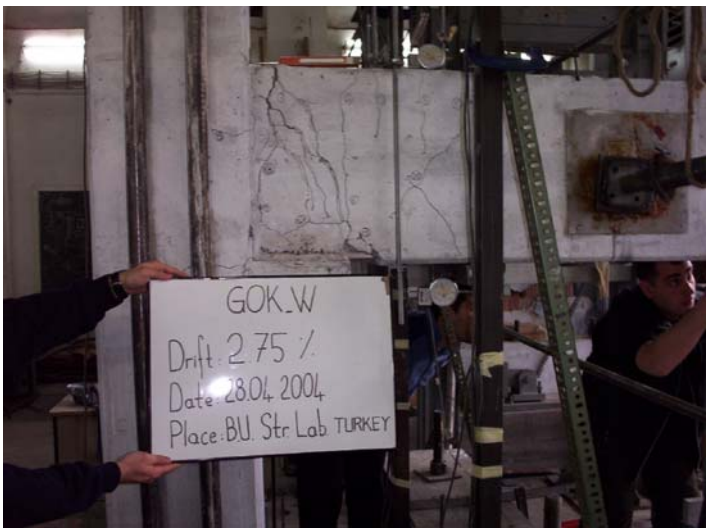

Figure 4.15. Crack distribution of specimen GOK-W at 2.75 per cent story drift

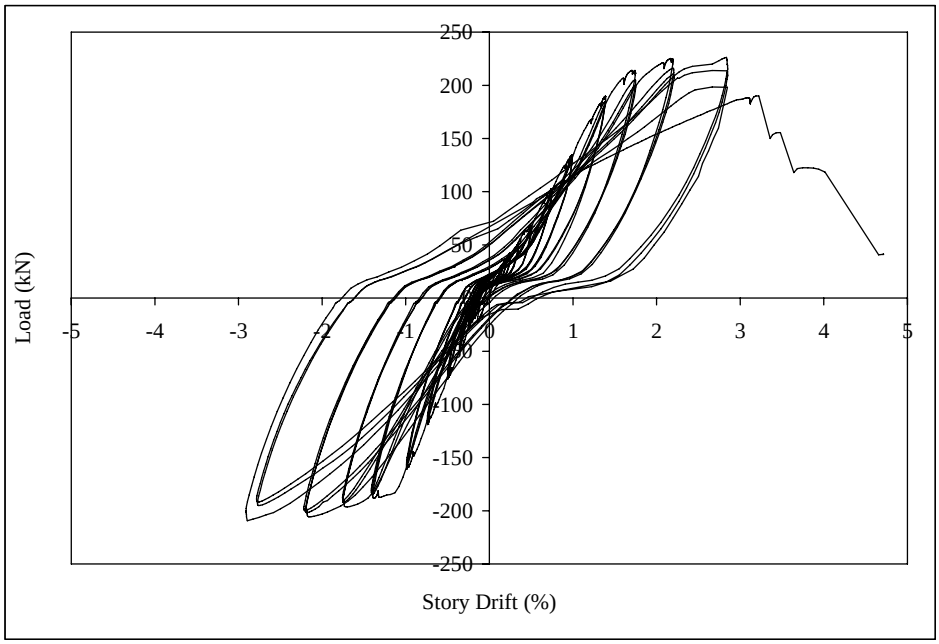

Figure 4.16. Load vs. story drift response of specimen GOK-W

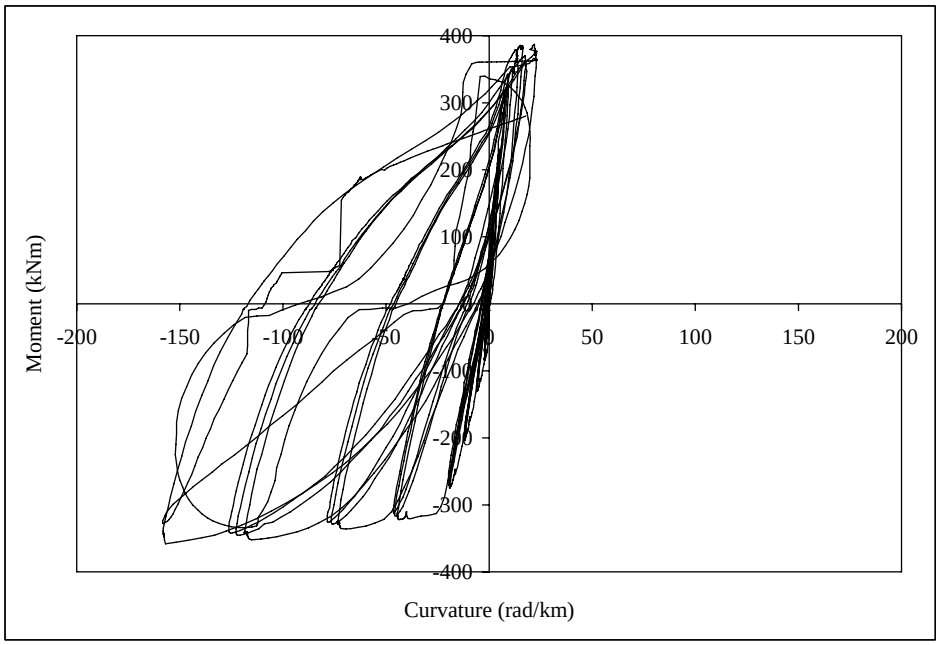

Figure 4.17. Moment vs. curvature response of specimen GOK-W

4.5. Bolted Connection (specimen B and specimen Mod-B)

The cyclic response of bolted connection (B) was unsatisfactory as shown in Figure 4.18. Although the flexural cracks at the beam-column interface were first observed at the 0.50 per cent story drift level, the sliding of steel box relative to the precast beam was accelerated beyond this level. Therefore, the bolts could not be forced up to their yielding load level. The deficiencies of specimen B were highlighted during and after the test, hence specimen Mod-B was designed and constructed. During the test of specimen Mod-B, no relative slip between the steel boxes and the beam concrete was observed. The flexural cracks were concentrated to the beam-column interface and there were no observation for diagonal crack at the joint core as shown in Figure 4.19 and Figure 4.20. Steel plates at the face of the beam prevented the crushing of concrete at lower drift levels. At 3.50 per cent story drift level, top bolts were ruptured and the experiment was terminated. The behavior of specimen Mod-B may well be considered as satisfactory and the response of the specimen is presented in Figure 4.21 and Figure 4.22. The overall performance of the Mod-B connection was better than that of monolithic and the other type of connections. Due to the pre-tensioning applied to the bolts, initial stiffness was greater in specimen Mod-B and the bolts were yielded at smaller drift levels as compared to the other subassemblies. Mod-B connection behaved similar to a friction damper. On the other hand, at higher story drift levels, sliding were observed between the precast beam and the column. The maximum recorded lateral load was 110 kN and -116 kN during the last forward and backward cycles.

4.6. Post-Tensioned Specimens

Post-tensioned connections had predetermined crack location at the beam-column interface because of the imposed cold joint. During the load cycles, a predetermined crack opening/closing type of response was observed at the connection region and minor cracks were observed on the precast beams and columns. Specimens PTM0, PTM10 and PTM30 behaved as self-centering systems while the behavior of PTM50 and PTM65 approached the response of monolithic subassembly.

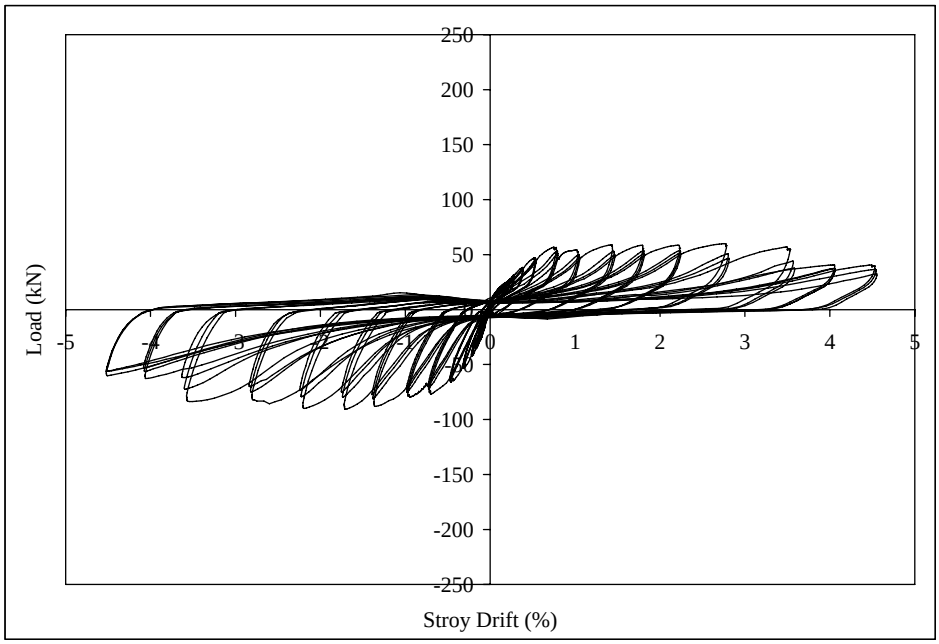

Figure 4.18. Load vs. story drift response of specimen B

Figure 4.19. Crack distribution of specimen Mod-B at 1.75 per cent story drift

Figure 4.20. Crack distribution of specimen Mod-B at 3.50 per cent story drift

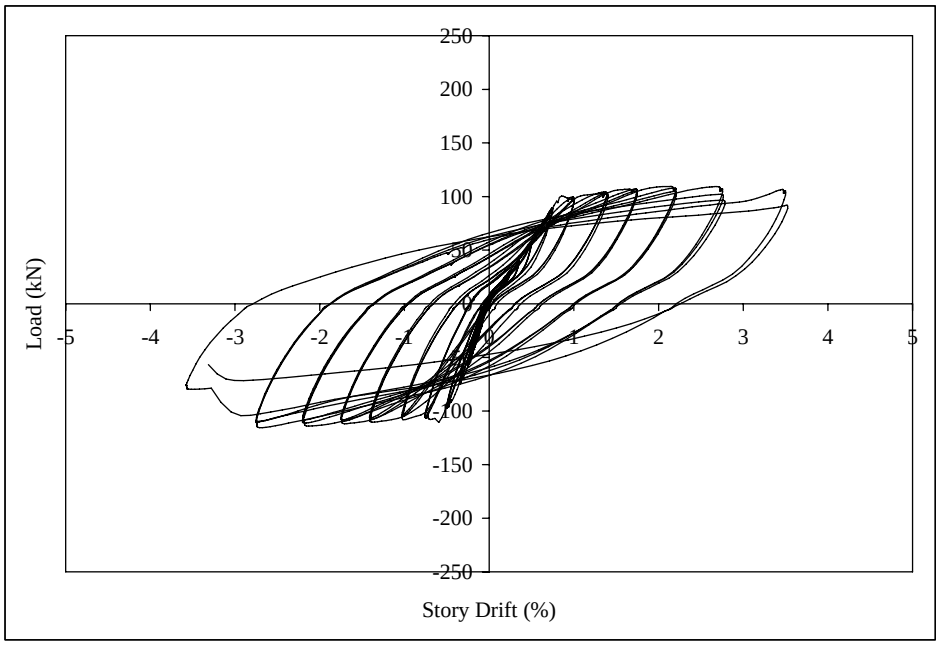

Figure 4.21. Load vs. story drift response of specimen Mod-B

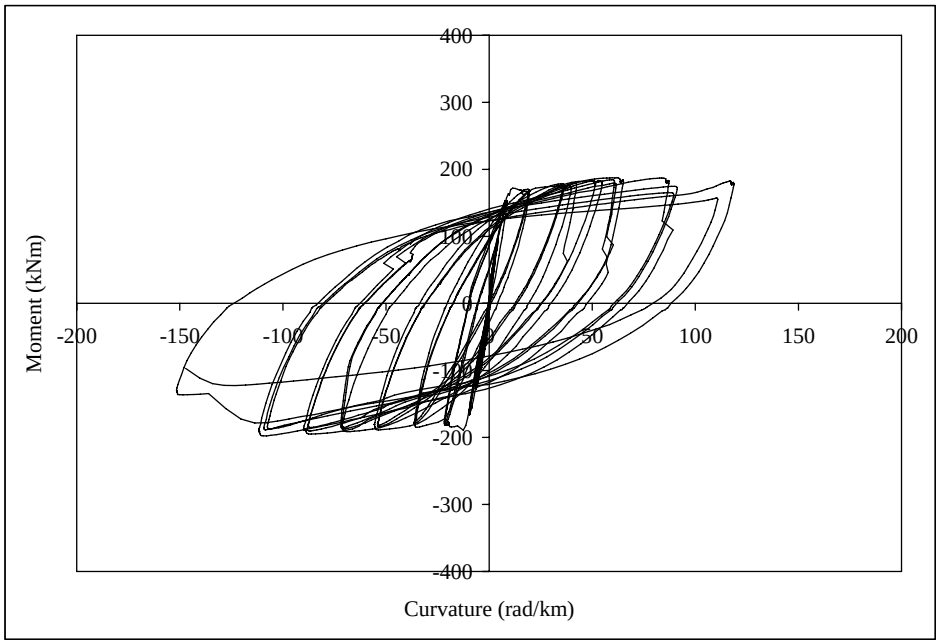

Figure 4.22. Moment vs. curvature response of specimen Mod-B

4.6.1. Post-Tensioned Specimen-No Mild Steel Effect (PTM0)

No flexural or diagonal cracks were observed until 0.35 per cent story drift cycle. At this level, a hairline crack was initiated at the beam-column interface and this crack widened at increasing story drift levels. No cracking or crushing was observed at the precast elements. At the end of the test, there were no visible cracks and no residual displacement at the subassembly. In order to compare damage level of post-tensioned specimens with other classical connection types, some photos were presented in the following figures. Figure 4.23 and Figure 4.24 shows the damage level at 1.75 per cent and 3.50 per cent story drift respectively. The behavior of specimen PTM0 was like a bilinear spring as shown in Figure 4.25. The maximum lateral load was 92 kN for forward and -89 kN for backward cycles. Also, the average maximum stress on the strands was measured as 65 per cent of the ultimate capacity throughout the loading history. The behavior of post-tensioned specimens is different from the monolithic system due to the pre-cracked section therefore moment-rotation behavior is illustrated in Figure 4.26 instead of moment-curvature relation.

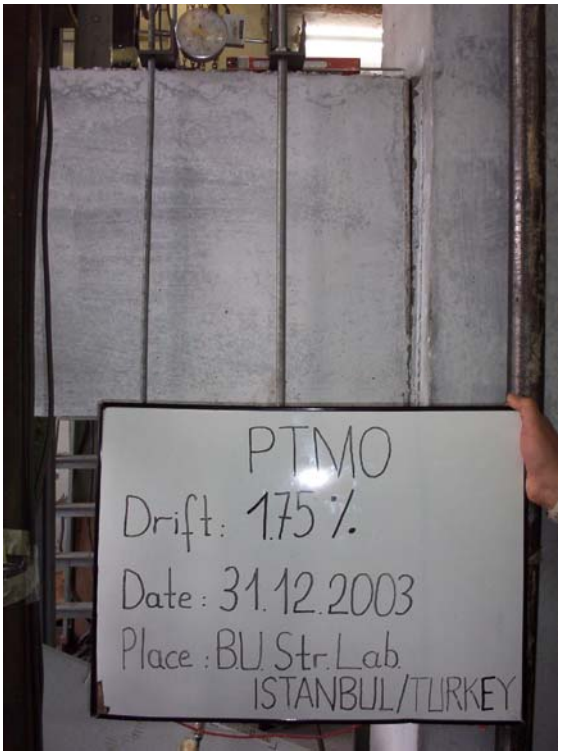

Figure 4.23. Damage level of specimen PTM0 at 1.75 per cent story drift

4.6.2. Post-Tensioned Specimen-10 per cent Mild Steel Effect (PTM10)

The first visible crack was observed at 0.25 per cent story drift level at the beam-column interface. At 0.75 per cent story drift, a flexural crack was observed near the reservation channel and the mild steel at the connection was yielded according to the strain gage readings. The ϕ10 mild steel rebars at the connection were ruptured at 2.20 per cent story drift cycle due to the insufficient unbonded length. There was not any indication on the bond deterioration around ϕ10 steel bars at the end of the test. After the rupture of mild steel, the specimen behaved like PTM0. No significant damage observed at the precast members as shown in Figure 4.27 and Figure 4.28. The effect of small amount of mild steel content was minor for the overall hysteretic behavior as presented in Figure 4.29 and Figure 4.30. The maximum load for the forward and backward cycles were 97 kN and -101 kN and the maximum average stress on prestressing tendons was 68 per cent of the ultimate capacity. The residual displacement at the end of the test was less than 1 mm.

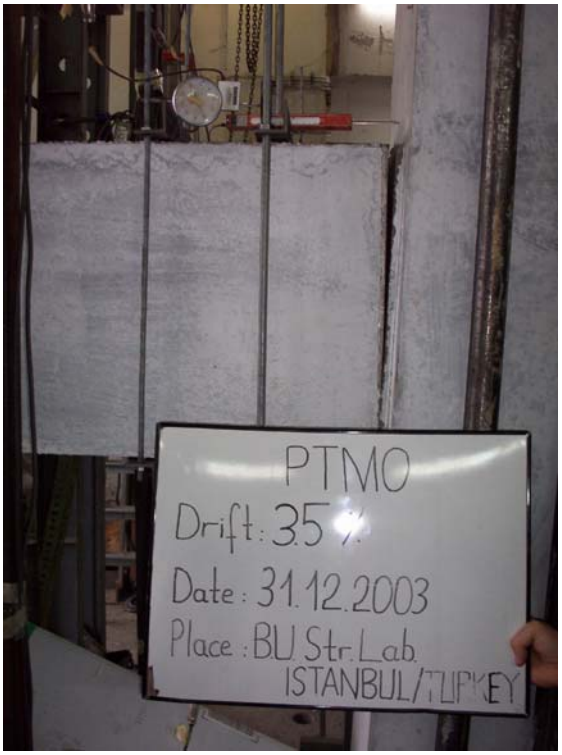

Figure 4.24. Damage level of specimen PTM0 at 3.50 per cent story drift

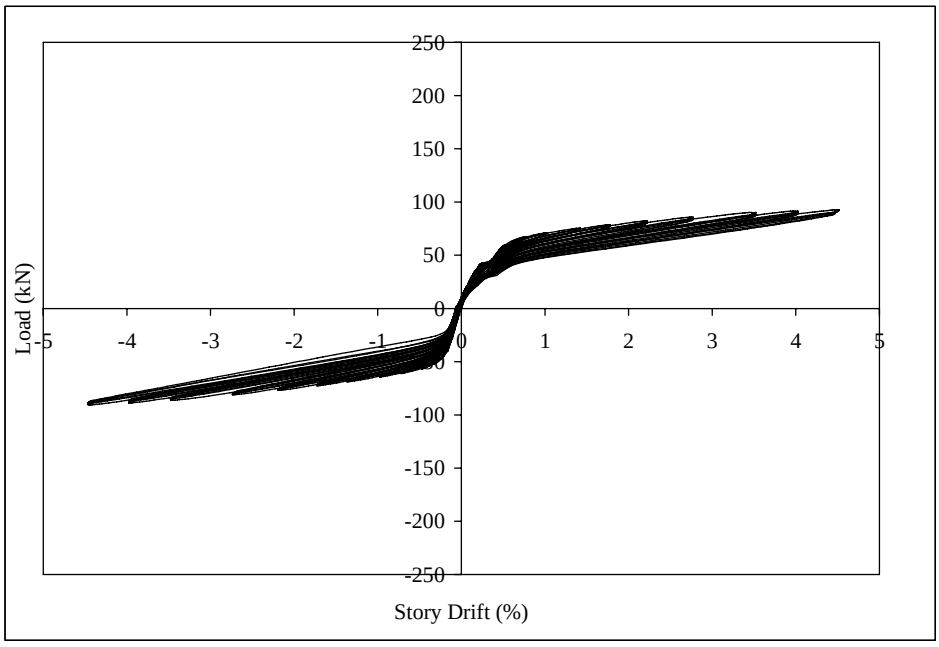

Figure 4.25. Load vs. story drift response of specimen PTM0

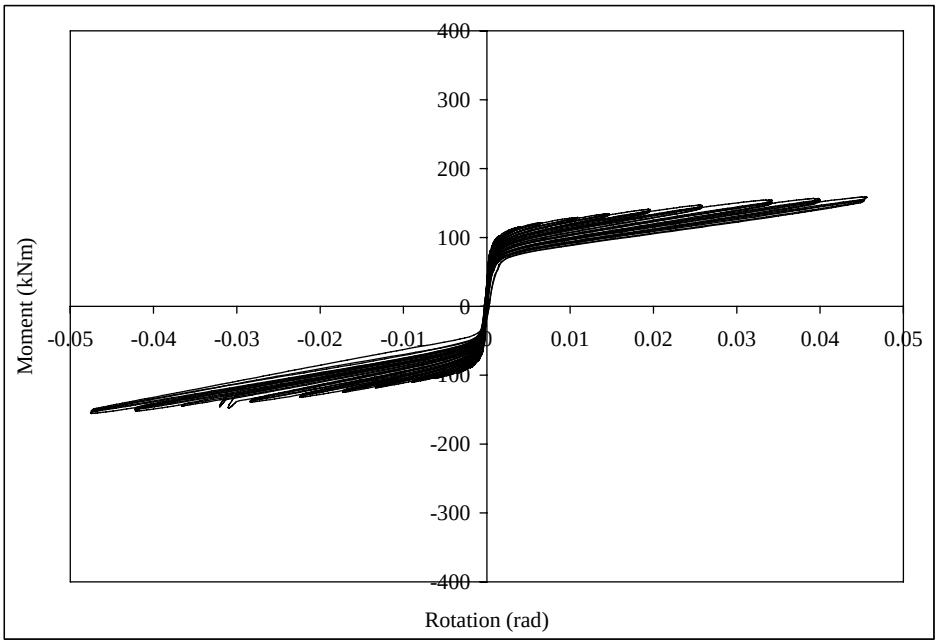

Figure 4.26. Moment vs. rotation response of specimen PTM0

Figure 4.27. Damage level of specimen PTM10 at 1.75 per cent story drift

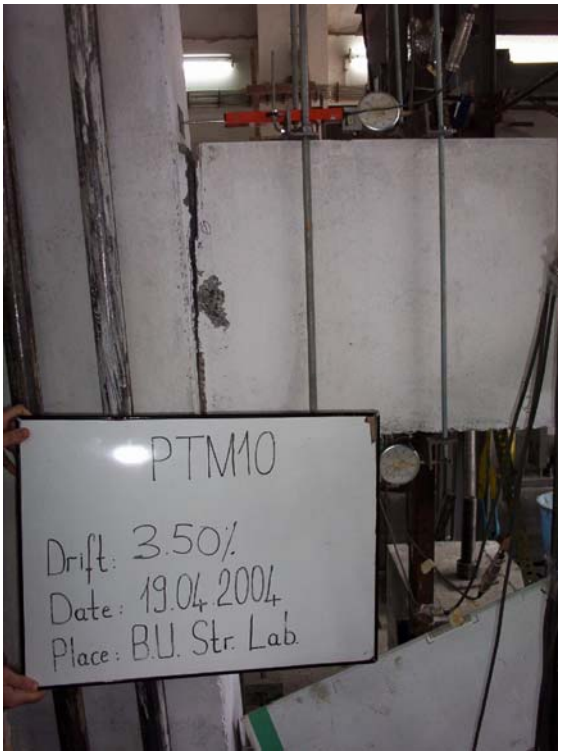

Figure 4.28. Damage level of specimen PTM10 at 3.50 per cent story drift

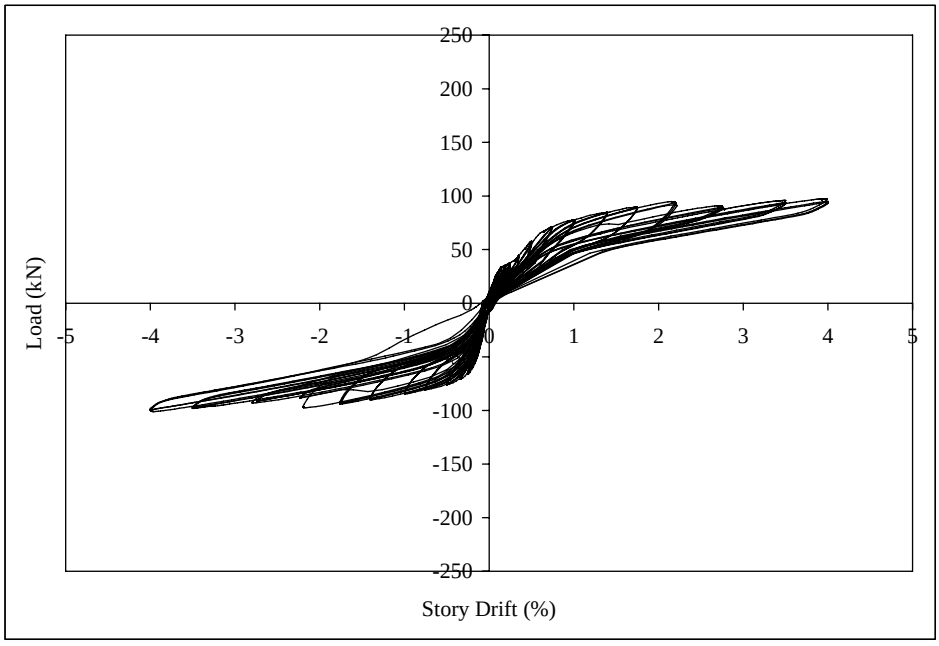

Figure 4.29. Load vs. story drift response of specimen PTM10

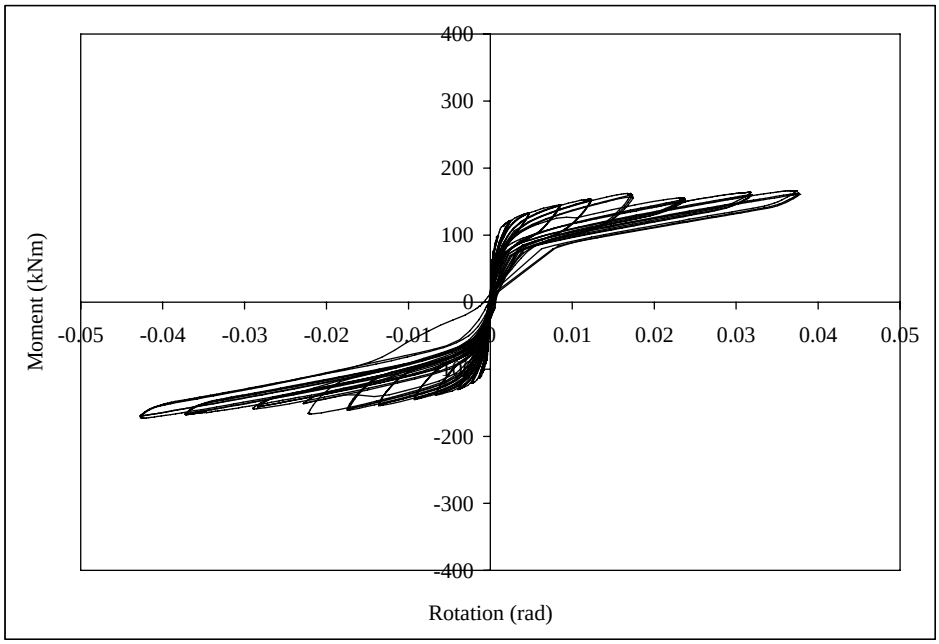

Figure 4.30. Moment vs. rotation response of specimen PTM10

4.6.3. Post-Tensioned Specimen-30 per cent Mild Steel Effect (PTM30)

A minor flexural crack on the beam was observed around 50 cm away from the column face at 0.75 per cent story drift level. Also, the damage levels and minor cracks can be seen in Figure 4.31 and Figure 4.32 for 1.75 and 3.50 per cent story drift cycles respectively. When the flexural contribution of mild steel was increased, the load vs. story drift response of the test specimen was improved as shown in Figure 4.33. The effect of mild steel on the hysteretic loops at high drifts was dominant as shown in Figure 4.34, and the residual displacement was negligible. At 4.00 per cent story drift level, 7 mm permanent displacement at test subassembly was observed. The maximum lateral loads were 124 kN and -133 kN for forward and backward loadings respectively. The prestressing tendons were forced up to 63 per cent of their ultimate capacity indicating an elastic response.

Figure 4.31. Damage level of specimen PTM30 at 1.75 per cent story drift

4.6.4. Post-Tensioned Specimen-50 per cent Mild Steel Effect (PTM50)

Minor flexural cracks were observed at the mid length of the precast beam at 0.50 per cent story drift level. Mild steels were yielded at the 0.75 per cent drift cycle. The first diagonal crack at the joint core was observed at the 3.50 per cent story drift level. There were more flexural cracks at the precast beams than the first three post-tensioned specimens as presented in Figure 4.35 and Figure 4.36. The hysteretic behavior of PTM50 approached to the response of monolithic specimen as illustrated in Figure 4.37 and Figure 4.38. The maximum measured lateral load was 158 kN for the forward cycle and –174 kN for the backward cycle. The maximum average stress on the prestressing strands was 60 per cent of their ultimate value and the residual displacement at column was 35 mm. This permanent displacement was greater for minimum damage criteria despite this mild steel content was within the limits of ACI T1.2-03 [49] recommendations.

Figure 4.32. Damage level of specimen PTM30 at 3.50 per cent story drift

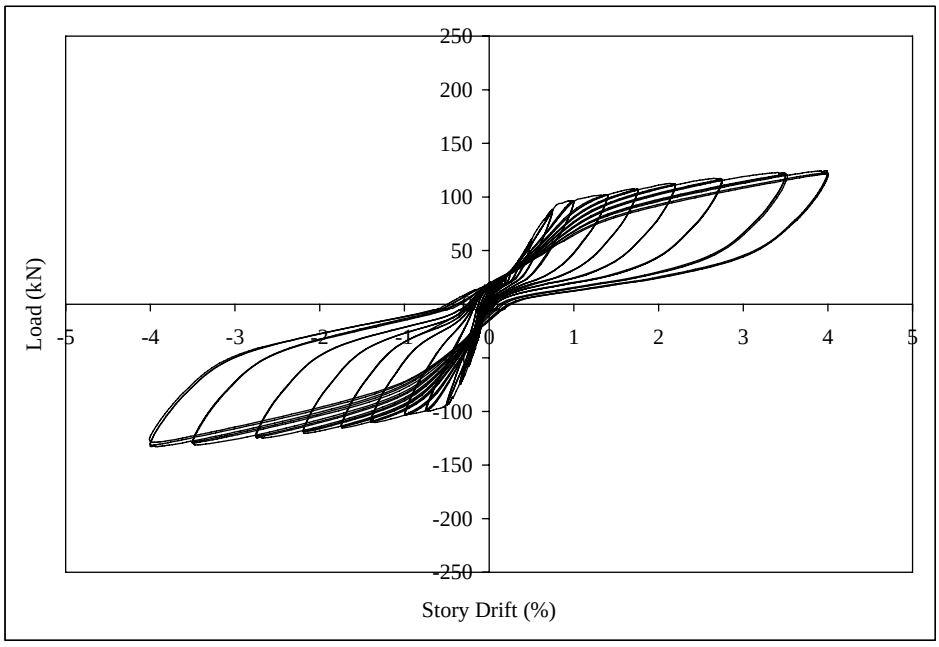

Figure 4.33. Load vs. story drift response of specimen PTM30

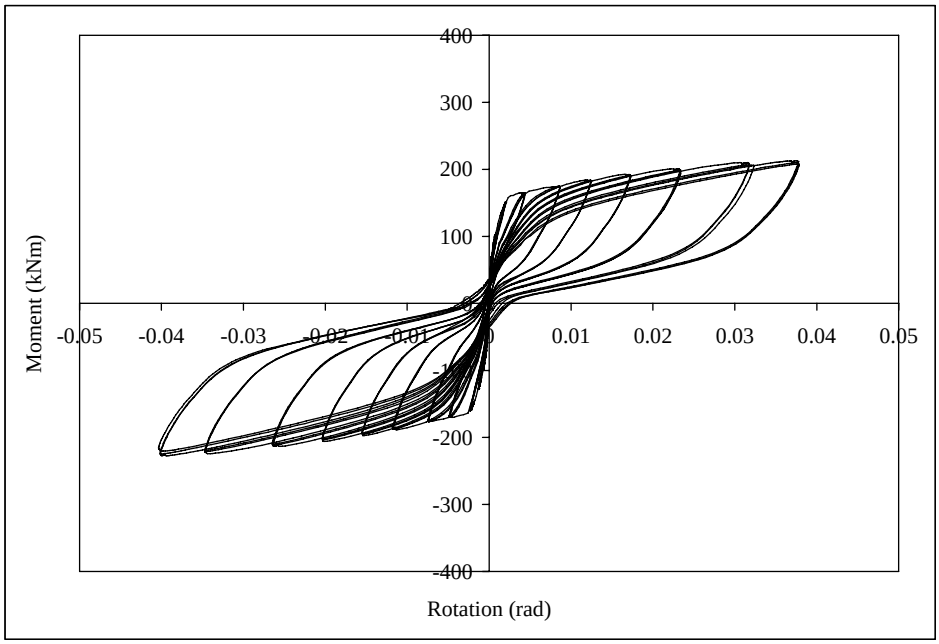

Figure 4.34. Moment vs. rotation response of specimen PTM30

Figure 4.35. Damage level of specimen PTM50 at 1.75 per cent story drift

Figure 4.36. Damage level of specimen PTM50 at 2.75 per cent story drift

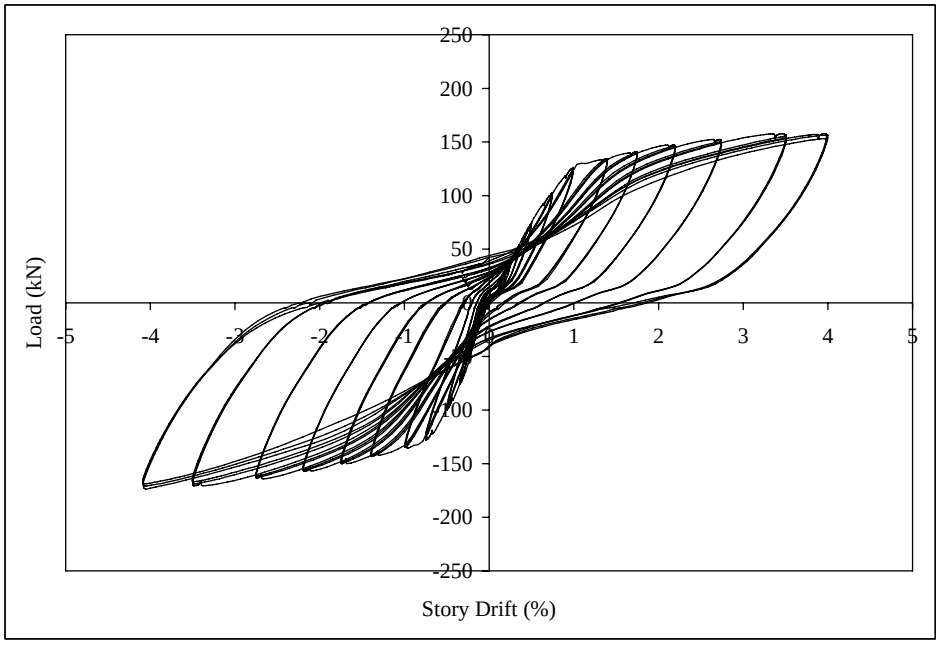

Figure 4.37. Load vs. story drift response of specimen PTM50

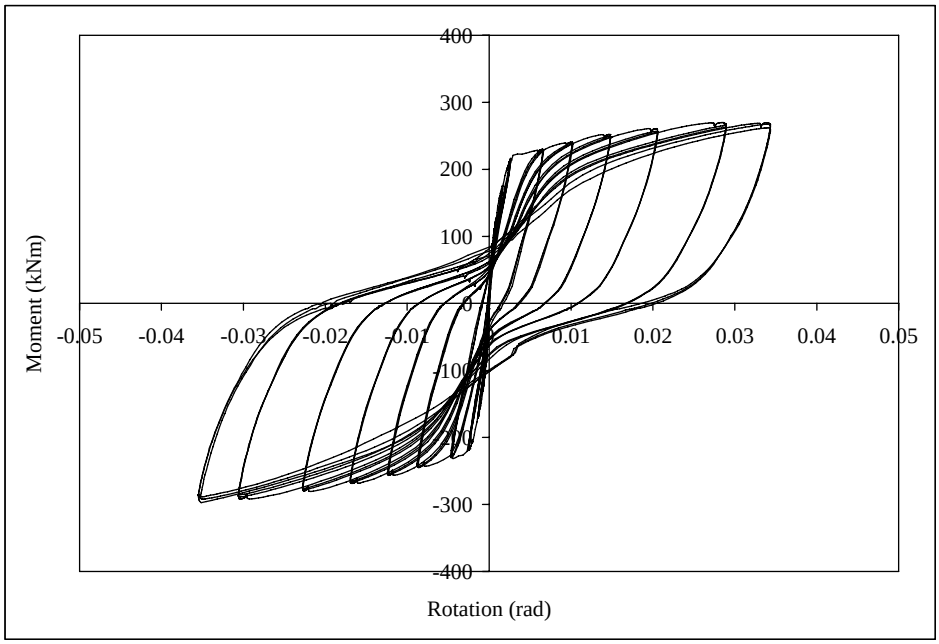

Figure 4.38. Moment vs. rotation response of specimen PTM50

4.6.5. Post-Tensioned Specimen-65 per cent Mild Steel Effect (PTM65)

A hairline crack appeared at the reservation channel location on the precast beam at 0.50 per cent story drift level. In addition to that, some flexural cracks were observed at these regions at higher drifts as shown in Figure 4.39 and Figure 4.40. Top mild steels at the connection were ruptured at the second and third cycles of the 4.00 per cent story drift level. The response of PTM65 was very similar to the monolithic specimen as shown in Figure 4.41 and Figure 4.42 due to the high content of mild steel. The permanent displacement at column was 50 mm and the measured maximum lateral load was 117 kN and –124 kN for forward and backward cycles respectively. The tendons were loaded up to 63 per cent of their ultimate strength at 4.00 per cent loading cycles.

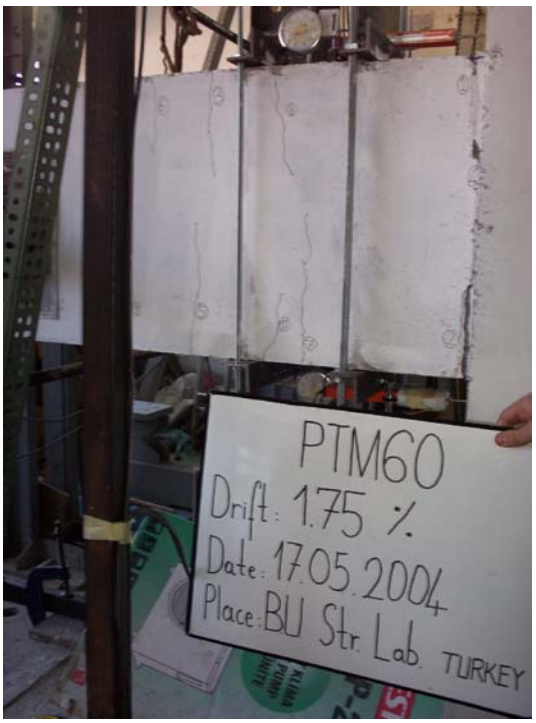

Figure 4.39. Damage level of specimen PTM65 at 1.75 per cent story drift

Figure 4.40. Damage level of specimen PTM65 at 3.50 per cent story drift

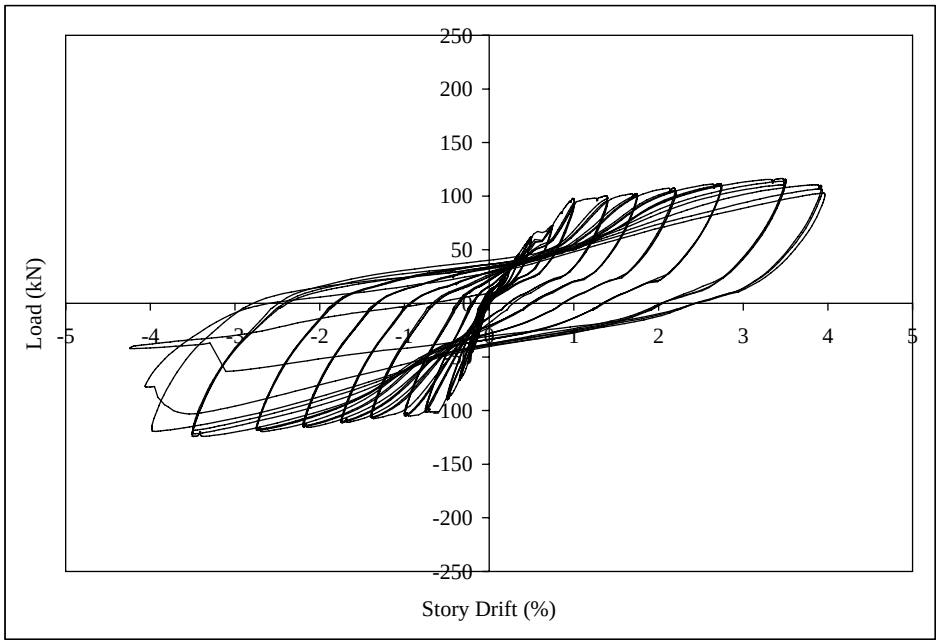

Figure 4.41. Load vs. story drift response of specimen PTM65

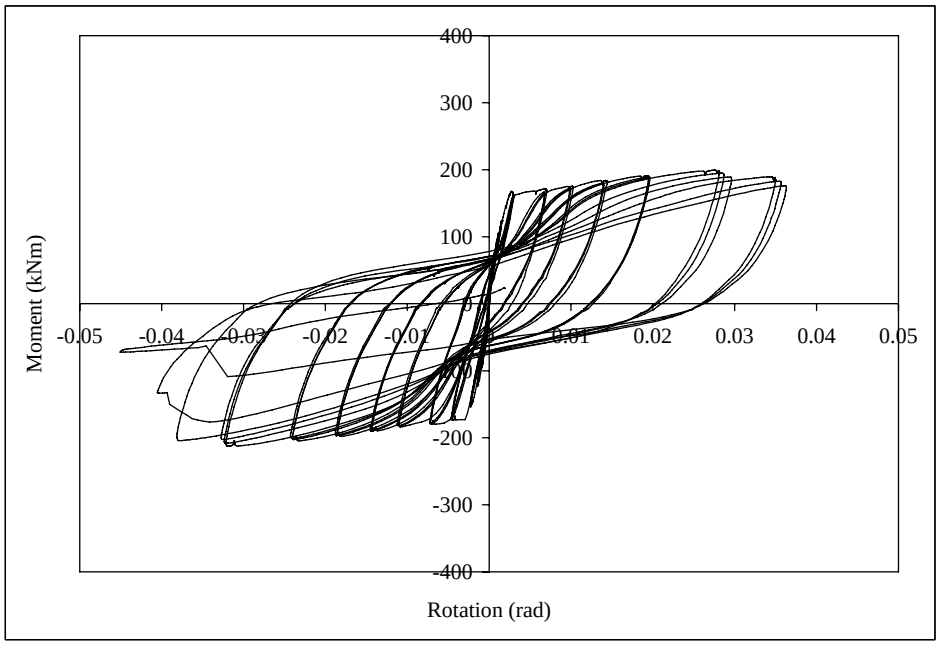

Figure 4.42. Moment vs. rotation response of specimen PTM65

5. EVALUTION OF TEST RESULTS

Monolithic, CIPC, CIPB, GOK-W and Mod-B test specimens were grouped as Phase I specimens and they were compared according to their strength predictions, ductility, stiffness degradation and energy dissipation properties. The discussion on specimen B is omitted due to its poor performance and also due to the existence of redesigned companion specimen Mod-B.

Post-tensioned specimens (PTM0, PTM10, PTM30, PTM50 and PTM65) were called as Phase II specimens. Experimental capacities of these test specimens were compared with the capacity predictions based on ACI T1.2-03 [49] design procedure. Besides, ductility, stiffness degradation, energy dissipation characteristics and residual displacements of the hybrid specimens were compared with that of the monolithic specimen like Phase I specimens.

5.1. Strength, Failure Modes and Ductility

Prior to testing, yield (M_{cal-y}) and ultimate (M_{cal-u}) moment capacities of each connection were calculated for the forward (+) and backward (-) cycles for Phase I specimens. The experimental results and predicted capacities are given in Table 5.1. The predictions are very important to define the connection performance in terms of flexural strength. When comparing the calculated yield moment and test result, yield moment calculation was observed a bit greater than testing in Phase I except Mod-B specimen. The reason of it can be explained with moment-shear (M-V) interaction that was defined in ASCE-ACI 445 committee report [50].

Most codes of practice use sectional methods for design of conventional beams under bending and shear. They assume that flexure and shear can be handled separately for the worst combination of flexure and shear at a given section. The interaction between flexure and shear is addressed indirectly by detailing rules for flexural reinforcement cutoff points. [50].

The shear stress that the crossection of a beam can resist is a function of the longitudinal straining in the crossection. The larger this longitudinal straining becomes, the smaller the shear stress required to fail. For design calculations, ε_x can be approximated as the strain in the tension chord of the equivalent truss as given Equation 5.1.

$$\varepsilon_x = \frac{(M_u / d_v) + 0.5N_u + 0.5V_u \cot\theta}{E_s A_s} \tag{5.1}$$

Where A_s = area of nonprestressed longitudinal reinforcement on the flexural tension side of the member; M_u = moment at the section, taken as positive; and N_u = axial load at the section, taken as positive if tensile and negative if compressive. The determination of ε_x for a nonprestressed beam is illustrated in Figure 5.1. The longitudinal strain parameter (ε_x) accounts for the influence of moment, axial load, and amount of longitudinal reinforcement on the shear strength of a section [50]. The inclination angles of shear cracks (cotθ) widely are affected from quantity of stirrups, concrete strength and level of shear stresses.

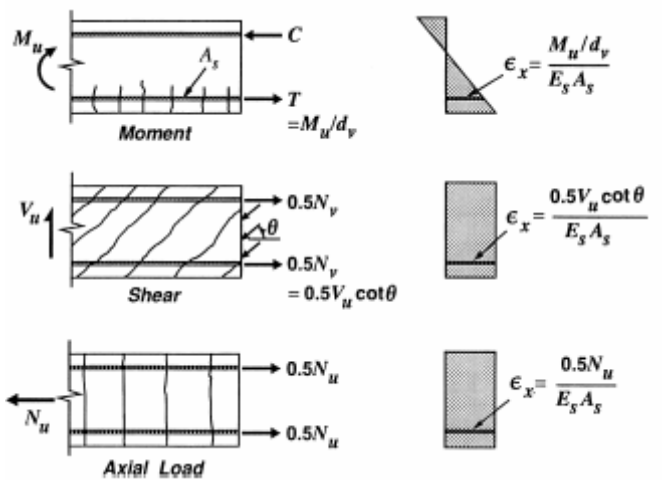

Figure 5.1. Determination of the strains in the tension cord [50]

Shear causes tensile stresses in the longitudinal reinforcement as well as in the stirrups. If a member contains an insufficient amount of longitudinal reinforcement, its shear strength may be limited by yielding of this reinforcement. Figure 5.2 illustrates the influence of shear on the tensile force required in the longitudinal reinforcement. Whereas the moment is zero at the simple support, there still needs to be considerable tension in the

longitudinal reinforcement near this support. The required tension, T, at a simple support can be determined from the free-body diagram as shown in Figure 5.2 [50].

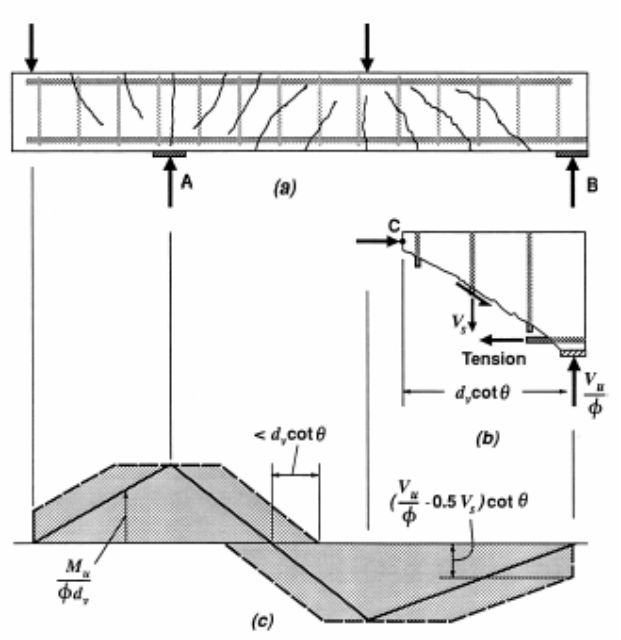

Figure 5.2. Influence of shear on tension in longitudinal reinforcement [50]

Although failure type of all connection was flexure, high shear forces were occurred at the connection due to low a/d ratio. When crack orientations were examined, shear cracks were observed for all test specimens except Mod-B specimen in Phase I. Under these circumstances, longitudinal reinforcement may be yielded earlier under lower flexural moments. Besides that, at high drift levels, bottom cover concrete of the beam spalled off and bottom flexural rebars were buckled. Therefore, the ratios of ultimate moment capacities to the predicted values were smaller. The capacity prediction for the backward cycle of specimen GOK-W was less than the experimentally measured value due to the existence of corbel, which serves as a haunched beam end. In addition, the yield capacities of specimen Mod-B were the same as the predicted values. Moreover, the ultimate capacity of the connection is five per cent grater than the expected. This may be due to the existence of steel plates located at the crossectional surface of the beam and due to the confining effect of closed stirrups located in the beam at the connection region.

Table 5.1. Capacity predictions and ductility ratios for Phase I specimens

Specimen		M	CIPC	CIPB	GOK-W	Mod-B
f_c'(MPa)	(1)	40	52	49	55	30
f_y (MPa)	(2)	472	472	472	503	472
f_u (MPa)	(3)	574	574	574	662	574
A_s (mm^2)	(4)	942	942	942	1570	942
A_s' (mm^2)	(5)	1256	942	942	942	942
M_y (kNm)	(6)	176/-243	168/-183	172/-178	309/-313	171/-180
M_u (kNm)	(7)	195/-255	183/-190	175/-186	326/-357	188/-199
μ	(8)	4+	4	4	2	5
M_{cal-y} (kNm)	(9)	188/-248	190/-190	188/-188	340/-262	173/-173
M_{cal-u} (kNm)	(10)	221/-279	221/-221	221/-221	379/-328	190/-190
(6)/(9)	(11)	0.94/0.98	0.88/0.96	0.91/0.95	0.91/1.19	0.99/1.04
(7)/(10)	(12)	0.88/0.91	0.83/0.86	0.79/0.84	0.86/1.09	0.99/1.05

Plastic moment capacities and ultimate stress values at prestressing tendons for each post-tensioned connection were calculated according to ACI T1.2-03 [49] at 4.00 per cent story drift level. True prediction of the gap opening in calculating the flexural strength of the connection is of prime importance. Therefore, coefficient of the effective additional debonded length (α_b) has to be chosen accordingly. Although this coefficient was proposed to be 5.5 by Cheok *et al.* [51], Raynor *et al.* [52] recommended a value of 2 for the same mild steel reinforcement. In the design of precast specimens of the current investigation, and their ultimate moment capacity calculations the α_b value was chosen as 3, and it was observed in experiments that α_b=3 yielded the best predictions for the Phase II specimens. Predicted capacities, test results and the experimental over calculated ratios are given in Table 5.2. Since the amount of top and bottom mild steel at the connection was equal within each specimen, calculated flexural strength (M_{cal}) and stress on the prestressing strands (f_{pt-cal}) were the same for the forward and backward cycle. The strength predictions are believed to be very important in defining the connection performance in terms of lateral load capacity. All tested connection types approached to nearly their calculated flexural yield and ultimate moment capacities. It is observed in Table 5.2 that experimental results

for the moment capacity were nearly the same as calculated values (M_{cal}). This reveals that, all connections had adequate capacities. Stress predictions on the prestressing strands (f_{pt-cal}) were very close to the test results for specimens PTM0, PTM10 and PTM30. On the other hand, the estimation of stress on tendons was greater than the measured values for PTM50 and PTM65. This may due to the changing behavior of the hybrid connection towards that of the monolithic subassembly with increasing mild steel content and resulting permanent displacements. The relation between the story drift angle and the gap opening angle measured on the beam-column interface is linear until the load point at which the beam body starts cracking. This relation is important for capacity calculations as defined by Cheok et al. [51].

Failure type and location of connections is important for seismic regions, therefore damages and failure modes are presented from Figure 5.3 to Figure 5.12. In these figures, photos are given before and after testing the specimens to visualize and compare the level of damage. In addition to that, design philosophy of post-tensioned specimens based on the damage level of connection according to ACI T1.02-03 document [49]. This means that after a major seismic event, that moment frame can be expected to exhibit minimal damage in beam-column regions and negligible permanent displacements [49].

Figure 5.3 presents the reference specimen crack propagations. The plastic hinges occurred at the end of the beam and cracks usually well distributed over the beam. At high story drifts, concrete cover was spalled of and longitudinal reinforcement was buckled. This means that the connection cannot be recovered again. Similar comments can be said for CIPC connection. Plastic hinging was occurred at the tip of precast beam as illustrated in Figure 5.4. There was no diagonal crack at the joint core because of the steel fiber reinforced concrete. On the other hand, failure was occurred at the precast beam and 50 cm away from the column face for CIPB connection as shown in Figure 5.5. Cast-in-place part was designed according to strong connection concept; therefore all damages were concentrated in these regions. Specimen GOK-W showed the highest damage level as compared to the monolithic specimen, as presented in Figure 5.6. Failure was occurred at the end of the corbel with rupture of bottom longitudinal reinforcement with flexure-shear failure.

Table 5.2. Capacity predictions and ductility ratios for Phase II specimens

Specimen		PTM0	PTM10	PTM30	PTM50	PTM65
f_c'(MPa)	(1)	60	67	52	52	43
f_y (MPa)	(2)	-	472	472	472	472
f_u (MPa)	(3)	-	574	574	574	574
A_s (mm^2)	(4)	-	78.5	314	628	628
A_s' (mm^2)	(5)	-	78.5	314	628	628
F_{pt} (kN)	(6)	450	450	450	450	225
M_c (kNm)	(7)	158/-152	166/-173	212/-228	271/-298	200/-212
f_{pt}/ f_{ptu} (%)	(8)	68/66	67/69	62/64	60/61	59/64
μ	(9)	5+	6+	6+	5+	5
M_{cal-c} (kNm)	(10)	164/-164	183/-183	228/-228	296/-296	223/-223
f_{pt-cal}/f_{ptu} (%)	(11)	66/66	66/66	65/65	64/64	68/68
(7)/(10)	(12)	0.96/0.93	0.91/0.95	0.93/1.00	0.92/1.00	0.90/0.95
(8)/(11)	(13)	1.03/1.00	1.02/1.05	0.95/0.98	0.94/0.95	0.87/0.94

The plastic hinging was occurred at the beam-column interface for Mod-B connection. All cracks were concentrated at the failure zone. No concrete crushing and buckling of rebars was observed. The test was stopped when longitudinal rebars were fractured. As shown in Figure 5.7, all damage located at the beam-column interface. Also, sliding of precast beam with respect to columns with yielding of mild steel was observed.

The damage level and the distribution in post-tensioned specimens were widely different than the other precast connections and the monolithic specimen. Generally, a few minor cracks were observed on the precast beam and column. Plastic hinging was concentrated at beam-column interface for all post-tensioned specimens.

Figure 5.3. Damage level of specimen M

Figure 5.4. Damage level of specimen CIPC

Figure 5.5. Damage level of specimen CIPB

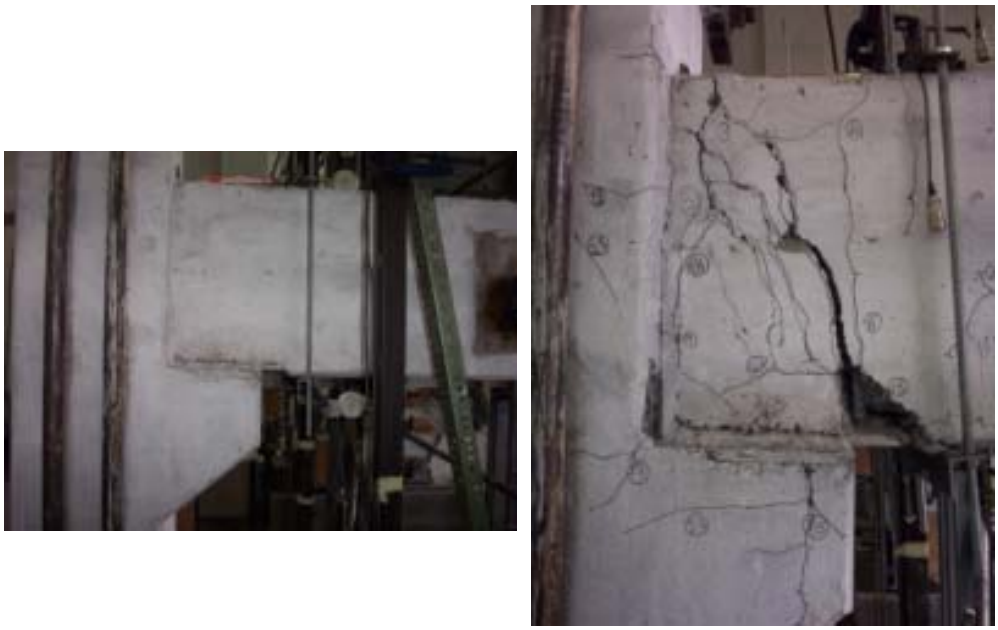

Figure 5.6. Damage level of specimen GOK-W

Figure 5.7. Damage level of specimen Mod-B

As presented in Figure 5.8, no diagonal or flexural cracks and sliding was observed at specimen PTM0. Also, no residual displacement at the beam-column connection was monitored. In addition to that, the damage performance of PTM10 was the same as PTM0 as illustrated in Figure 5.9. Although the mild steel reinforcement was ruptured in specimen PTM10, the effect of mild steel was negligible.

Figure 5.8. Damage level of specimen PTM0

Figure 5.9. Damage level of specimen PTM10

Damage level and crack distribution in specimen PTM30 was slightly different than the first two post-tensioned specimens as shown in Figure 5.10. Some minor flexural cracks were observed in the specimen under loading and these cracks closed when the loading was finished.

Figure 5.10. Damage level of specimen PTM30

Figure 5.11 and Figure 5.12 show crack patterns on specimens PTM50 and PTM65. More flexural cracks and connection damage was observed as compared the other post-tensioned specimens. Despite the response of specimens PTM50 and PTM65 was similar to that of the monolithic specimen, all damages could be repaired easily.

Figure 5.11. Damage level of specimen PTM50

Figure 5.12. Damage level of specimen PTM65

There are some regulations about precast moment resisting connections in the Turkish earthquake code. The first one, moment resisting connections shall be proven through analytical methods with appropriate references from the literature or tests that moment resisting connections of prefabricated building frames possess strength and

ductility that are equivalent to the monolithic behavior under cyclic and repeated loading due to earthquakes. The second one, connections shall possess sufficient strength to transfer moments, shear forces and axial forces to be developed at the ultimate strength level without any reduction in strength and ductility. The last one, connections must be arranged in sufficient distance from the potential plastic hinges that can develop within the elements connected [7]. Therefore, lateral load vs. story drift backbone curves of each connection with respect to monolithic specimen are presented the following figures. All backbone curves were normalized according to their yield load level, since the longitudinal reinforcement ratio at the connection is somewhat different in each specimen. Displacement ductility comparison is also illustrated. Displacement ductility factor was defined as the maximum deformation divided by the corresponding deformation when yielding takes place. The use of ductility factors permits the maximum deformations to be expressed in non-dimensional terms as indices of inelastic deformation for seismic design and analysis [53]. Yield displacement was calculated by using Figure 5.13 for Phase I specimens. At post-tensioned specimens except PTM0, yielding point is determined from strain gages that were installed on the mild steels. As shown in Figure 5.14 and Figure 5.15, the behavior of CIPC and CIPB connection is identical to the monolithic specimen M up to 2.75 per cent story drift. Therefore, the displacement ductility of these specimens was similar. The yield point of these three specimens was around 1.00 per cent story drift. On the other hand, GOK-W specimen had the lowest ductility value that was 2 as illustrated in Figure 5.16. The first reason of such a low ductility may be attributed early failure of GOK-W specimens at the forward cycle. The second is the yielding point of welded section, which was around 1.75 per cent story drift. Bolted connection showed the best performance among Phase I specimen. The overall behavior of Mod-B is very similar to the monolithic connection. The initial stiffness of Mod-B is greater than the conventional system as presented in Figure 5.17. Due to the pretension bolts, yielding point was around 0.50~0.75 per cent story drift, therefore ductility was around 5.

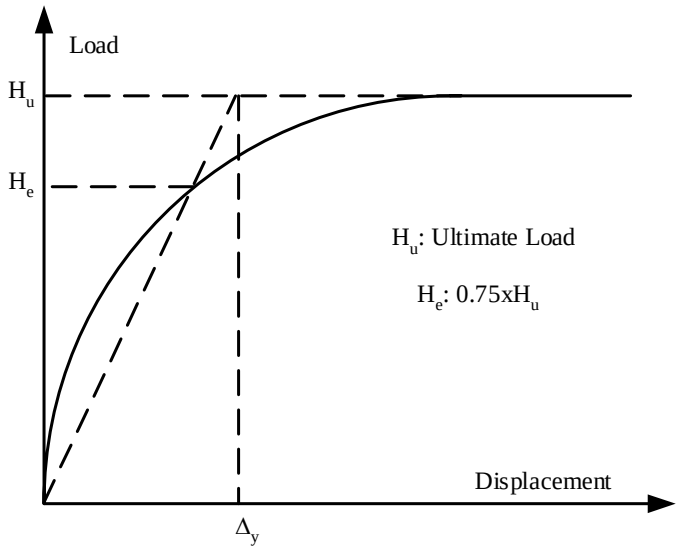

Figure 5.13. Definition of ductility [53]

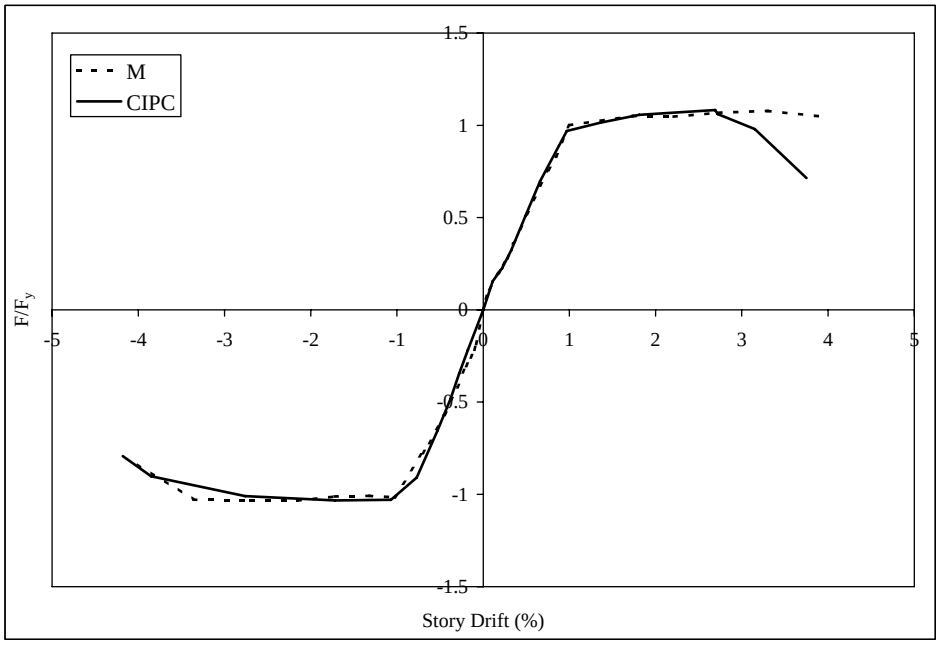

Figure 5.14. Backbone curve of specimen CIPC

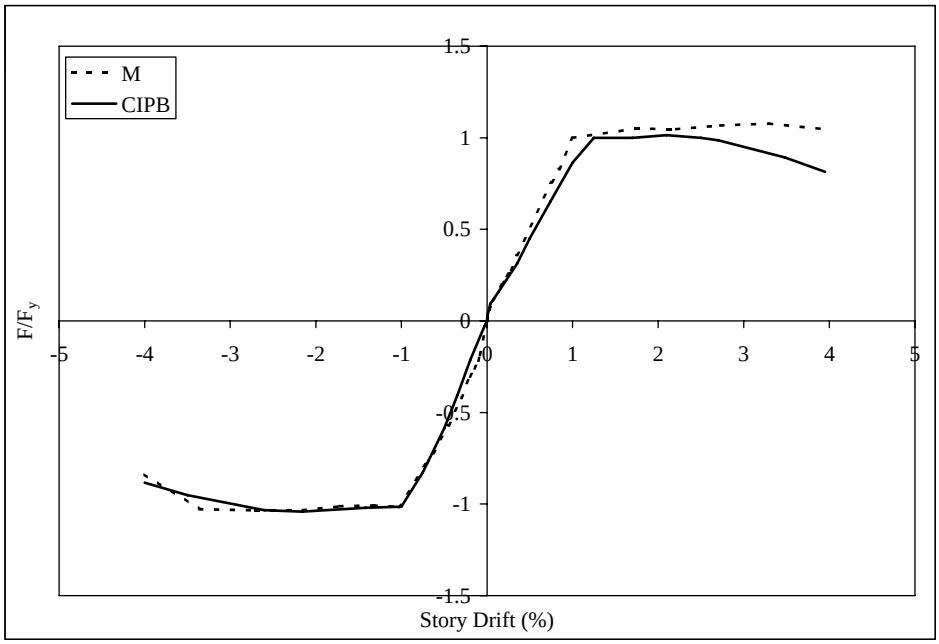

Figure 5.15. Backbone curve of specimen CIPB

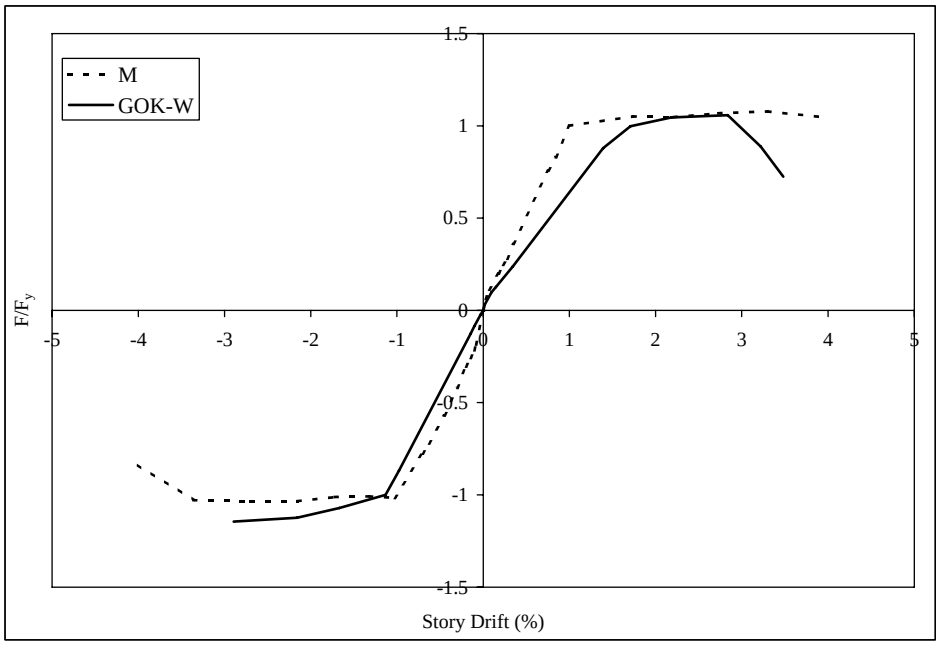

Figure 5.16. Backbone curve of specimen GOK-W

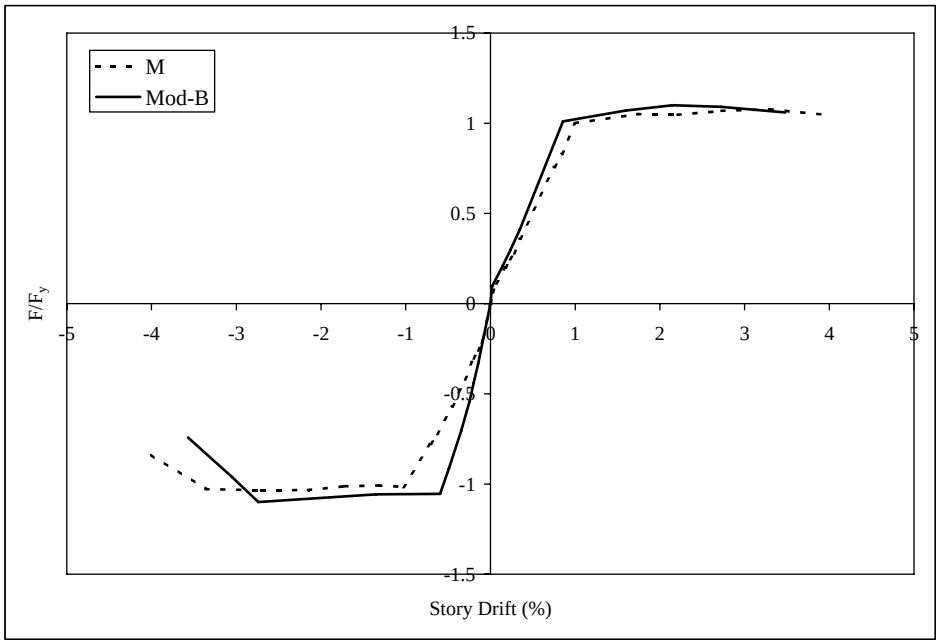

Figure 5.17. Backbone curve of specimen Mod-B

The behavior of post-tensioned specimens was different than the monolithic specimen depending on the level of contribution of prestressing tendon on flexure. As presented in Figure 5.18, the initial stiffness and ductility of PTM0 was greater than that of the reference specimen. Initial yield displacement was defined as significant changing point on the curve. As seen in Figure 5.19, the response of PTM10 was similar to the PTM0. This means that the effect of small amount mild steel was negligible. With increasing mild steel content in the connection, the behavior of post-tensioned connection approached the conventional monolithic specimen as given in Figure 5.20. The yielding point of PTM30, PTM50 and PTM65 was around 0.50~0.75 per cent story drift. As a result, the ductility level of these three specimens was greater than monolithic specimen. The backbone curve of PTM50 and PTM65 was approximately the same as monolithic specimen response especially up to the yielding point as shown in Figure 5.21 and Figure 5.22.

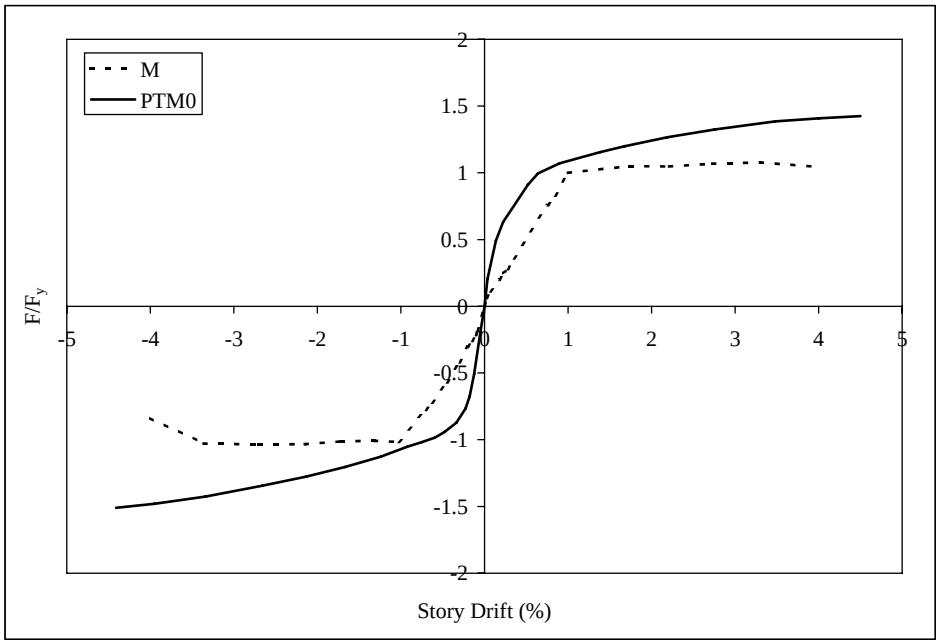

Figure 5.18. Backbone curve of specimen PTM0

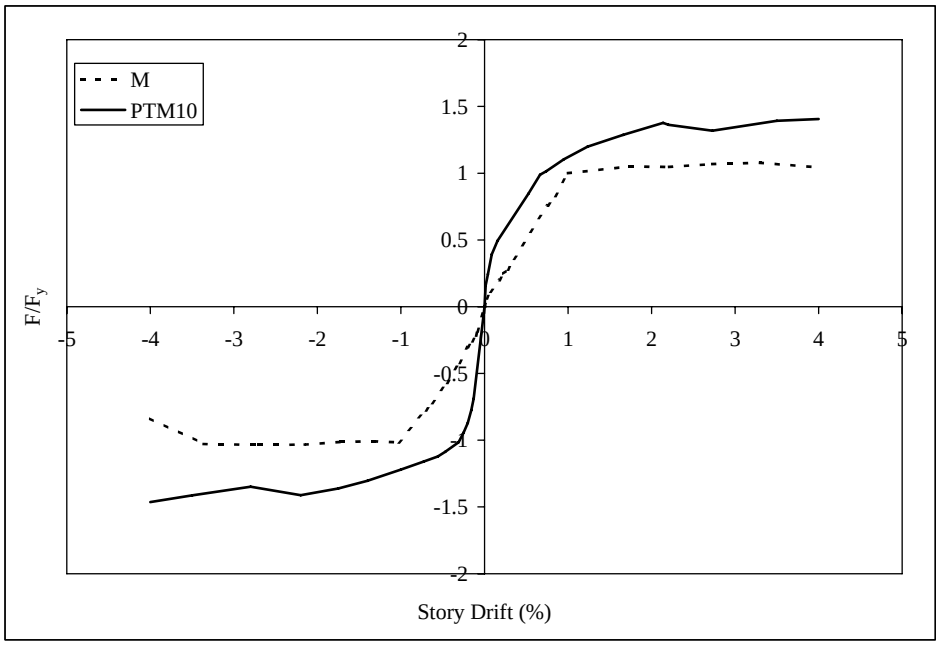

Figure 5.19. Backbone curve of specimen PTM10

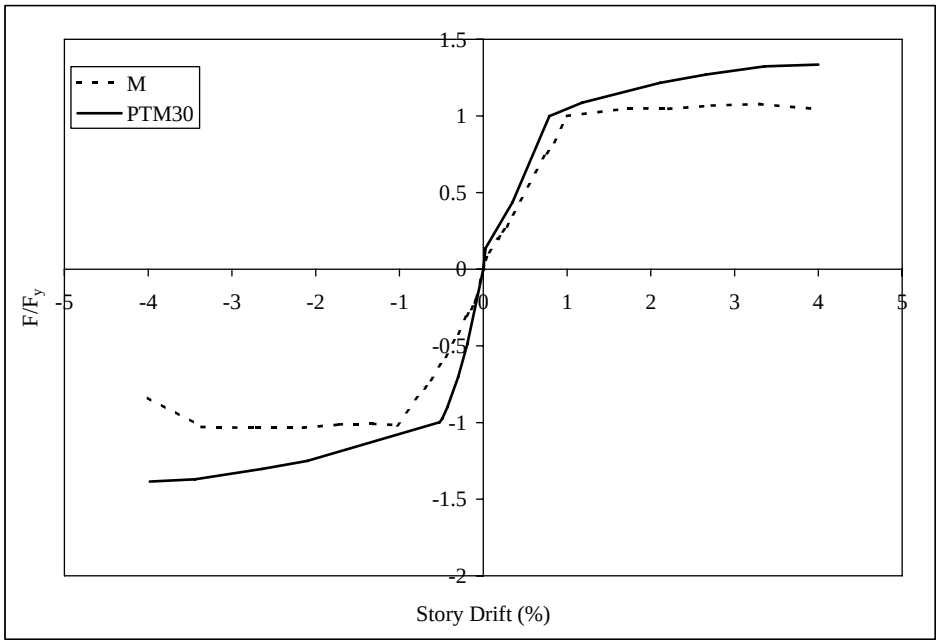

Figure 5.20. Backbone curve of specimen PTM30

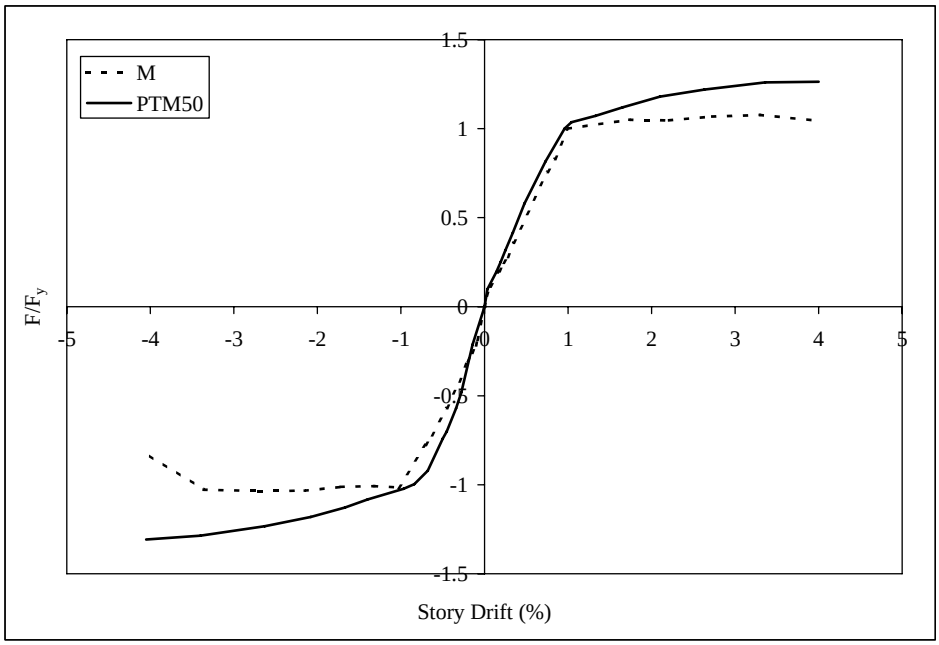

Figure 5.21. Backbone curve of specimen PTM50

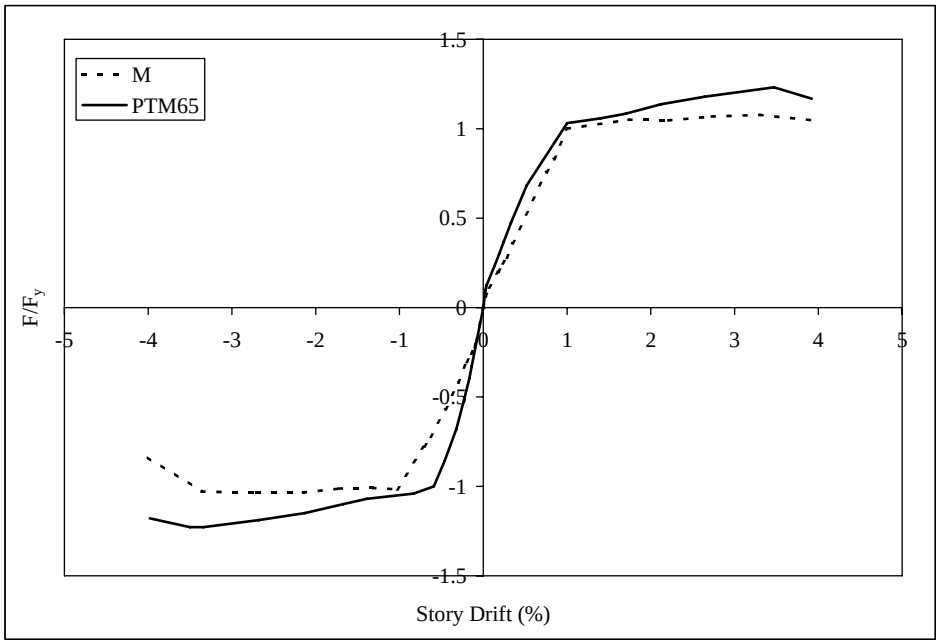

Figure 5.22. Backbone curve of specimen PTM65

5.2. Stiffness Degradation

Stiffness degradation of test specimens was discussed based on the secant stiffness changes. Secant stiffness (K_{sec}) calculated at the last cycle of each successive story drift level was used for the comparison of stiffness degradation among the test specimens. The secant stiffness is defined as the slope of the straight line between the maximum drift levels of that specific load cycle. It is also called peak-to-peak stiffness and illustrated in Figure 5.23. Each secant stiffness value of a specific specimen was normalized (K_{norm}) with respect to the secant stiffness measured at 0.15 per cent story drift level for a possible comparison between the test specimens. Stiffness value for specimen GOK-W was computed up to 2.75 per cent story drift level since it failed during the 3.50 per cent drift cycle. Besides, the stiffness of specimen Mod-B was calculated for the first cycle of 3.50 per cent story drift since connection was failed during the second cycle of this load step.

It is observed that the stiffness degradation of specimens M, CIPC and CIPB are very similar, especially at higher drift levels. The loss of initial stiffness for these three connections was approximately 75~80 per cent at the end of the last cycle as shown in Figure 5.24. On the other hand, there was no significant stiffness degradation in specimen

GOK-W up to the 1.00 per cent story drift. At 2.75 per cent story drift, approximately 50 per cent of the initial stiffness was reserved in specimen GOK-W. The initial stiffness of Mod-B connection was greater as compared to the other specimens, however its stiffness degradation was more pronounced due to the gap opening at the column surface.

Initial stiffness of the post-tensioned specimens was greater than that of the monolithic specimen. Figure 5.25 presents the stiffness degradation of monolithic and post-tensioned test specimens. The secant stiffness of the post-tensioned specimens was significantly degraded with the gap opening at the beam-column interface. The stiffness of PTM0 and PTM10 decreased tremendously, and the loss of stiffness at 4.00 per cent drift level was approximately 90 per cent. Therefore, displacement based design methodology may be more rational to be fully utilized [54]. With the addition of mild steel to the connection, the stiffness degradation response changed significantly and approached to that of the conventional monolithic specimen M.

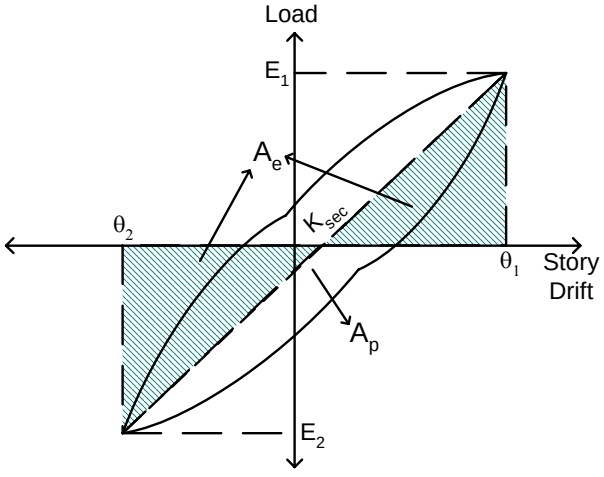

Figure 5.23. Representation of secant stiffness and equivalent damping ratio

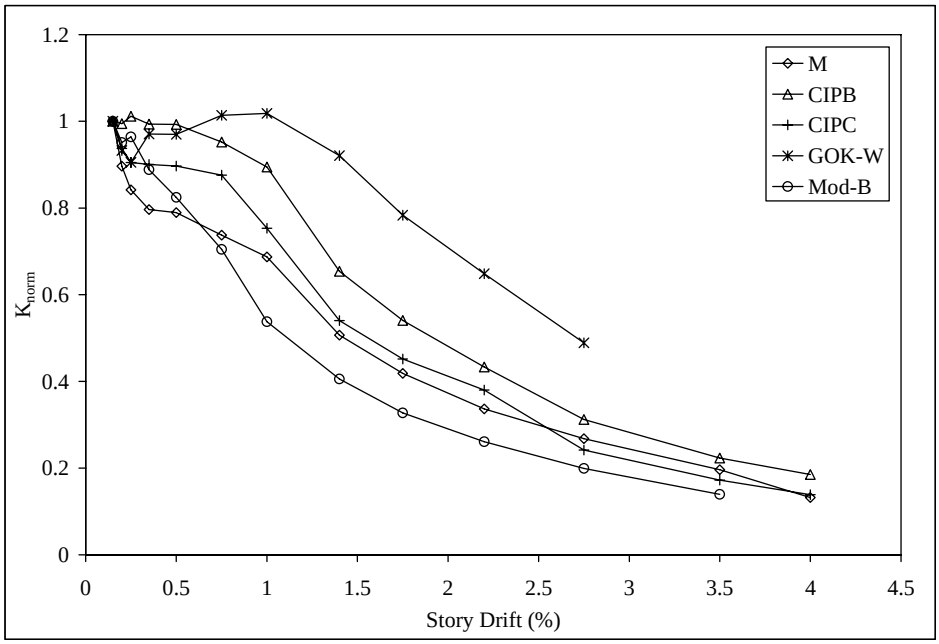

Figure 5.24. Stiffness degradation of Phase I specimens

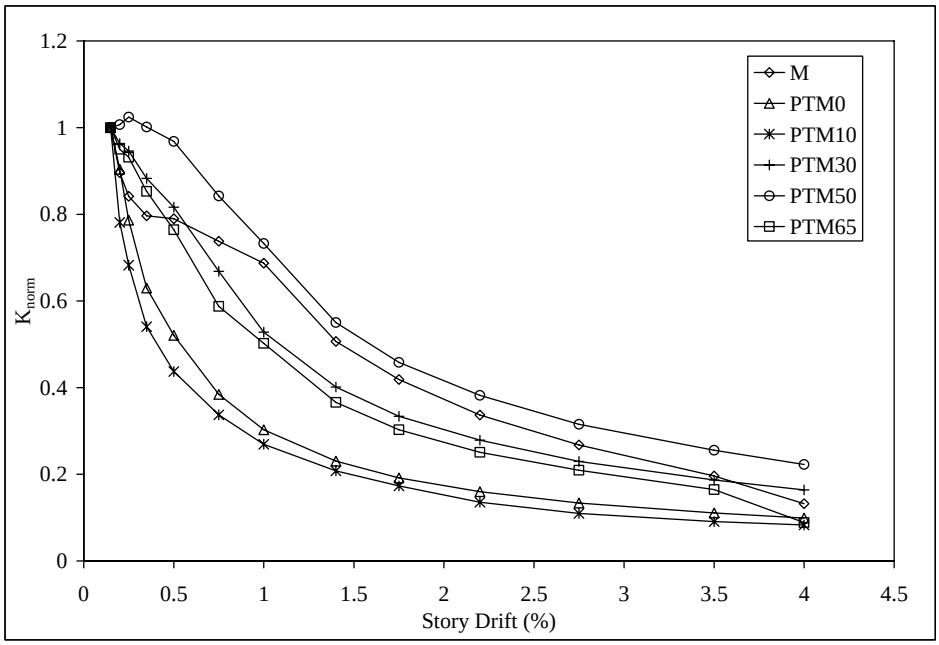

Figure 5.25. Stiffness degradation of Phase II specimens

5.3. Energy Dissipation

In order to discuss the energy dissipation characteristics of the test specimens, two widely used methods were chosen. The first one, the equivalent viscous damping ratio (ζ_{eq}), was plotted against the story drift as illustrated in Figure 5.26 for Phase I specimens. Energy dissipation of test specimen was computed from the last cycle of each successive story drift level. The equivalent viscous damping ratio was defined by Chopra [55] as equating the energy dissipated in a vibration cycle of the actual structure to an equivalent viscous system. For an actual structure the resisting force-displacement relation obtained from an experiment under cyclic loading is illustrated in Figure 5.23. The energy dissipated in the actual structure is given by the area A_p enclosed by the hystresis loop. A_e is the strain energy that is calculated from the assumed linear elastic behavior of the same specimen. This definition is formulated in Equation 5.2 [55].

$$\zeta_{eq}(\%) = \frac{1}{2\pi}\frac{A_p}{A_e}\times 100 \tag{5.2}$$

In general, equivalent viscous damping increased with the increasing story drift as shown in Figure 5.26 for Phase I specimens. The trends of M, CIPC, CIPB and GOK-W were very similar. The response of Mod-B connection in terms of energy dissipation was more satisfactory as compared to the monolithic specimen, M. At 2.00 per cent story drift, which may be called as design drift level, the equivalent viscous damping ratio of specimen Mod-B was around 20~25 per cent while the other connections were experiencing 10 to 15 per cent damping. Also, the damping ratio of specimen Mod-B reached 35 per cent at 3.50 per cent story drift level.

The second method was defined in ACI T1.1-01 as acceptance criteria for such subassemblies [46] as illustrated in Figure 5.27. The dissipated energy can be measured as the hatched area (A_h) in the third cycle of a given story drift level. Normalization of this value is done with respect to the elasto-plastic behavior of specimen at this specified load cycle. The initial stiffness (K and K') values and peak loads (E_1 and E_2) may be different for the forward and backward cycles in the elasto-plastic behavior. The relative energy dissipation ratio is defined as the hatched area divided by the area of the effective circumscribing parallelograms. This definition is formulated and given in Equation 5.3. As

an acceptance criterion according to the ACI T1.1-01 [46] document, the relative energy dissipation ratio of a subassembly must be equal to or exceed 1/8 at the third cycle of the 3.50 per cent story drift.

$$\beta(\%) = \frac{A_h}{(E_1 + E_2) \times (\theta_1' + \theta_2')} \times 100 \tag{5.3}$$

In order to highlight the energy dissipation characteristics of the test specimens, the relative energy dissipation ratio (β) was plotted against the story drift level as shown in Figure 5.28 for the Phase I specimens. The behavior of the normalized energy dissipation depending on story drift was similar to the equivalent damping ratio trend. All β values for Phase I specimens exceeded 1/8 ratio at 3.50 per cent story drift.

For Phase II specimens, equivalent damping and energy dissipation ratio was calculated at each story drift as shown in Figure 5.29 and Figure 5.30 respectively. While the damping ratios of PTM0, PTM10 were less than five per cent, this value for the other post-tensioned specimens was similar to the monolithic specimen. Furthermore, the relative energy dissipation ratio enhances with the increasing the story drift level as shown in Figure 5.30, except PTM0 and PTM10. The energy dissipation characteristics of PTM50 and PTM65 were similar to the monolithic reference specimen at high drift levels. On the other hand, PTM0 and PTM10 had widely different characteristics when compared with the monolithic specimen, M. The energy dissipation of specimen PTM10 increased up the point of the rupture of the mild steels at the connection. After that, its behavior was very similar to the specimen PTM0. At 2 per cent story drift level, which may be adopted as possible design level, β values were around 2~7 per cent for PTM0 and PTM10, while these values reached up to 20~25 per cent for PTM50 and PTM65. PTM30 could be located in the midpoint of these specimens for energy dissipation performance. Furthermore, PTM30, PTM50 and PTM65 test specimens satisfied the acceptance criteria for relative energy dissipation ratio at 3.50 per cent story drift level according to ACI T1.1-01 [46]. The calculated β values for these test modules exceeded β=1/8 value. It may be concluded that approximately 20 to 30 per cent mild steel contribution for flexural strength may be adequate to create damping on the precast, post-tensioned structures.

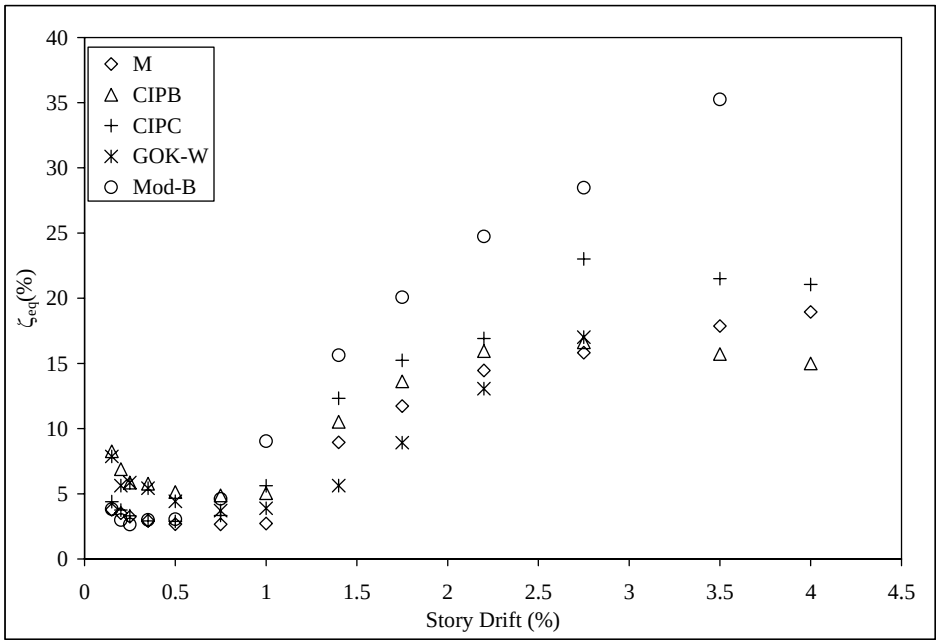

Figure 5.26. Equivalent damping ratio vs. story drift for Phase I specimens

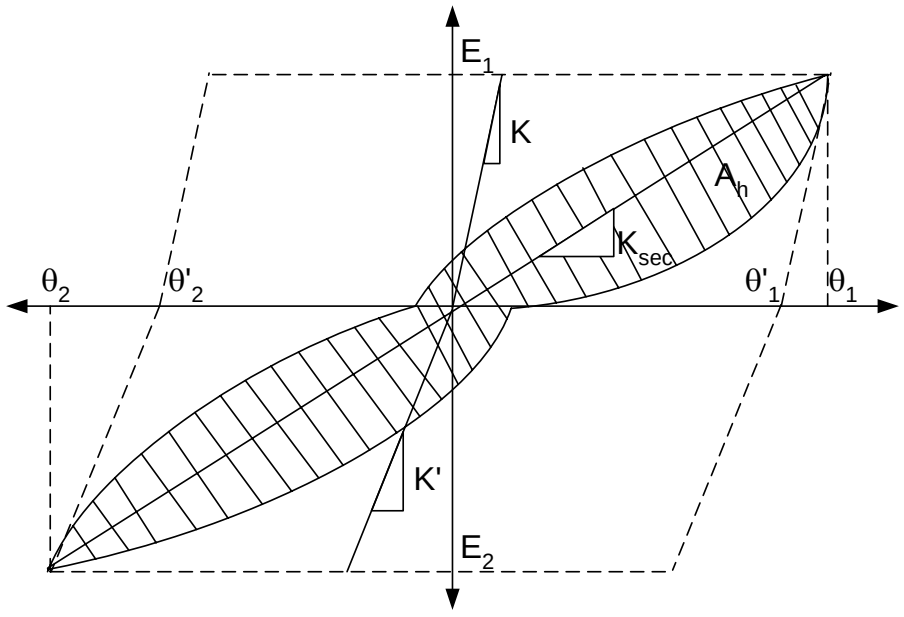

Figure 5. 27. Representation of energy dissipation and normalization

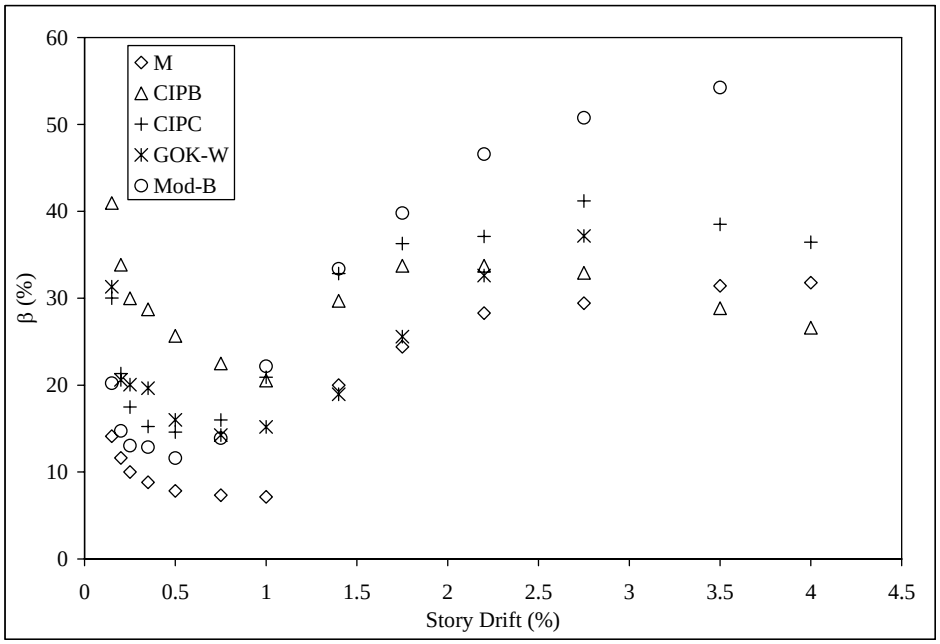

Figure 5.28. Normalized energy dissipation vs. story drift for Phase I specimens

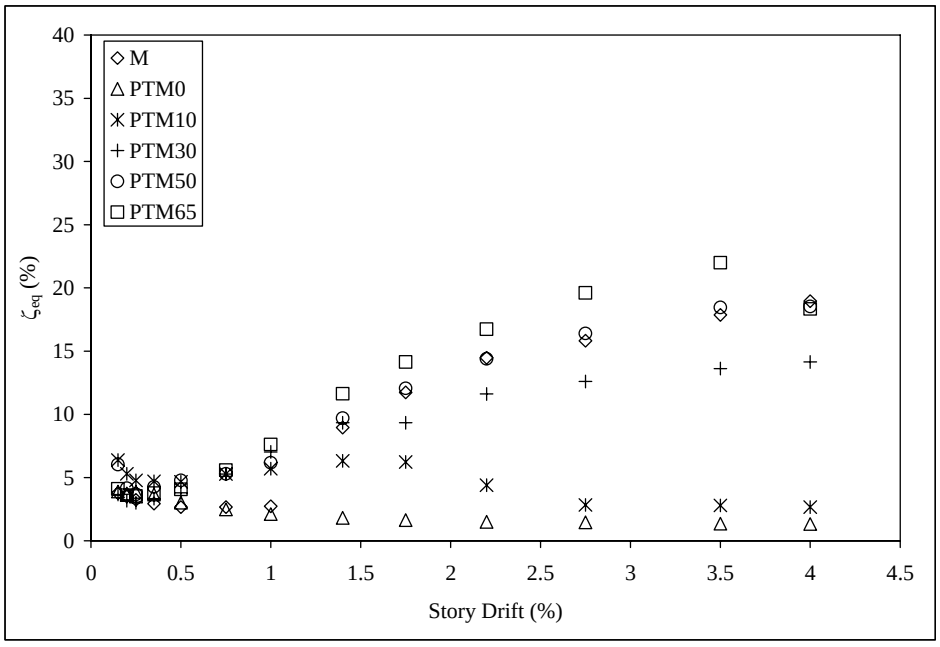

Figure 5.29. Equivalent damping ratio vs. story drift for Phase II specimens

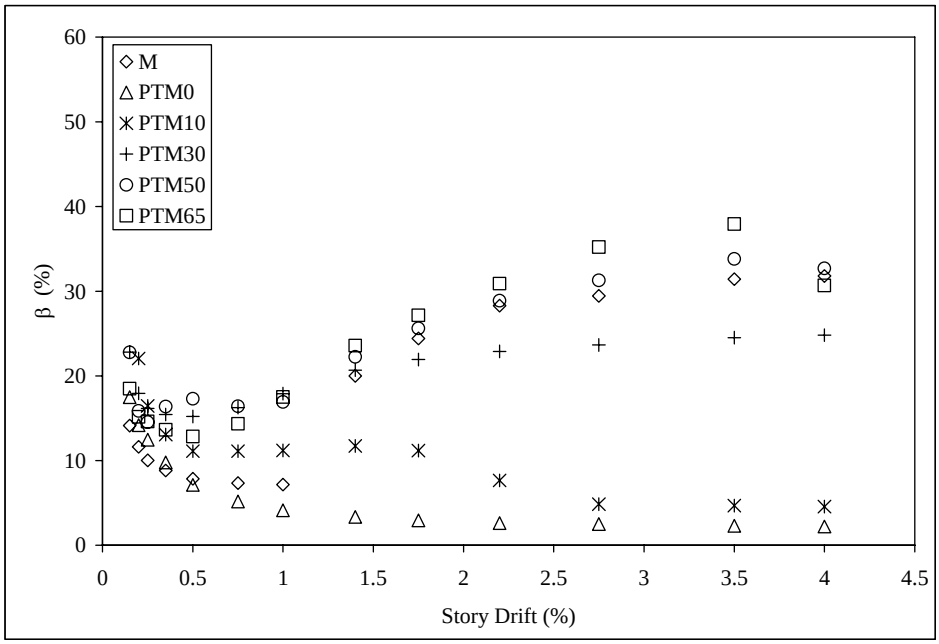

Figure 5.30. Normalized energy dissipation vs. story drift for Phase II specimens

5.4. Residual Displacements

Residual displacements of Phase I specimens were identical with monolithic specimens as presented in Figure 5.31. Permanent displacements and damage were directly related and these factors were expected due to the design mentality of ductile conventional systems. On the other hand, post-tensioned connections are designed as self-centering systems. In the design philosophy of hybrid systems, the moment resisting frame is expected to exhibit minimal damage in beam-column connection regions and negligible residual displacements after a major seismic event. The residual displacements of the test specimens are presented in Figure 5.32. Up to 30 per cent mild steel contribution level for flexural moment capacity, the permanent displacement was negligible. At 4.00 per cent story drift level, 7 mm residual displacement was recorded for specimen PTM30. Prior to yielding of mild steels in specimens PTM50 and PTM65, residual displacements were at a minor level. After that point, the permanent displacements built up and reached to 35~50 mm at the end of the test.

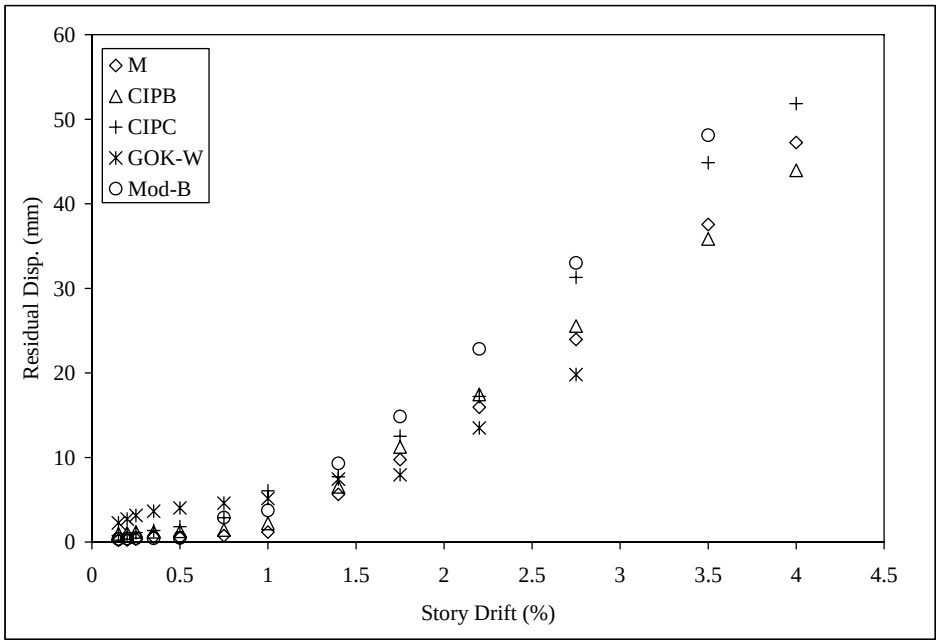

Figure 5.31. Residual displacement on Phase I specimens

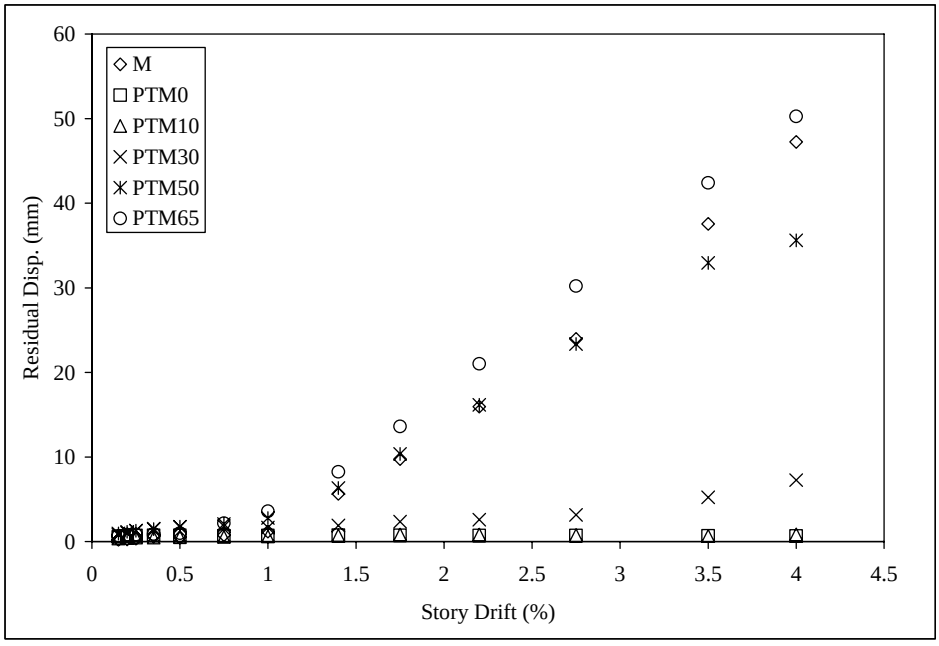

Figure 5.32. Residual displacement on Phase II specimens

6. NUMERICAL ANALYSIS

This chapter describes the design criteria and the analysis steps of post-tensioned connections with a case study on the design of a multi-story precast concrete building. A new hysteretic model for hybrid connections is also proposed and illustrated.

In the first part of the study, performance criteria of post-tensioned beam-column connections which were explained in ACI T01-2-03 [49], are discussed. In the second part of this chapter, plastic analysis equations that were taken directly from the ACI T01-2-03 [49], are presented with proposed some equations for the Turkish design standards based on ACI T01-2-03 approach. In the third part, modeling of moment-rotation behavior of post-tensioned connections with mild steel is explained with a simple algorithm. Finally, the proposed hysteretic behavior model of post-tensioned connections is illustrated.

6.1. Design Steps of Post-Tensioned Connection

The design philosophy of post-tensioned connections is different than the monolithic structures. In the post-tensioned connections, most of the deformations of the frame occur from the opening and closing of the connection at the interface between the precast beam and the column. In contrary, monolithic frames may suffer significant cracking, crushing and spalling in the plastic hinging regions of the beam, the beam-column joint or the both. After a major seismic event, post-tensioned moment frame can be expected to exhibit minimal damage in beam-column regions and negligible permanent displacements. Such post-tensioned moment frames do not satisfy the prescriptive requirements of ACI 318 [56] which for is the frames of monolithic construction. The acceptance of such precast frames requires demonstration by experimental evidence and analysis that the frames have strength and toughness equal to or exceeding those provided by comparable monolithic frames [49].

In order to validate the performance criteria mentioned above, the post-tensioning tendons should be unbonded from anchor to anchor and concentrically located within the cross section of the beam and designed to remain elastic during a major earthquake. The

upper bound of initial post-tensioning may be set to 40 per cent of tendons ultimate strength in order to ensure the predicted behavior. The role of such a post-tensioning level may be summarized as creating a shear resistance between the beam and the column interface in order to resist the gravity or earthquake induced shear forces. The central post-tensioned tendons and mild steel rebars located at the top and the bottom of the crossection mainly creates the base of moment capacity of the connection. Besides, mild steel rebars enhance the energy dissipation properties of the hybrid connections. These rebars are grouted in ducts and deliberately debonded for a short length in the beam adjacent to the beam-column interface in order to reduce the high cyclic strains.

In order to reach the expected performance level of hybrid connections the following equations which are mainly taken from ACI T1-02-03 [49] need to be satisfied. The equation number suffix “a” in the following equations indicates that the equation taken directly from ACI T1-02-03 [49] while “b” indicates that it is the proposed version for the Turkish designer by considering the safety factors and load combinations.

The minimum post-tensioning force created by the tendons should be equal to the gravity load induced shear force at the beam-column interface which is calculated according to the factored loads as shown in Equation 6.1. The main difference for the Turkish standard is the factored gravity load level (Equation 6.1b).

$$A_{pt} f_{pi} = \frac{1.4V_D + 1.7V_L}{\phi \mu_f} \tag{6.1a}$$

$$A_{pt} f_{pi} = \frac{1.4V_G + 1.6V_Q}{0.85 \mu_f} \tag{6.1b}$$

In the design of hybrid connections, the lower bound for the amount of the mild steel reinforcement is chosen such that the unfactored gravity load induced shear forces at the interface is carried by the mild steel. The shear strength of the mild steel can be taken as the half of the yield strength as given in Equation 6.2 where the tension and compression steel is assumed to be equal. In Equation 6.2b, the design yield strength of the mild steel which is divided by the material factor, 1.15 issued. At the same time, the amount of the mild steel at the connection region should be satisfied energy dissipation ratio. On the

other hand, the effect of mild steel on flexural strength of the connection should be limited with 50 per cent or less since high mild steel ratio increases the residual displacements.

$$\frac{A_s f_y + A_s' f_y}{2} = A_s f_y = \frac{V_D + V_L}{\phi} \tag{6.2a}$$

$$\frac{A_s f_{yd} + A_s' f_{yd}}{2} = A_s f_{yd} = V_G + V_Q \tag{6.2b}$$

The calculation of flexural strength of the connection is based on the rotation at the beam-column interface at the ultimate strength of the mild steel as shown in Figure 6.1.

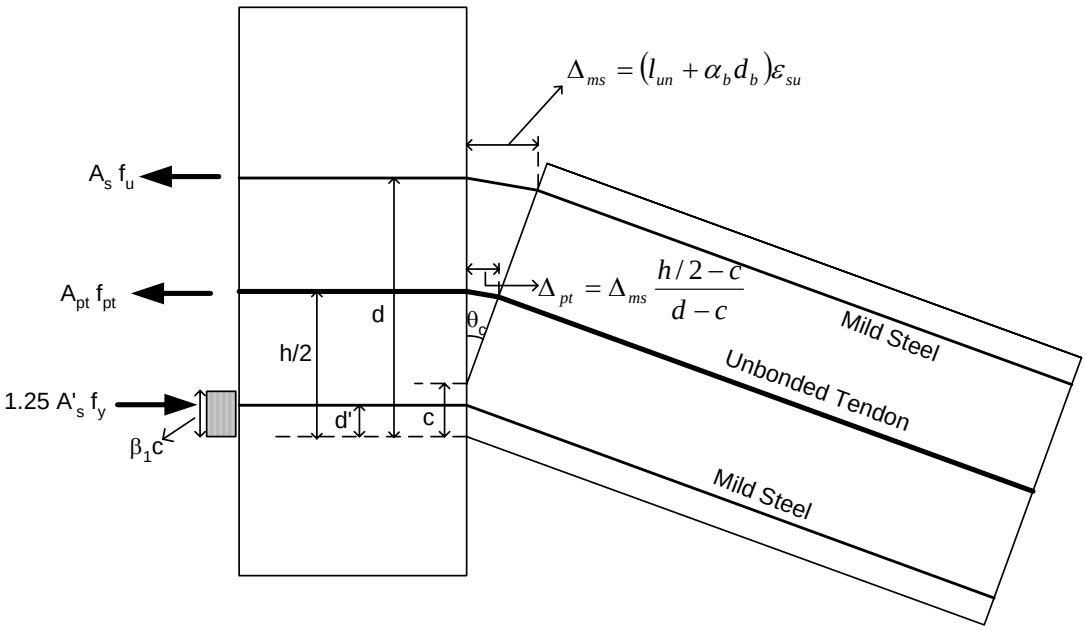

Figure 6.1. Rotation at the beam-column interface

The elongation in mild steel reinforcement is calculated according to Equation 6.3 where α_b is a coefficient depending on the bond deterioration of the rebar and it ranges between 2 and 5.5.

$$\Delta_{ms} = (l_{un} + \alpha_b d_b)\varepsilon_{su} \tag{6.3}$$

ε_{su} is taken as 90 per cent of the ultimate strain (ε_u) that mild steel can reach at its ultimate strength. The reason of using such a reduction factor is to eliminate the possibility of fracture of mild steel bars before reaching the required displacement level. The elongation of prestressing tendons can be calculated easily by using similar triangles as illustrated in Figure 6.1 and as given in Equation 6.4. The total strain developed in the prestressing tendon due to the rotation of the connection and due to the initial prestressing is calculated by Equation 6.5 where L_{un} shows the unbonded tendon length.

$$\Delta_{pt} = \Delta_{ms} \frac{h/2 - c}{d - c} \tag{6.4}$$

$$\varepsilon_{pt} = \frac{\Delta_{pt}}{L_{un}} + \varepsilon_{pi} \tag{6.5}$$

By using the Equation 6.6 and Equation 6.7, the contribution of mild steel and prestressing strands on the flexural moment capacity of connection can be calculated respectively. In proposed Equations 6.6b and 6.7b, design yield strength of mild steel and design compressive strength of concrete are used as 1.15 and 1.40 respectively for calculating moment capacity and compression block depth.

$$M_{ms} = A_s f_u \left(d - \frac{\beta_1 c}{2} \right) - A_s' 1.25 f_y \left(d' - \frac{\beta_1 c}{2} \right) \tag{6.6a}$$

$$M_{ms} = A_s f_{yd} \left(d - \frac{k_1 c}{2} \right) - A_s' f_{yd} \left(d' - \frac{k_1 c}{2} \right) \tag{6.6b}$$

$$M_{pt} = A_{pt} f_{pt} \left(\frac{h - \beta_1 c}{2} \right) \tag{6.7a}$$

$$M_{pt} = A_{pt} f_{pt} \left(\frac{h - k_1 c}{2} \right) \tag{6.7b}$$

The total flexural moment capacity of the connection, M_c can be calculated by summing up the contributions of mild steel, M_{ms} and prestressing tendon, M_{pt}. The

effective depth of the compression block is calculated by force balance as shown in Equation 6.8.

$$\beta_1 c = \left[\frac{A_{pt} f_{pt} + A_s f_u - A_s' 1.25 f_y}{b(0.85 f_c')} \right] \tag{6.8a}$$

$$k_1 c = \left[\frac{A_{pt} f_{pt} + A_s f_{yd} - A_s' f_{yd}}{b(0.85 f_{cd})} \right] \tag{6.8b}$$

In the calculation of flexural strength of the connection, the following conditions must be satisfied:

- The behavior of prestressing strands must be in the elastic region and should satisfy the Equation 6.9. The f_{pt} is defined as the stress in the prestressing tendon throughout the loading history.

$$\frac{f_{pt}}{f_{ptu}} < 0.80 \tag{6.9}$$

- The contribution of mild steel on the flexural moment capacity of the connection should not exceed 50 per cent of the overall capacity as given in Equation 6.10 [49]. Besides, this flexural contribution should not be less than 10 per cent of the overall capacity according to the Turkish standard TS3233 [48]. It should be recalled the results presented in Chapter 5 and it may be concluded that this 10 per cent limit is not adequate for a desired response of the hybrid connection.

$$\frac{M_{ms}}{M_c} \leq 0.50 \tag{6.10}$$

- In order to reach the 3.50 per cent story drift, the rotation at beam-column interface should be around 0.035 radians as given in Equation 6.11.

$$\theta_c = \frac{\Delta_{ms}}{d - c} \approx 0.035 \tag{6.11}$$

- Gravity load induced shear force at the beam column interface should be limited with the Equation 6.12, where C designates the compressive force created at the compression block.

$$V_u = 0.75\left(1.4V_D + 1.7V_L\right) + \frac{M_{c1} + M_{c2}}{L_n} = \phi\,\mu_f\,C \tag{6.12a}$$

$$V_u = V_{dy} + \frac{M_{c1} + M_{c2}}{L_n} = 0.85\,\mu_f\,C \tag{6.12b}$$

6.2. Case Study for Multi-Story Precast Structures with Hybrid Connections

In the study, presented under this subheading, three similar buildings with changing span lengths in one direction were analyzed and designed with precast members connected via hybrid connections. The building had 60 m x 20 m foot-print dimensions and four stories. The story height was 3.20 m. It is assumed that these buildings were constructed as student dormitory in the first earthquake zone with Z3 soil type according the Turkish Earthquake Code [7]. The precast frame was chosen as moment resisting frame with an earthquake load reduction factor (R) of 6. The structures were modeled with linear elastic material and analyzed by using SAP2000 V.8 computer program.

In this case study, the main variable was chosen as the beam span length as 5, 7.5 and 10 m for the long direction of building. For the transverse direction, span length was kept constant at 5 m as illustrated from Figure 6.2 to Figure 6.4. In the analysis, loads were taken from TS500 [57], TS3233 [48] and the Turkish Earthquake Code [7]. Depending on the span length, the precast beam and column dimensions were changed. At the foundation level, the total crossectional area of the columns was kept approximately equal for all the structures. The geometric properties of the structures are given in Table 6.1.

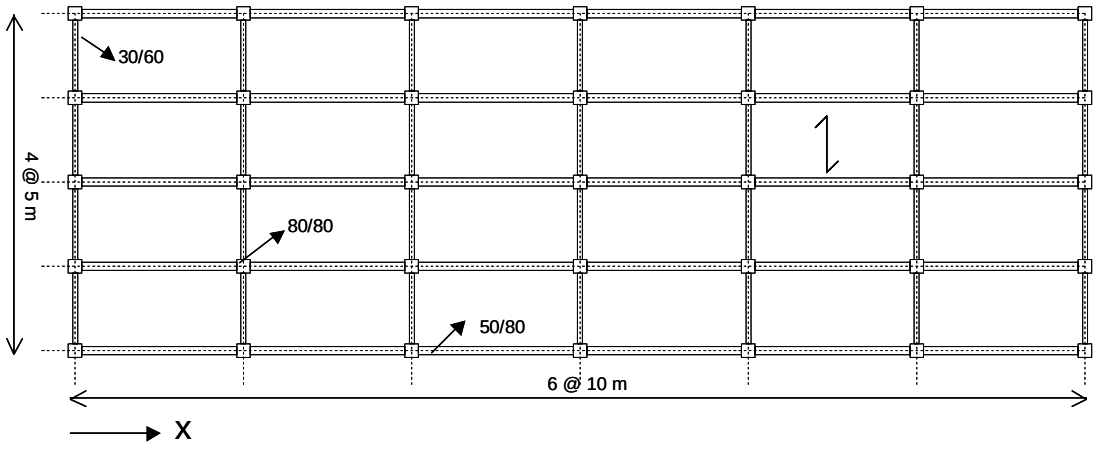

Figure 6.2. The plan view of structure Type I

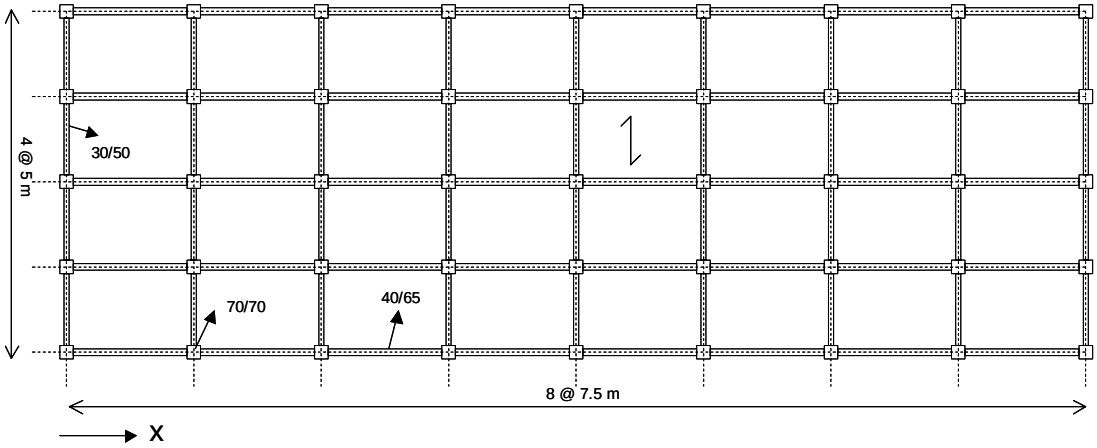

Figure 6.3. The plan view of structure Type II

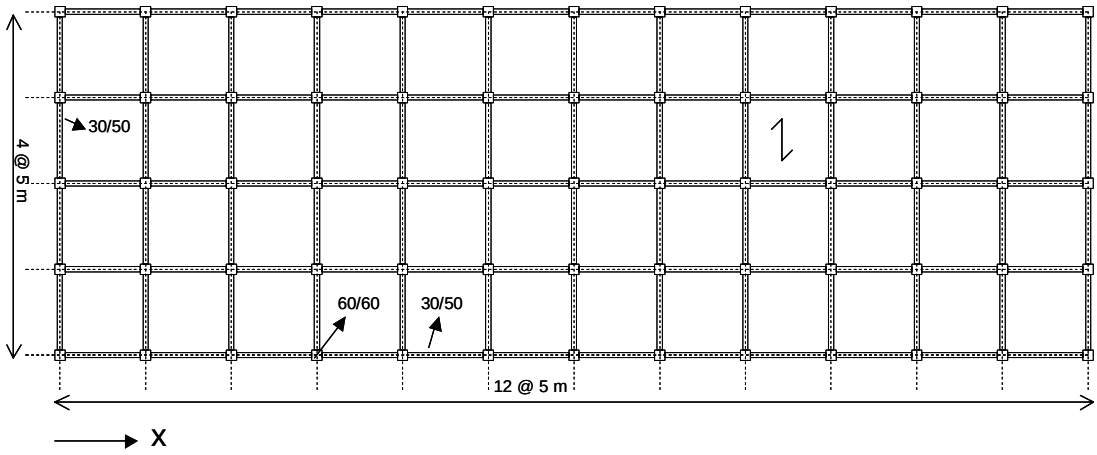

Figure 6.4. The plan view of structure Type III

Table 6.1. Geometric properties of the structures

	Type I	Type II	Type III
Span length in X direction (m)	10	7.5	5
Span length in Y direction (m)	5	5	5
Beam dimensions in X direction (cm)	50/80	40/65	30/50
Beam dimensions in Y direction (cm)	30/60	30/50	30/50
Column dimensions (cm)	80/80	70/70	60/60

The reason of choosing three different span lengths was to investigate the range of shear forces occur under gravity loading at the beam-column interface and to present the boundary amount of mild steel and prestressing strands. For the precast members, the concrete class was chosen as C40. The mild steel was S420a and the mechanical properties were taken from TS500 [57]. The post-tensioning force was applied with prestressing strands that had 13 mm nominal diameter and 1860 MPa ultimate strength. The coefficient of bond deterioration (α_b) was taken as 3.

In the detailing part, the worst case was chosen from the load combinations according to Turkish standards and all connections were detailed and presented in Table 6.2 according to these results. In this table, first four columns are defined the location of the connections. These columns present the type of the structure, story number, connection direction and type of joint. Only some critical joints details were given in Table 6.2 to clarify ranges of post-tensioning detailing. Fifth and sixth columns shows the reinforcement detailing of the connections and the next three columns gives unbonded length on the mild steel, unbonded length of prestressing tendon and post-tensioning level respectively. Unbonded length of the tendons can be taken as half of the span length.

Two different capacity and performance calculations were performed according to ACI T01-2-03 plastic analysis and proposed Turkish standards respectively and presented at last four columns in Table 6.2. They were flexural moment capacity of the connection, mild steel contribution, maximum stresses on the tendons and connection rotation capacity. In the detailing part, mild steel contribution on the moment capacity ranges from 28 per cent to 48 per cent. This condition satisfies the requirements of ACI T1-1-01. Besides that,

the rotation capacity of connection is greater than 0.035 radians. On the other hand, this rotation capability is chosen less 0.04 radians in order to eliminate second order effects. When designing of hybrid connections, firstly, mild steel contribution on the flexural capacity should be decided and secondly the amount of prestressing tendons and the post-tensioning force level should be optimized. The determination of unbonded length of mild steel can be found a trial and error with depending on the mild steel effect and the rotation limits.

The behavior of post-tensioned connections considers not only strength-based design but also performance based criteria; therefore, last three columns are very important. When comparing the proposed Turkish standard and plastic analysis concept, following conclusions may be drawn:

- In proposed Turkish Standard, the contribution of mild steel for flexural strength is less than plastic analysis results. This means that, in real behavior, the effect of mild steel on moment capacity may be grater than 50 per cent
- Stress calculations at tendons according to proposed equation are less than the ACI results. This may be caused that the prestressing strands behavior might be at non-linear region.
- There is difference between results of rotation calculations. By contrast, analysis result according to the Turkish standard is greater than ACI T1-02-03 values. The result directly affects the decision of unbonded length on the mild steel.

Briefly, there is a consistency between ACI procedure and experimental results. Due to the considering the material factor of safety, the strength capacities of the connection that were calculated according to proposed equations, are less than the ACI results as expectedly. This situation is not a problem because the plastic analysis is conservative side. On the other hand, performance criteria according to proposed standard diverge from the plastic analysis. Therefore; performance criteria checks should be done with plastic analysis method. Finally, the hybrid connection system may be suitable for medium range span length because the number of strands increases tremendously with increasing span length.

Table 6.2. Result analysis and detailing

Structure	Story	Axis	Location	# of Mild Steel	# of Strand (13 mm)	l_{un} (mm)	L_{un} (m)	f_{pi}/f_{ptu}	Code	M_c (kNm)	M_{ms}/M_c	f_{pt}/f_{ptu}	θ_c (%)
(1)	(2)	(3)	(4)	(5)	(6)	(7)	(8)	(9)	(10)	(11)	(12)	(13)	(14)
Type I	2nd	X	Middle	2 ϕ 24	18	120	5	0.5	ACI	1042	0.28	0.68	3.8
									Prop. TS	886	0.24	0.65	4.2
Type I	2nd	Y	Edge	3 ϕ 24	9	25	2.5	0.5	ACI	539	0.48	0.72	3.8
									Prop. TS	440	0.43	0.68	4.5
Type II	2nd	X	Middle	3 ϕ 18	12	80	3.75	0.6	ACI	633	0.31	0.76	3.5
									Prop. TS	530	0.27	0.72	4.0
Type III	2nd	X	Middle	3 ϕ 18	9	40	2.5	0.6	ACI	373	0.40	0.73	3.7
									Prop. TS	302	0.35	0.68	4.3
Type III	4th	Y	Edge	1 ϕ 20	4	60	2.5	0.5	ACI	185	0.33	0.77	3.6
									Prop. TS	161	0.30	0.75	3.8

6.3. Modeling of Hybrid Connections

6.3.1. Theoretical Background of Analysis

Well-known classical section analysis rules cannot be applied directly to the precast hybrid connections due to the existence of unbonded prestressing tendon and partially bonded mild steel. In the proposed section analysis below, moment-rotation behavior of the connections was developed by providing an additional debonding length formulation for the mild steel. In the literature some numerical approaches are reported for similar precast concrete or steel frames and precast walls [58-69].

In the theoretical background of the modeling of moment-rotation response for post-tensioned connections, state of the art of such models need be discussed.

Firstly, a simple tri-linear idealization of unbonded post-tensioned connection was developed by Priestly and Tao in 1993 [68]. There were three key points at the definition of the force-displacement relation of the connection. They were decompression, linear limit and proportionality limit of steel. The first point was defined as the precompression stress at the extreme fiber was lost and crack started to propagate. The second point was the end of the elastic behavior and this point was approximately two times of the first point. The last point was the limit of proportionality on the steel-strain stress curve, since it was reasonable to assume at this stage that concrete ultimate conditions were approached [68].

Secondly, a parametric study was performed by Cheok *et al*. about the hybrid connections [58] by using IDARC [70] that is capable of nonlinear structural analysis. The proposed model was characterized by seven unique feature parameters that were developed from experimental observations. Hysteretic parameters were identified for five different connections types. The parameters were calibrated using the experimental load-deformation data which was scaled using similitude requirements to account for the reduced scale of test specimens [58].

Another study about modeling the post-tensioned precast concrete connections was developed by El-Sheikh [62, 63]. This study was based on spring and fiber model on DRAIN-2DX [71] software. In the content of this model, limit state points were defined. The first point defined was the estimation of the linear behavior limit. The linear limit moment was considered to be the smaller of the two values; the first value accounted for concrete softening and the second value accounted for the geometric softening due to the gap opening. The linear limit rotation was calculated assuming the beam was uncracked. The second point was the definition of yield limit state with several assumptions, given below:

- The elastic flexural deformations over the length was negligible
- The center of rotation at the beam-column interface was at the neutral axis
- The cover concrete was spalled

The last point of the moment-rotation curve defined by El-Sheikh was the estimation of the ultimate limit state. In this state, ultimate moment was equal to the yield moment and the ultimate rotation capacity of the connection was calculated from the ultimate strain of the confined concrete and critical failure length [62, 63].

The modeling of unbonded post-tensioned connections with mild steel was discussed by Pampanin *et al.* in 2001 [67]. The reported model provided an iterative section analysis method, incorporating, an analogy with equivalent cast-in-place solution named “monolithic beam analogy”, as an additional condition on the member global displacement [67]. A similar approach was presented for post-tensioned steel frame connections by Christopoulos [60].

A flag-shaped model and hysteretic rules were defined by Christopoulos for self-centering post-tensioned connections [59]. In this model, loading, unloading and reloading stiffness values were defined and a parametric study about post-yield stiffness and energy dissipation characteristics were presented. The details of flag-shaped hysteretic behavior will be discussed further in the following pages under the subheading of cyclic modeling.

6.3.2. Procedure for Moment-Rotation Analysis

In the previous part, the behavior of hybrid connections and some of the available numerical approaches are discussed. There is some complexity in the section analysis of unbonded post-tensioned connections, since the classical analysis procedures of monolithic reinforced concrete for moment-curvature relationship is not directly applicable. In this part of the study, definition of the moment-rotation behavior of a post-tensioned section with mild steel will be discussed. The hybrid connection concept is defined as unbonded strands in the mid-depth of the crossection and mild steel at the top and the bottom of the beam crossection with partially unbonded length as defined in ACI-T1.02 [49]. For the analysis of such type of connections, a simple and iterative procedure using the equilibrium equations was previously defined by Pampanin *et al.* [67]. The current procedure was based on this approach and a new debonding length estimation formula for the mild steel, which is in the steel duct with high-strength grout, is incorporated.

The flow chart to calculate the moment-rotation response of a hybrid connection is presented in Figure 6.5. In the first step, the gap opening angle (rotation angle, θ_c) between beam and column is imposed. Secondly, a neutral axis depth (c) for the crossection is assumed. The application of monolithic beam analogy for precast members that was defined by Pampanin *et al.* [67] is used to find the concrete compression fiber strain (ε_c) (Equations 6.13 and 6.14). Pampanin claims that, if two beams, which one of them was hybrid and the other one was monolithic connection had identical geometry and reinforcements the elastic deformations would be the same and, when imposing the same total displacement, the plastic contributions can be equated [67]. The plastic hinge length (l_p) may be calculated according to Paulay *et al.* [72].

$$l_p = 0.08L_{cant} + 0.022d_b f_y \tag{6.13}$$

L_{cant} represents the length of the cantilever and d_b and f_y is the bar diameter and yield strength of the reinforcement respectively. The concrete strain at the hybrid connection can be defined as:

$$\varepsilon_c = \frac{\theta_c \times c}{l_p} \tag{6.14}$$

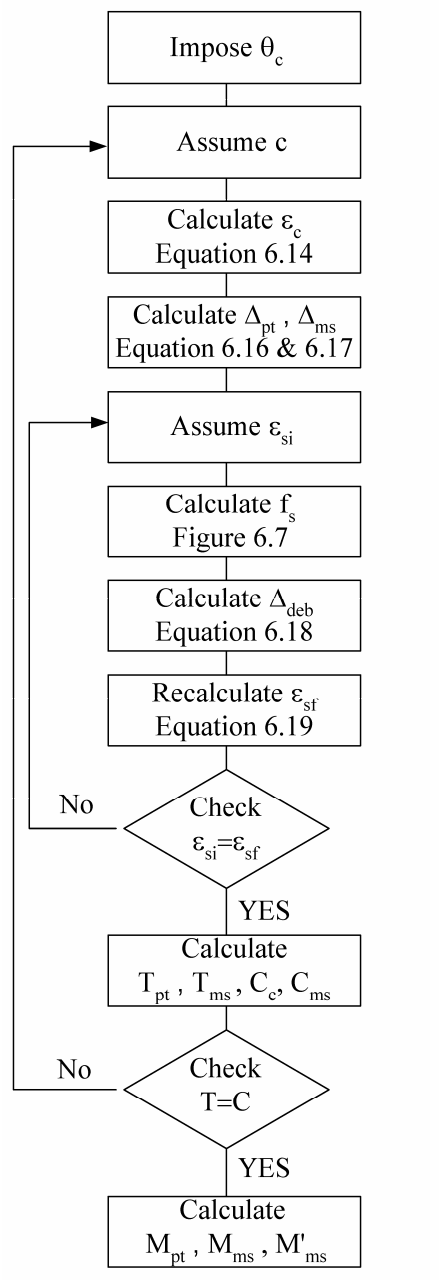

Figure 6.5. The algorithm for the moment-rotation behavior

Equation 6.14 is a simplified illustration for the relation between strain in concrete and the rotation at the connection. The differences between the accurate calculation as defined in Equation 6.15 and the approximate one (Equation 6.14) for precast members were reported at a minor level by Pampanin *et al*. [67].

$$\varepsilon_c = \left[\frac{\left(\theta_c \times L_{cant}\right)}{\left(L_{cant} - \frac{l_p}{2}\right) l_p} + \phi_y \right] c \tag{6.15}$$

In the fourth step, as shown in Figure 6.6, by using similar triangles and using Equation 6.16 and Equation 6.17, the elongation at strands (Δ_{pt}) and mild steel (Δ_{ms}) can be calculated easily.

$$\Delta_{pt} = \theta_c \left(\frac{h}{2} - c \right) \tag{6.16}$$

$$\Delta_{ms} = \theta_c \left(d - c \right) \tag{6.17}$$

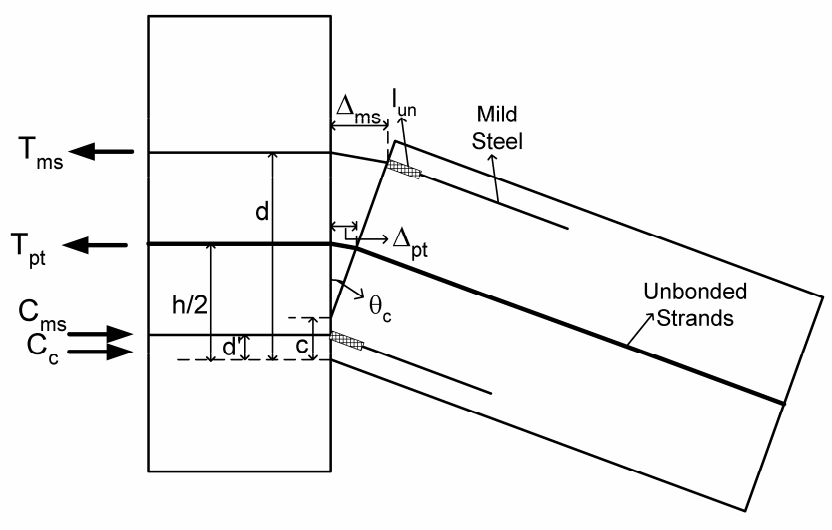

Figure 6.6. Schematic representation of gap opening

In the fifth step, there is a second assumption which is about the strain level of the mild steel (ε_{si}). By using Figure 6.7, that is tri-linear idealization of mild steel, the stress on the mild steel (f_s) is calculated. Other constitutive equations were reported by Restrepo [73] for modeling steel bars but the first model was chosen since tri-linear idealized behavior was simple especially for designers. During the tests of the current study, the strain level at the mild steels and the gap opening at the connection region was monitored. These tests showed that the elongation of mild steel was not only related to the initially

imposed unbonded length (l_{un}). When the comparisons with strain level and the elongations were made, strain penetration towards to the steel ducts was observed. In order to determine the length of the additional debonded length (Δ_{deb}), some experimental test data taken from the bond tests which were performed in Bogazici and Kocaeli Universities [74-77] were used. These researches showed that the debonded length was directly related with stress and strain level on the mild steel. In these tests, debonding length was increased even if the steel was in the yield plateau. The other factors were the concrete or grout compressive strength (f_g), bar diameter (d_b) and the cover thickness. The similar approaches were reported by Raynor *et al*. for bond-slip response of reinforcing bars grouted in ducts [52]. In the current proposed model in Equation 6.18, the cover thickness parameter is not considered because the mild steels are in the steel ducts and the strain penetration is occurred in two sides- to the column and to the beam.

$$\Delta_{deb} = 2\left(0.40\frac{f_s \times \varepsilon_{si} \times \sqrt{d_b}}{\sqrt{f_g}}\right) \quad mm \tag{6.18}$$

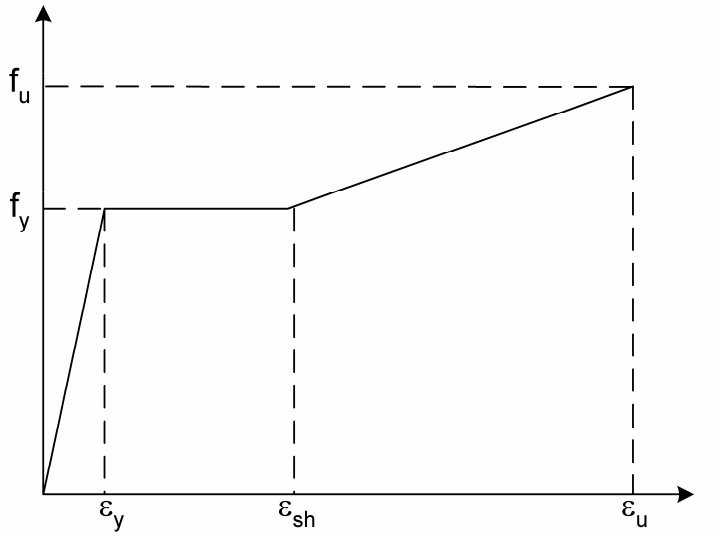

Figure 6.7. Idealized stress-strain behavior of mild steel

In the next step, the calculated final strain in the mild steel (ε_{sf}) by using Equation 6.19 should be checked with the assumed initial strain (ε_{si}). Until convergence of assumed and final strains, iteration is to be performed on the assumption. In the next step, force balance condition at the crossection should be checked. Initially, strain at the strands (ε_{pt}) is calculated from Equation 6.20 where ε_{pi} is the initial strain due to post-tensioning and

L_{un} is the unbonded length of the strands. At this point, strain distribution along the unbonded length of the tendons is assumed uniform. After that, by using Ramberg-Osgood formulation as presented in Equation 6.21 for low relaxation tendon, the stress on strand (f_{pt}) is found.

$$\varepsilon_{sf} = \frac{\Delta_{ms}}{l_{un} + \Delta_{deb}} \tag{6.19}$$

$$\varepsilon_{pt} = \frac{\Delta_{pt}}{L_{un}} + \varepsilon_{pi} \tag{6.20}$$

$$f_{pt} = 200 \times 10^3 \varepsilon_{pt} \left\{ 0.025 + \frac{0.975}{\left[1 + \left(118\varepsilon_{pt}\right)^{10}\right]^{0.10}} \right\} \leq 1860\ MPa \tag{6.21}$$

Mander confined concrete model [78] for rectangular hoops may be chosen for the stress-strain relation since the connection region is heavily confined by high amount rectangular closed stirrups and steel plates at the beam-column interface. This configuration delays the concrete crushing hence, confined model is more appropriate instead of unconfined model. Strain distribution on the compressive block is assumed linear. Using this model, compression force component due to the concrete block (C_c) is calculated. Finally, until section equilibrium that is defined in Equation 6.22 is satisfied, the assumption of neutral axis depth is iterated.

$$T_{pt} + T_{ms} = C_c + C_{ms} \tag{6.22}$$

T_{pt}, T_{ms} are the tension force components due to the strand and mild steel respectively, while C_{ms} is the compression force resultant due to the mild steel. When two assumptions are satisfied, the flexural moment capacity of crossection is calculated with considering contribution of prestressing strand (M_{pt}) and the mild steel (M_{ms}, M'_{ms}).

6.3.3. Experimental Validation for Moment-Rotation Behavior

The experimental program that was performed on post-tensioned connections with different mild steel ratio yielded envelope curves of specimens having different flexural moment contributions from the mild steel (PTM10, PTM30, PTM50, and PTM65). The

details and the behavior of test specimens were discussed in the previous chapters. The comparisons on the proposed numerical and experimental results in terms of moment-rotation behavior of the hybrid connections, are presented in Figure 6.8 to Figure 6.11. Generally, the numerical moment-rotation behavior coincided with the backbone curve of the experimental results. For specimen PTM10, the predicted rupture of mild steel was a bit later than the experimental result. In specimen PTM10, a smaller mild steel diameter was used in the huge steel duct as compared to the other specimens. Therefore, the debonded length prediction was probably a bit longer than the experimental value. Hence rupture of mild steel in the simulation was delayed. The numerical response was the same as experimental result in both elastic and inelastic region for PTM30 and PTM50 with only minor difference for the ultimate flexural moment capacity around 0.04 radian. When the predicted elastic response of PTM65 was compared with test result, numerical curve was slightly stiffer.

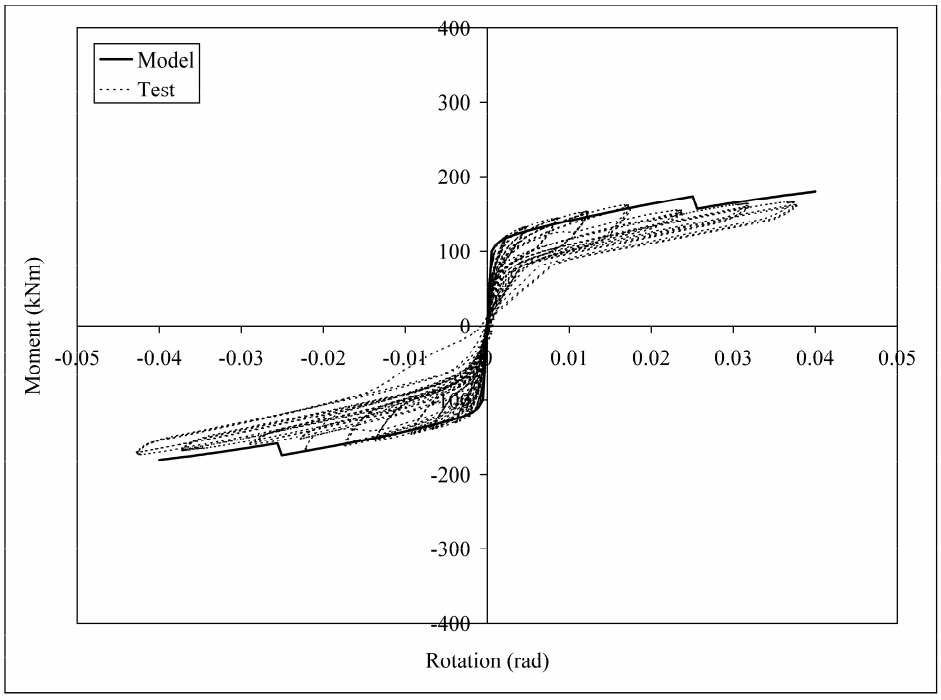

Figure 6.8. Comparison test result vs. the model for moment-rotation behavior of PTM10

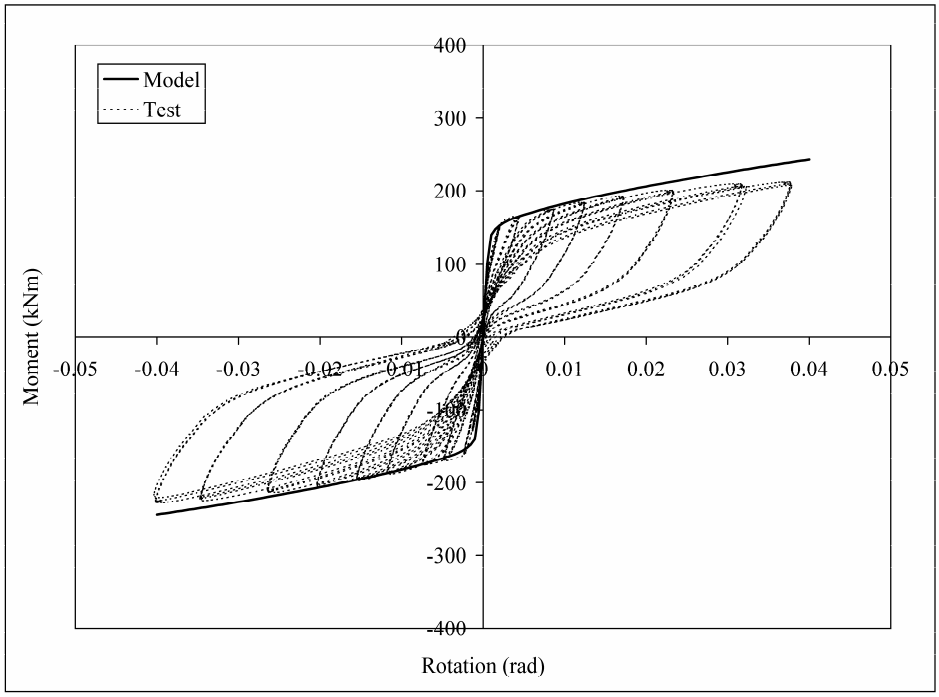

Figure 6.9. Comparison test result vs. the model for moment-rotation behavior of PTM30

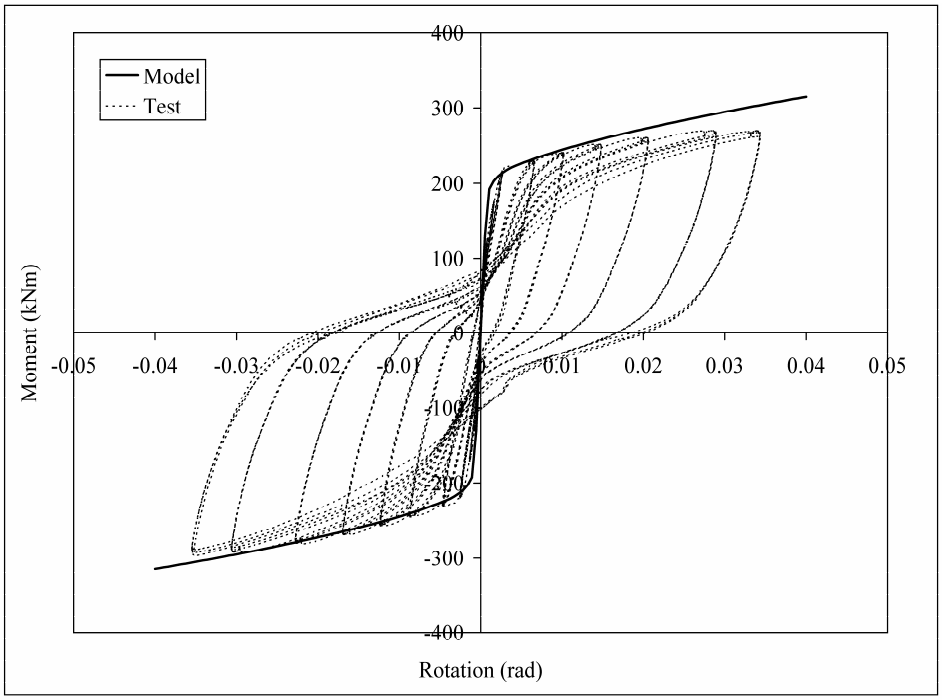

Figure 6.10. Comparison test result vs. the model for moment-rotation behavior of PTM50

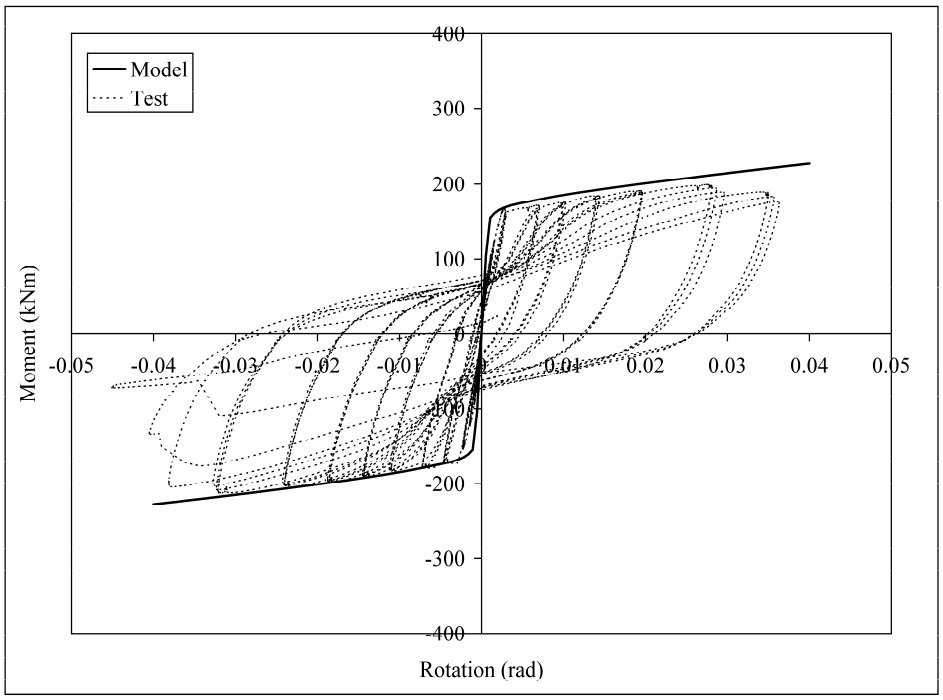

Figure 6.11. Comparison test result vs. the model for moment-rotation behavior of PTM65

6.3.4. Hysteretic Modeling of Beam-Column Subassemblies

In the current part of the study, a hysteretic response model is proposed by considering the residual displacements measured in the hybrid connection subassemblies. The proposed model will be compared with the reversed cyclic test results and energy dissipation values of the current investigation. Three hysteretic models which are bilinear self-centering spring model, modified Takeda model and flag-shaped model are considered in the establishment of the hybrid connection cyclic response model. Bilinear self-centering spring model is suitable for representing the behavior of unbonded post-tensioned specimens [68]. The Takeda model [79] is widely accepted for the modeling of monolithic reinforced concrete structures as presented in Figure 6.12. In the Takeda model K_i and K_p are the initial and post yielding stiffness values of R/C structures, while K_r is the unloading stiffness value with considering the stiffness degradation that can be calculated by using Equation 6.23. The value of γ is given as 0.3 for pure R/C system as discussed by Christopoulos *et al.* [61] and μ represents the displacement ductility level of the latest hysteretic load cycle.

$$K_r = \frac{K_i}{\mu^{\gamma}} \tag{6.23}$$

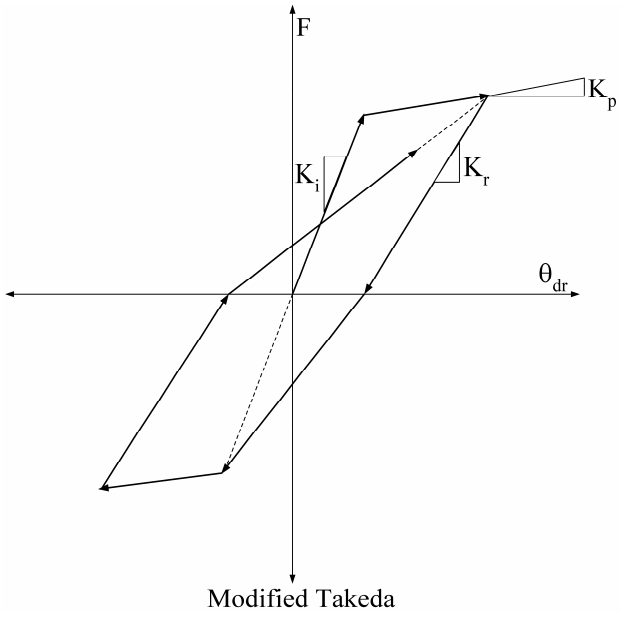

Figure 6.12. Representation of modified Takeda model

The flag-shaped hysteretic model as illustrated in Figure 6.13 was developed for the self-centering post-tensioned structures. In this model, post yield stiffness ratio of Ψ and an energy dissipation coefficient value of β depending on the stress-strain behavior of mild steel and the mild steel contribution to the flexural moment capacity is issued. β value ranges from 0 to 1.0 [59]. Also, the clear span and the depth of the beam affects the post-yielding stiffness in flag-shaped model. Christopoulos *et al*. proposed Ψ and β values as 0.10 and 0.70 respectively for typical post-tensioned connection to represent flag-shaped models [61]. Flag-shaped model does not consider the residual displacements because of the self-centering concept of fully post-tensioned connections. On the other hand, when mild steel content contribution for flexural strength was more than 30 per cent, residual displacements are observed. Therefore, flag-shaped hysteretic models may not be sufficient for such specimens.

The proposed model within in the framework of this study can be defined as the combination of bilinear spring model and the modified Takeda model as shown in Figure

6.14. The first step in the proposed overall model is to calculate and draw the backbone curve of the test subassembly. All damage and nonlinear action is assumed to accumulate in the connection region for hybrid subassemblies and the behavior structural of elements is assumed in the elastic response range both in the design and the analysis of hybrid connections. Hence, by using the virtual work theorem that is formulated in Equation 6.24, lateral force (F_h) and the top displacement (Δ_{top}) of the column in the experimental subassembly of this study can easily be calculated and the lateral load-lateral displacement response of specimens can be reproduced.

$$F_h \times \Delta_{top} = M_c \times \theta_c + \int M_{beam} \times \phi_{beam} + \int M_{col} \times \phi_{col} \tag{6.24}$$

M_c, M_{beam}, M_{col}: Flexural moment at connection, beam and column respectively

ϕ_{beam}, ϕ_{col} : The curvature value at beam and column respectively

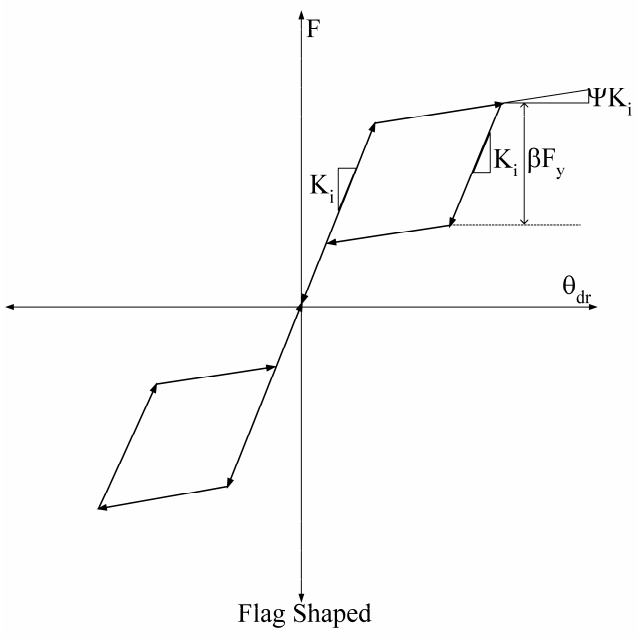

Figure 6.13. Representation of flag-shaped model

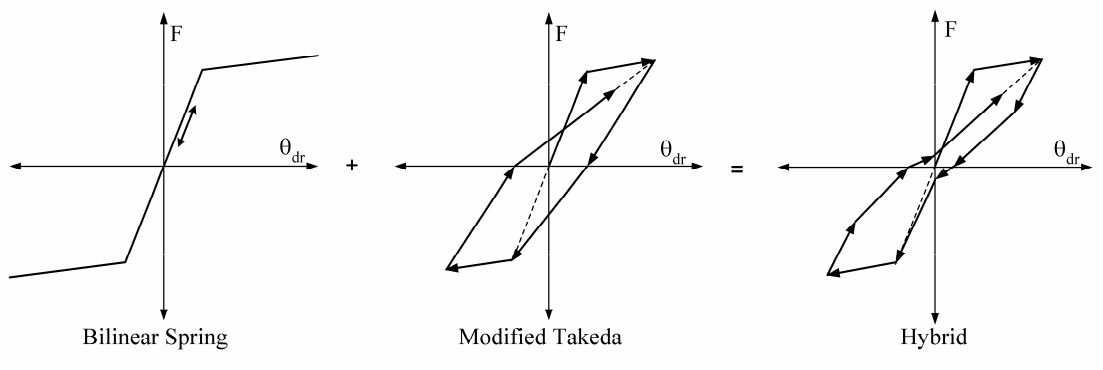

Figure 6.14. Components of the hybrid model

The cyclic response of the experimental subassemblies follows the calculated backbone curve which is created by using the Equation 6.24 and the procedure defined in Figure 6.5. The response curve may be divided into two according to the relative contributions of mild steel and prestressing tendons for the flexural strength. The behavior of unbonded strand is simulated by bilinear self centering spring system. The remaning part of the response curve behaves like monolithic reinforced concrete members. Therefore, this type of structure may be called as partially a R/C structure. The similarities of the hybrid system to classical R/C members are directly related to the level mild steel content at the connection and this relation is derived from the test results and represented with the square root of mild steel contribution to the moment capacity of the connection ($\alpha^{0.5}$), where α is calculated as presented in Equation 6.25.

$$\alpha = \frac{M_{ms}}{M_c} \tag{6.25}$$

In the proposed model, the loading branch can be defined as the summation of the effects of the post-tensioned and R/C parts that are presented like bilinear spring and Takeda models respectively. The unloading branch is based on the flag-shape model and the Takeda model as shown in Figure 6.15. The unloading stiffness is calculated similar to the Takeda model, but γ value is calculated based on the mild steel contribution to the flexural capacity (Equation 6.26).

$$\gamma = 0.3 \times \alpha^{0.5} \tag{6.26}$$

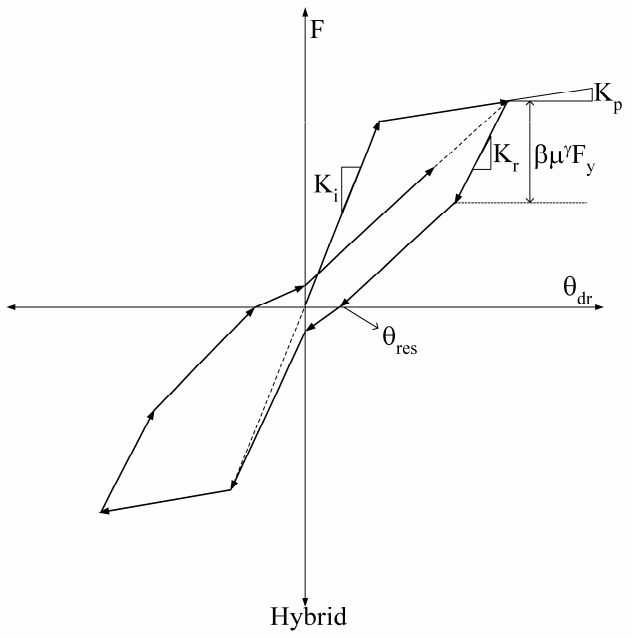

Figure 6.15. Presentation of the proposed hybrid model

In Equation 6.26, when the mild steel contribution is 1, γ is 0.3 and that is purely RC structure. On the other hand, if the mild steel contribution is 0, γ is 0 and this represents purely the post-tensioned system. In the next step, the definition of the energy dissipation coefficient (β) was made. By using the test results with depending on the mild steel content, β is changed from 0.3 to 0.75 as shown in Figure 6.16. Again, the tests showed that, this unloading branch was depended not only the β value and yield force level (F_y) but also displacement ductility at the current hysteretic load cycle with increasing residual strain in the mild steel. Another critical point was to define the residual displacement or the residual story drift level (θ_{res}). The 1996 Japanese seismic design code for bridges defined the residual displacement (δ_r) that was reported by Kawashima [80] and presented in Equation 6.27 where δ_y is the yield displacement and c_r is a factor depending on the stiffness ratio. Based on this approach, a residual story drift equation (Equation 6.28) was defined and calibrated by the test results. This calibration value (λ) changes from 0.1 to 1.0 depending on mild steel content and illustrated in Figure 6.17. For low mild steel contribution, the calculation of residual story drift is minor or negligible level.

$$\delta_r = c_r\left(1-\frac{K_p}{K_i}\right)(\mu-1)\delta_y \tag{6.27}$$

$$\theta_{res} = \lambda\alpha^{0.5}\left(1-\frac{K_p}{K_i}\right)(\mu-1)\theta_y \tag{6.28}$$

θ_y represents the yield story drift.

The last critical point for the cyclic modeling is the lateral load value at zero story drift level. Due to the self-centering effect, pinching behavior was observed during the tests. The reason was that when the story drift was zero, the contribution of strand was zero because of bilinear model. As a result, the lateral load is directly calculated from Takeda model because of sole mild steel contribution.

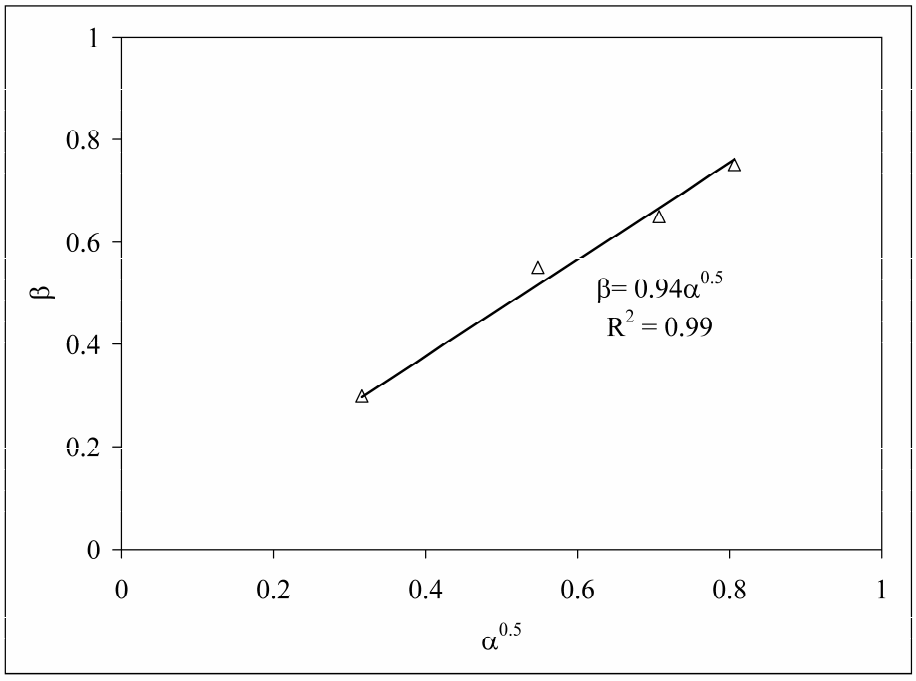

Figure 6.16. Calibration of energy dissipation coefficient

6.3.5. Verification of the Proposed Model

Four different hybrid connection test results were used to verify the current model. As discussed earlier, the behavior of post-tensioned connections with different mild steel content was investigated in this study. Briefly, the overall behavior of the numerical studies showed good agreement with the test results at initial loading, unloading and reloading parts of the response curve with minor error. In the test results, the behavior of forward and backward cycles were not symmetrical therefore, the current model results

generally coincided with the backward cycle. For PTM10 as presented in Figure 6.18, the proposed model behavior estimation up to rupture of mild steel can be acceptable when comparing the test results.

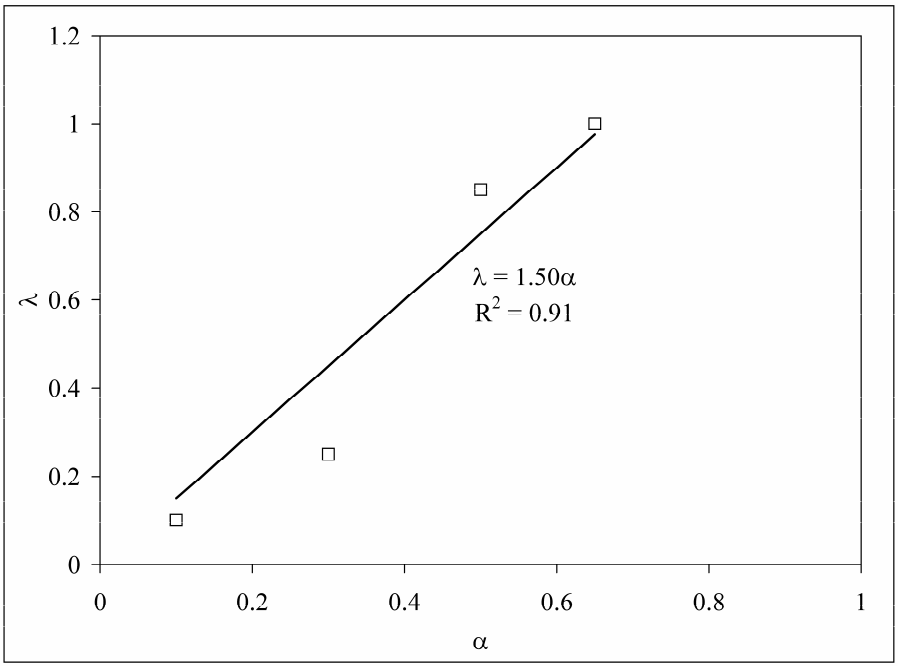

Figure 6.17. Calibration of residual displacement coefficient

After that point, the system behavior was simulated with bilinear spring. Figure 6.19 and Figure 6.20 illustrates the comparisons of test results and cyclic modeling for PTM30 and PTM50.These specimens yielded that this model has good estimation for residual story drift and self-centering effect. Although the behavior of PTM65 was widely similar to the monolithic behavior, the model also predicts specimen PTM65 relatively good as shown in Figure 6.21. Another comparison was done according to cumulative energy dissipation values of the specimens. Loading cycles were repeated three times at each story drift level during the test hence energy dissipation value for the specific story drift level was calculated by taking average of cumulative value of these three cycles and compared the test results. The energy performance values of numerical model and test results are identical with negligible errors except PTM10. Until the rupture of mild steel in PTM10, the energy dissipation values of the model and the tests resulted similar values as presented in Figure 6.22. After that point, due to the bilinear self-centering model, there was no

additional energy dissipation at the connection and error in prediction is observed. Figure 6.23 to Figure 6.25 illustrate the energy dissipation values of numerical and experimental studies and the analysis results have excellent calibration for these comparisons.

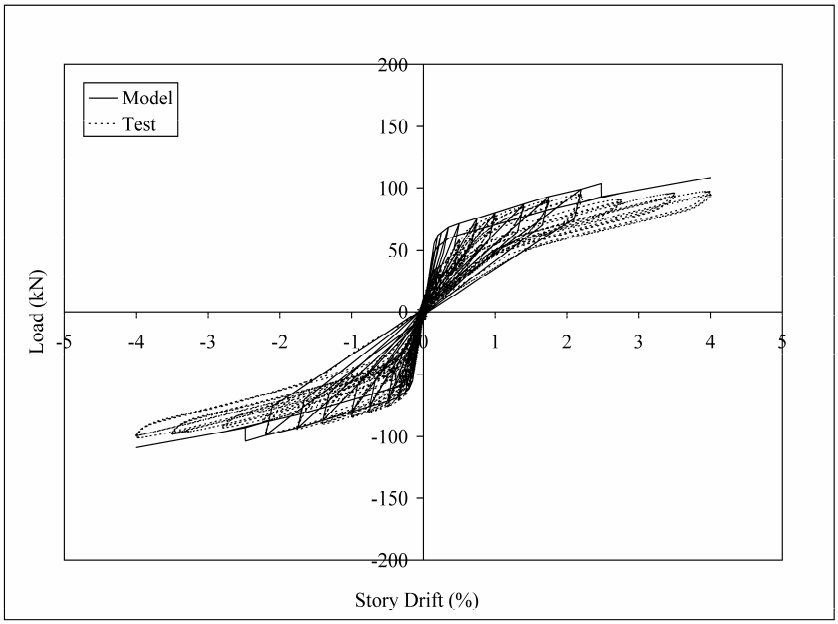

Figure 6.18. Verification of hysteretic model with test result for PTM10

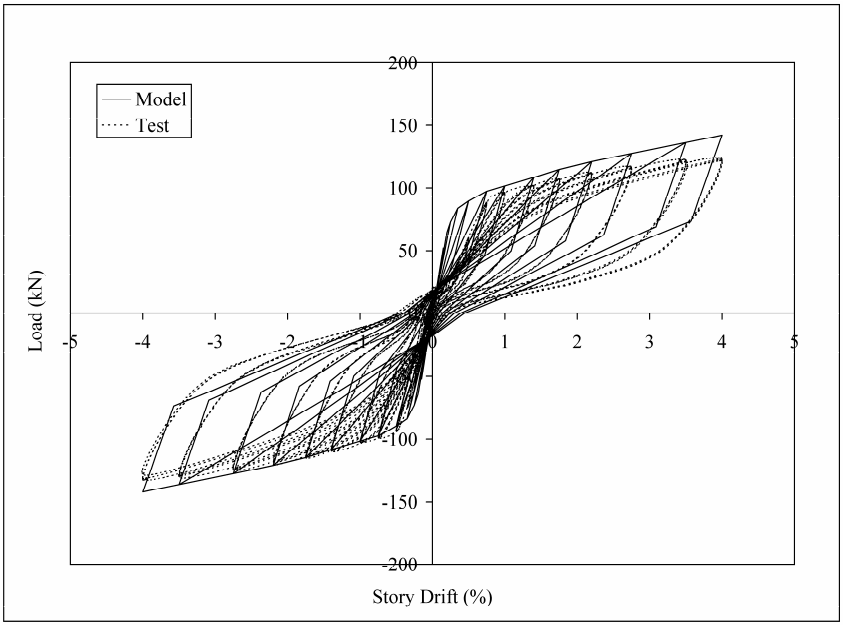

Figure 6.19. Verification of hysteretic model with test result for PTM30

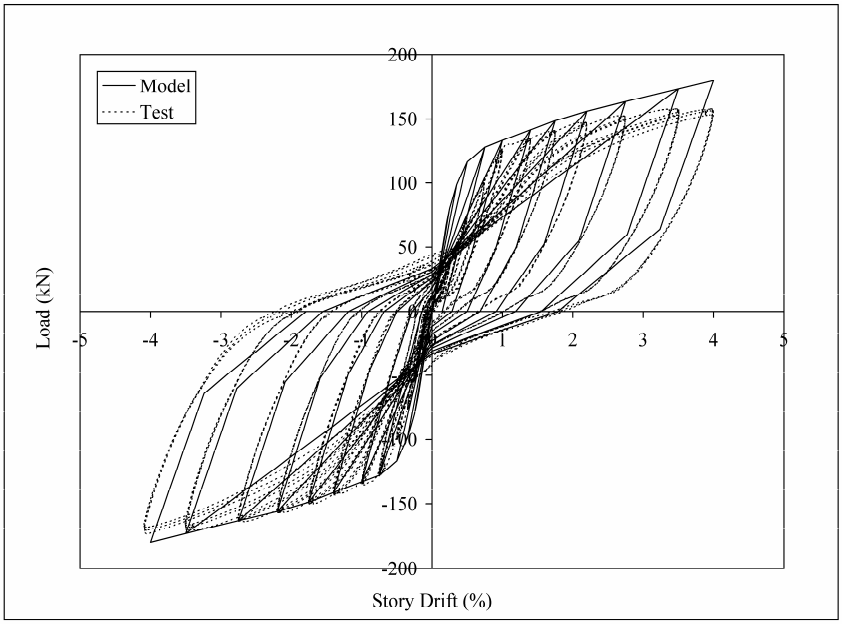

Figure 6.20. Verification of hysteretic model with test result for PTM50

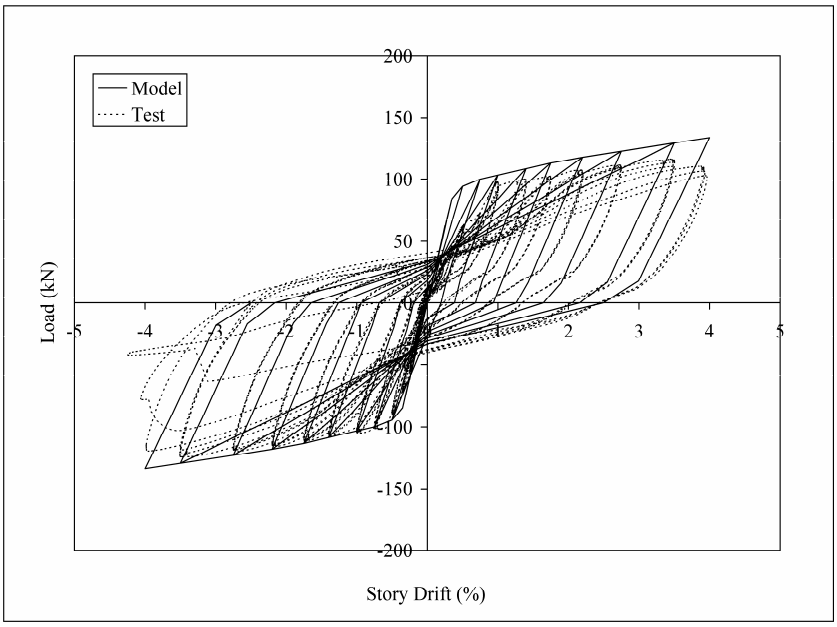

Figure 6.21. Verification of hysteretic model with test result for PTM65

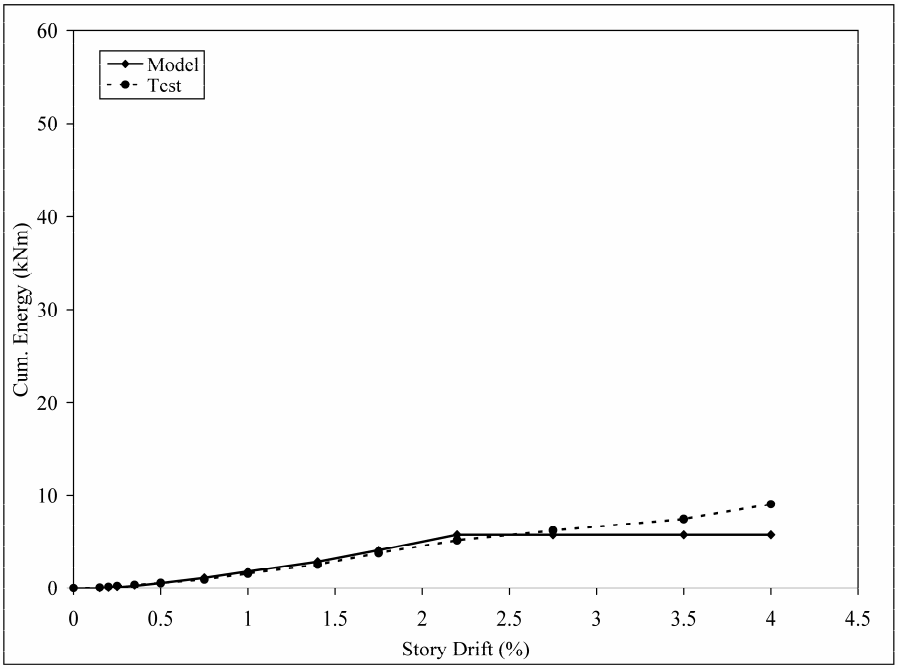

Figure 6.22. Comparison of test and simulation for energy dissipation values of PTM10

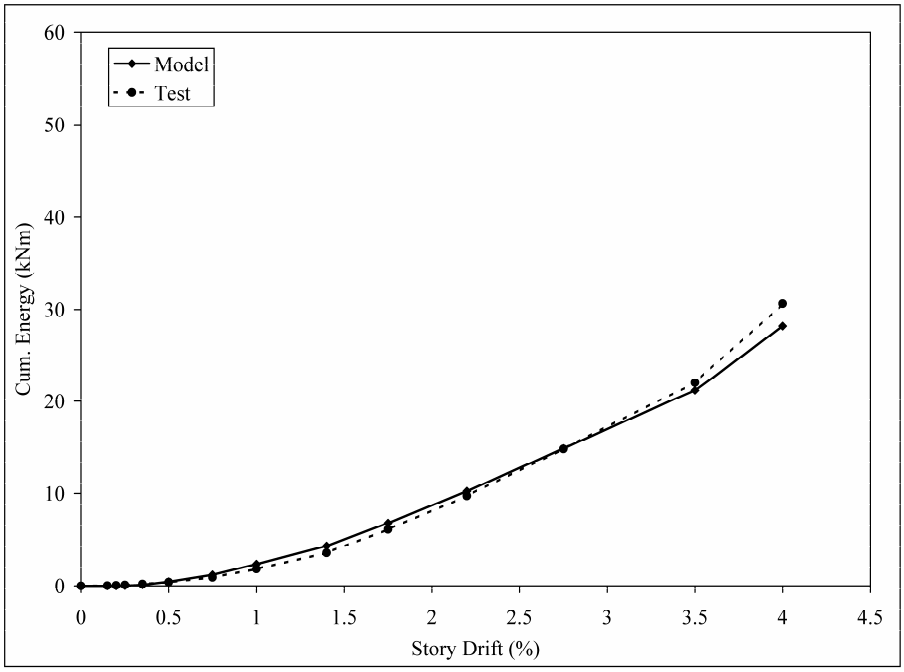

Figure 6.23. Comparison of test and simulation for energy dissipation values of PTM30

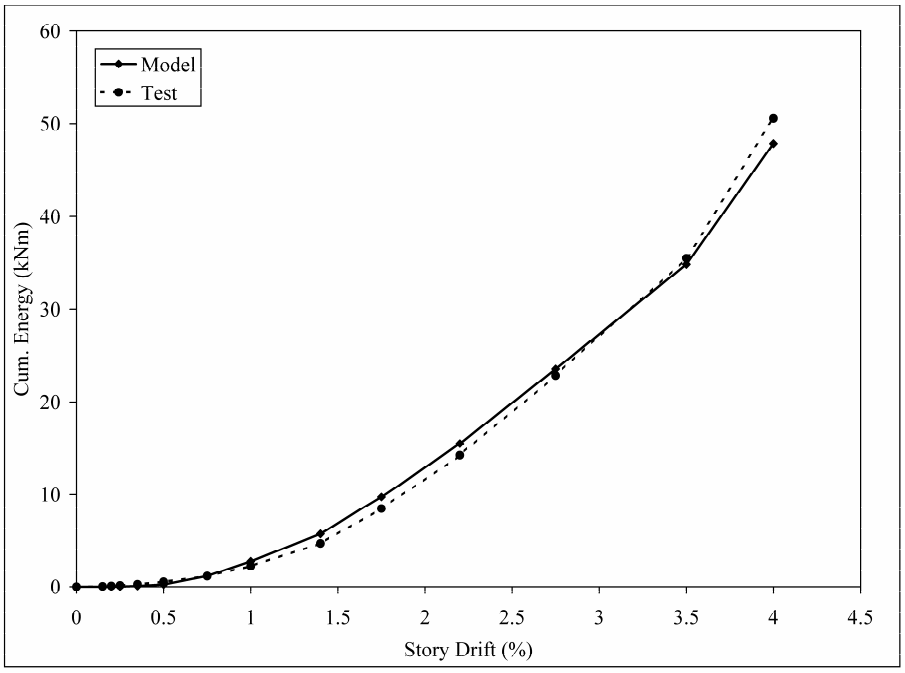

Figure 6.24. Comparison of test and simulation for energy dissipation values of PTM50

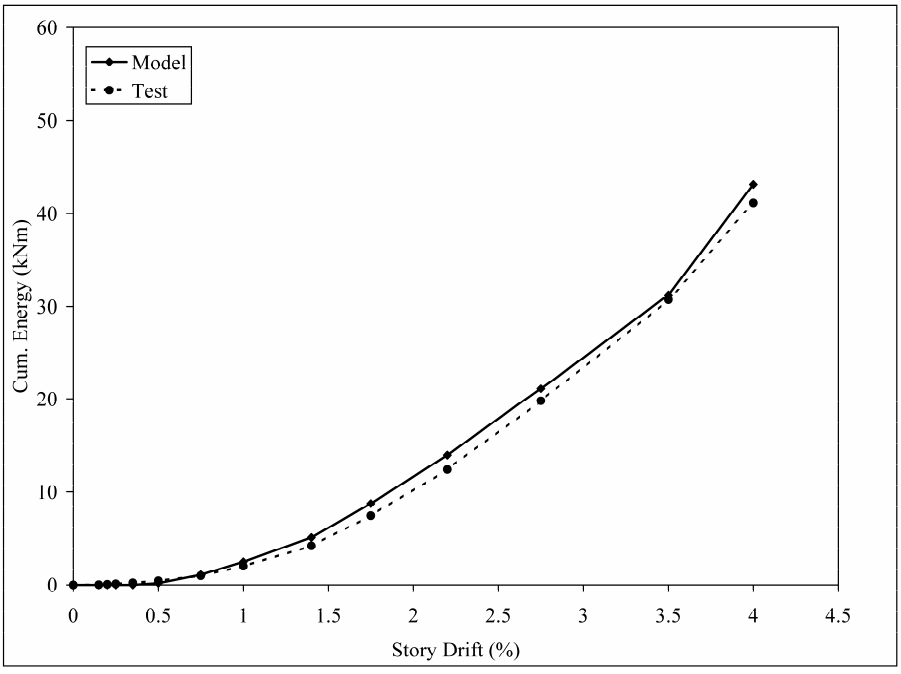

Figure 6.25. Comparison of test and simulation for energy dissipation values of PTM65

Also, the last comparisons were done according to secant stiffness estimations in model and test results as shown from Figure 6.26 to Figure 6.29. In this comparisons, generally up to 0.50 per cent story drift level the estimation of the secant stiffness some different. The reason of that, in the test part, the behavior of forward and backward cycles was different at the initial cycles. On the other hand, the secant stiffness estimation of the current model works properly in the high story drift level. Furthermore, this model has good agreement for the PTM10 and PTM65 test specimens at the initial cycles as illustrated in Figure 6.26 and Figure 6.29. For the PTM30 and PTM50 test specimens, the ratio of calculated stiffness to experimental one at the initial cycles is nearly doubled as illustrated in Figure 6.27 and Figure 6.28.

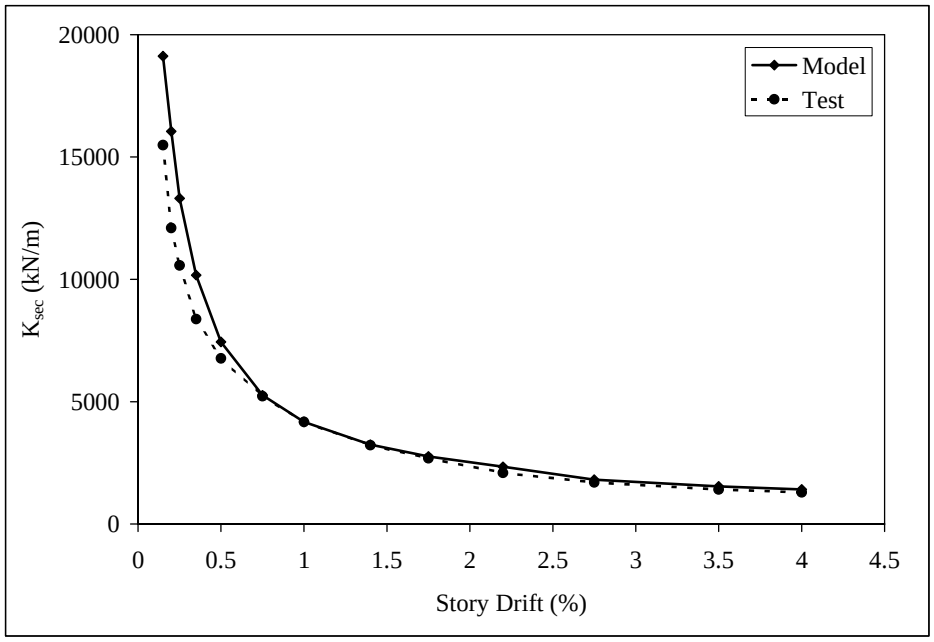

Figure 6.26. Comparison of test and model for stiffness degradation of PTM10

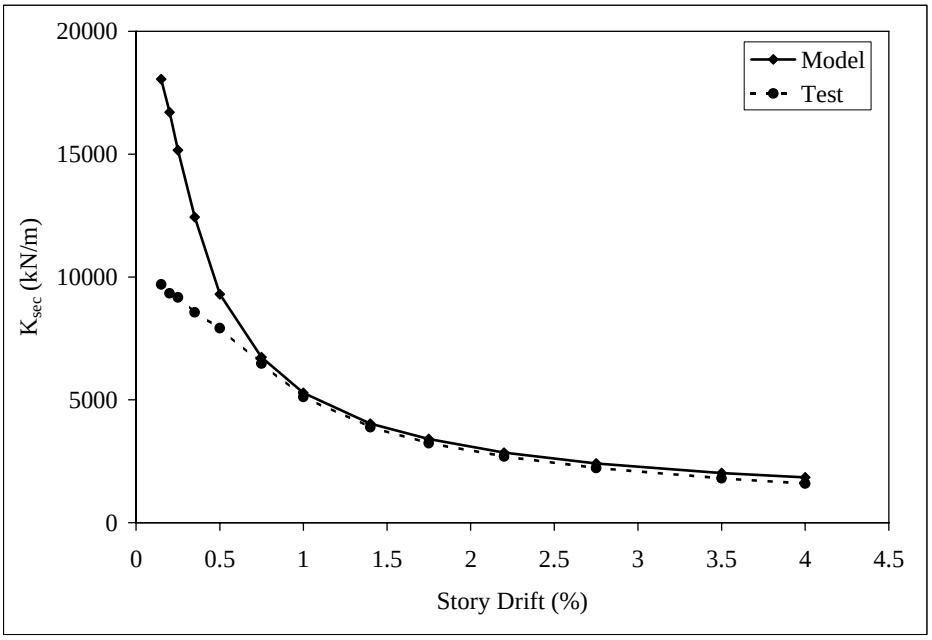

Figure 6.27. Comparison of test and model for stiffness degradation of PTM30

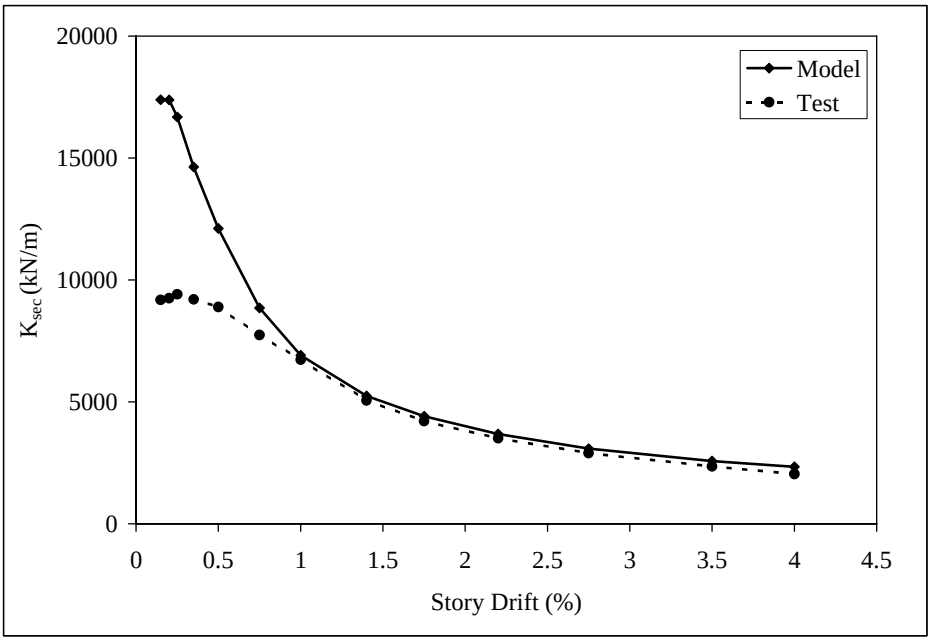

Figure 6.28. Comparison of test and model for stiffness degradation of PTM50

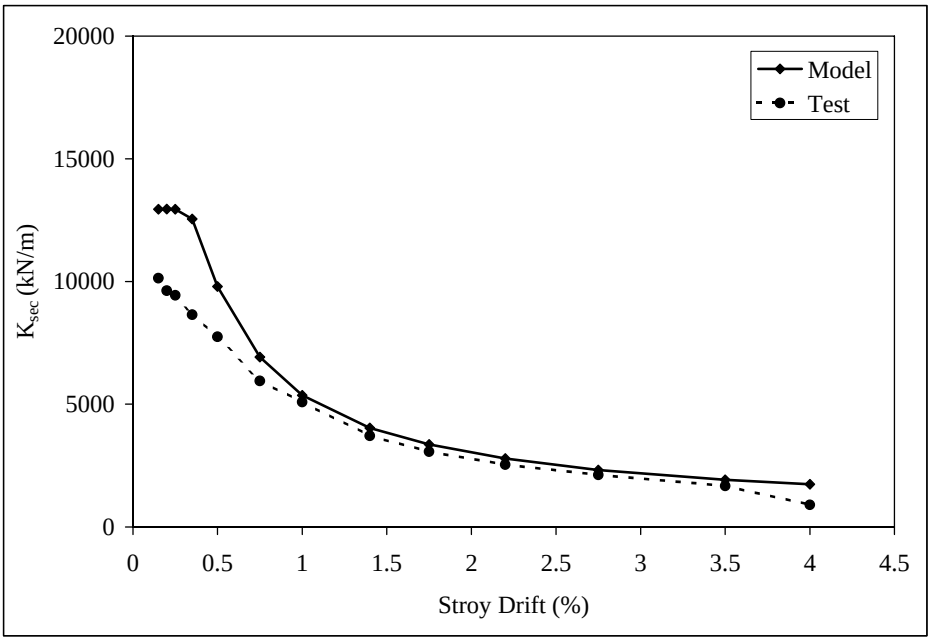

Figure 6.29. Comparison of test and model for stiffness degradation of PTM65

7. CONCLUSIONS AND RECOMMENDATIONS

Based on the test results, assembly process of connection, observations made during the reversed cyclic test and comparisons between proposed modeling and test, the following conclusions may be drawn:

- Specimen Mod-B yielded the best performance in terms of strength, ductility and energy dissipation in addition to easy and speed construction process among the Phase I specimens of this study.
- All Phase I connections are suitable for high seismic zones in terms of strength properties and energy dissipation.
- The hystresis behavior of cast-in-place and bolted connections is similar to monolithic specimen. Composite connection with welding yielded an inferior performance on displacement ductility as compared to the other type of connections tested.
- The Phase I precast connections reached nearly their calculated yield and ultimate flexural moment capacities. All of them had adequate strength capabilities.
- Except GOK-W connection, all Phase I specimens could sustain up to 3.50 per cent story drift. This means that, they have enough ductility level for seismic loads.
- Equivalent damping ratios of the Phase I connections are similar or better than the conventional systems.
- Pinching effect and excessive bond deterioration was not observed at cast-in-place connections due the use of steel fiber concrete and U shaped bars.
- For bolted connection, there is a risk about sliding of steel box or pipe with respect to beam concrete. Therefore, designers should consider the detailing of steel box or pipe which will eliminate the sliding problem.
- For the assembly process, cast-in-place connections need extra on-site formwork resulting increase in time and cost. For the case of composite specimen GOK-W, high quality control must be supplied for welding. On the other hand, assembly process of bolted connection is relatively rapid.

- All post-tensioned test specimens have adequate flexural strength and could sustain up to 4.00 per cent story drift level without major strength degradation. Generally the calculation of flexural strength and stress on the prestressing strands according to ACI T1.2-03 coincide with the experimental results. In addition to that, test results show that assumption of b=3 is rational.
- The hysteretic behavior of hybrid connections approaches to that of the monolithic subassembly with increasing mild steel content at the connection. On the other hand, damages on the precast beam and column are very small or negligible.
- The initial stiffness of the post-tensioned specimens is greater than the monolithic reference test, but the value of stiffness changes significantly with the opening of the precracked interface in hybrid subassembly. Therefore, displacement based design methodology may be more reasonable for seismic design of hybrid precast concrete frames.
- The energy dissipation characteristics of PTM50 and PTM65 are very similar to that of the monolithic specimen. On the other hand, PTM0 and PTM10 did not satisfy energy dissipation criteria at 3.50 per cent story drift level according to the ACI T1.1-01 document.
- Test results showed that the permanent displacement depends on the contribution of mild steel to the moment capacity at the connection. Up to 30 per cent mild steel contribution to flexural strength, residual displacements are negligible while these displacements for PTM50 and PTM65 reached around 35~50 mm.
- The optimum level mild steel contribution for the flexural strength is in the ranged of 20 to 30 per cent for the best connection design if the adequate strength, ductility and relative energy dissipation ratio, and the minimum permanent displacement criteria are considered.
- The moment-rotation modeling showed good correlation with the test results. This means that the monolithic beam analogy, the calculation algorithm and simulation of bond-slip behavior worked properly.
- The combination of bilinear self-centering and Takeda modeling to develop proposed hybrid model had excellent agreement as compared to the test results. Energy dissipation coefficient is directly related with the square root of the mild steel contribution for the flexural strength. The similar approach may be concluded for the

residual drift. There is a linear relation between the permanent deformation coefficient and mild steel contribution.

- For a specific load cycle in post-tensioned hybrid connection specimens, the unloading stiffness value and energy dissipation characteristics and permanent deformations are dependent on displacement ductility ratio at this level.
- Hysteretic model behavior demonstrated similar results with the test results. The estimation of residual drift coincided with the test results. Furthermore, the cumulative energy dissipation values were similar to experimental values for all specimens.
- For the future experimental research, firstly, inner joint test could be performed in order to highlight the behavior of post-tensioned connections. In these specimens, joint shear deformations can be more important depending on mild steel content. Furthermore, post-tensioning level and a/d ratio can be chosen as test parameters in these specimens. Another experimental research may be bidirectional loading to observe torsional behavior of post-tensioned connection that was the weakest point under seismic loading. In order to clarify non-linear hysteretic behavior, different loading pattern can be chosen as parameter for a typical post-tensioned connection

REFERENCES

1. Englekirk, R. E., "Seismic Design Consideration for Precast Concrete Multistory Buildings", *PCI Journal,* Vol. 35, No. 3, pp. 40-51, May-June 1990.

2. Erdik, M., *Report on 1999 Kocaeli and Düzce (Turkey) Earthquakes,* Boğaziçi University, 1999.

3. Özden, Ş. and H. Meydanlı, "Seismic Response of Pre-Cast Industrial Buildings During 1999 Kocaeli Earthquake" *SE-40EEE, Skopje Earthquake 40 Years of European Earthquake Engineering*, Skopje, Macedonia, August 26-29, 2003.

4. Çolakoğlu, H. K., *Seismic Resistant Design of Precast Industrial Building*, M.S. Thesis, Boğaziçi University, 2001.

5. Ersoy, U., T. Tankut, and G. Özcebe, *Damages Observed in the Precast Framed Structures in the 1998 Ceyhan Earthquake and their Rehabilitation*, METU, 1999.

6. Posada, M. and S. L. Wood, *Seismic Performance of Precast Industrial Buildings in Turkey*,http://ccee.oregonstate.edu/workshops/tubitak/reports/posada_evaluation_of_seismic 2001.

7. Turkish Civil Engineering Chambers, *Specifications for Structures to be Built in Disaster Areas*, Turkey, 1998.

8. ICBO, "Uniform Building Code: V. 2, Structural Engineering Design Provisions", *International Conferences of Building Officials*, Whittier, CA, May 1997.

9. Meydanlı, H., *Prefabrike Lambda Tipi Endüstri Yapıların Deprem Etkisi Altındaki Davranışı*, M.S. Thesis, Kocaeli University, 2003.

10. Ataköy, H., "17 Ağustos Marmara Depremi ve TPB Üyelerince Yapılan Prefabrike Yapılar", *Beton Prefabrikasyon,* No. 52, pp. 5-14, September 1999- January 2000.

11. Ataköy, H. "Prefabrike Taşıyıcı Sistem Birleşim Teknikleri" *Workshop, Prefabricated Structures and Earthquake,* Turkish Precast Concrete Association, pp.14-50, December, 1998.

12. Dolan, C. W. and S. P. Pessiki, "Model Testing of Precast Concrete Connections", *PCI Journal,* Vol. 34, No. 2, pp.84-103, March-April 1989.

13. Ersoy, U., G. Özcebe and T. Tankut, "1999 Marmara ve Düzce Depremlerinde Gözlenen Önüretimli Yapı Hasarları", *Earthquake and Prefabrication, 10th Prefabrication Symposium*, pp.1-10, İstanbul, May 2000.

14. Tankut, T. "Önüretimli Yapı Bağlantılarının Deprem Davranışı" *Workshop, Prefabricated Structures and Earthquake*, Turkish Precast Concrete Association, pp. 116-126, December1998.

15. Blakeley, R., " Prestressed Concrete Seismic Design", *Bulletin of the New Zealand Society for Earthquake Engineering,* Vol. 6, No. 1, pp. 18-42, 1973.

16. Camba, J. and R. Meli, "Case Study of the Performance of Prestressed Concrete Buildings during the 1985 Mexico Earthquake", *PCI Journal,* Vol. 38, No. 2, pp. 58-71, March-April 1993.

17. Ghosh, S. K., S. D. Nakaki and K. Krishan, "Precast Structures in Region of High Seismicty: 1997 UBC Design Provision", *PCI Journal,* Vol. 42, No. 6, pp. 76-93, November –December 1997.

18. Hawkins, N. M. and S. K. Ghosh, "Proposed Revisions to 1997 NEHRP Recommended Provisions for Seismic Regulations for Precast Concrete Structures Part 2", *PCI Journal,* Vol. 45, No. 5, pp. 34-44, September-October 2000.

19. Nakaki, S. D., R. E. Englekirk and J. L. Plaehn, "Ductile Connectors for a Precast Concrete Frame", *PCI Journal,* Vol. 39, No. 5, pp. 46-59, September-October 1994.

20. French, C. W., O. Amu and C. Tarzikhan, "Connections between Precast Elements Failure Outside Connection Region", *Journal of Structural Engineering, ASCE,* Vol. 115, No. 2, pp. 316-340, February 1989.

21. Bhatt, P. and D.W. Kirk, "Test on an Improved Beam Column Connection for Precast Concrete", *ACI Journal,* Vol. 82, No. 6, pp. 834-843, November-December 1985.

22. Pillai, S. U. and D. W. Kirk, "Ductile Beam-Column Connection in Precast Concrete", *ACI Journal,* Vol. 8, No. 6, pp. 480-487, November-December 1981.

23. Ersoy, U. and T. Tankut, "Precast Concrete Members with Welded Plate Connections under Reversed Cyclic Loading", *PCI Journal*, Vol. 38 No. 4, pp. 94-100, July-August 1993.

24. Ochs, J. E. and M. R. Ehsani, "Moment Resistant Connections in Precast Concrete Frames for Seismic Regions" *PCI Journal*, Vol. 38, No. 5, pp. 64-75, September-October 1993.

25. Yee, A.A., " Design Considerations for Precast Prestressed Concrete Building Structures in Seismic Areas", *PCI Journal,* Vol. 36, No. 3, pp. 40-55, May-June 1991.

26. Dolan, C.W., J.F. Stanton and R. G. Anderson, "Moment Resistant Connections and Simple Connections PCISFRAD Projects 1 and 4, Summary Paper", *PCI Journal*, Vol. 34, No. 2, pp. 62-85, March-April 1987.

27. French, C. W., M. Hafner and V. Jayashankar, "Connection between Precast Elements*", Journal of Structural Engineering, ASCE*, V. 115, No. 12, pp. 3171-3192, December 1989.

28. Nakaki S. D. and R. E. Englekirk, " PRESS Industry Seismic Workshops: Concept Development", *PCI Journal*, Vol.36, No.5, pp. 54-61, September-October 1991.

29. Blakeley, R. G., R. Park and R. Shephered, "A review of the Seismic Resistance of Prestressed Concrete", *Bulletin of the New Zealand Society for Earthquake Engineering*, Vol. 3, No. 1, pp.3-23, March 1970.

30. Park, R. and K. Thompson, "Cyclic Load Test on Prestressed and Partially Prestressed Beam-Column Joints", *PCI Journal,* Vol. 22, No. 5, pp. 84-110 September-October 1977.

31. Cheok, G. S. and H. S. Lew, "Model Precast Concrete Beam to Column Connections Subject to Cyclic Loading", *PCI Journal*, Vol. 38, No. 4, pp. 80-92, July-August 1993.

32. ACI 352R-02, *Recommendations for Design of Beam-Column Connections in Monolithic Reinforced Concrete Structures*, ACI-ASCE Committee 352, American Concrete Institute, 2002.

33. Cheok, G. and H. S. Lew, *Performance of 1/3 Scale Model Precast Concrete Beam-Column Connections Subjected to Cyclic Inelastic Loads*, *NISTIR 4589*, Report No. 2, NIST, June 1991.

34. Cheok, G. and W. Stone, *Performance of 1/3 Scale Model Precast Concrete Beam-Column Connections Subjected to Cyclic Inelastic Loads, NISTIR 5246,* Report No. 3, NIST, August 1993.

35. Cheok, G. and W. Stone, *Performance of 1/3 Scale Model Precast Concrete Beam-Column Connections Subjected to Cyclic Inelastic Loads, NISTIR 5436,* Report No. 4, NIST, June 1994.

36. Priestly, M. J. N. and G. A. MacRae, " Seismic Tests of Precast Beam to Column Joint Subassemblages with Unbonded Tendons", *PCI Journal*, Vol. 41, No. 1, pp. 64-80, January-February 1996.

37. Nakaki, S. D., J. F. Stanton and S. Sritharan, "An overview of the PRESS Five-Story Precast Test Building", *PCI Journal*, Vol. 44, No. 2, pp. 26-39, March-April 1999.

38. Precast Concrete Institute, *Seismic Design:* http ://www.pci.org/ markets/ markets.cfm? path=seismic_testing & id= connections.cfm, 2002

39. Priestley, M. J. N., S. Sritharan, J. Conley and S. Pampanin, "Preliminary Results and Conclusions from the PRESS Five-Story Precast Concrete Test Building", *PCI Journal,* Vol. 44, No. 6, pp. 42-67, November-December 1999.

40. Precast Concrete Institute, *Seismic Design:* http ://www.pci.org/ markets/ markets.cfm? path=seismic_testing & id= 5systems.cfm, 2002

41. Pınarbaşı, S., *Development and Seismic Performance of A Precast Concrete Beam-Column Connection by Post-Tensioning*, M.S. Thesis, METU, September 2000

42. Park, R., "A Perspective on the Seismic Design of Precast Concrete Structures in New Zealand", *PCI Journal,* Vol. 40, No. 3, pp. 40-59, May-June 1995.

43. Ohkubo, M. and M. Fujimura, "Lateral Deformation Behavior of Precast R/C Concrete Beam to Column Sub-Assemblages Jointed by Cast-in-Place Concrete", *Third Meeting of the U.S.-Japan Joint Technical Coordination Committee on PRESSS,* pp. 74-86, California, USA, November 18-20, 1992.

44. Soubra, K. S., J. K. Wight and A.E. Naaman, "Cyclic Response of Fibrous Cast-in-Place Connections in Precast Beam-Column Subassemblages", *ACI Structural Journal*, Vol. 90, No. 3, pp. 316-323, May-June 1993.

45. Vasconez, R. M., A. E. Naaman and J.K. Wight, "Behavior of HPFRC Connections for Precast Concrete Frames Under Reversed Cyclic Loading", *PCI Journal*, Vol. 43, No. 6, pp. 58-71 November-December 1998.

46. ACI T1.1-01, *Acceptance Criteria for Moment Frames Based on Structural Testing*, American Concrete Institute, 2001.

47. Mikame, A., H. Sasaki, M. Matsudo and H. Matsubara, "Test on Bent Bar Anchorage in Precast R/C Beam-Column Joints", *Third Meeting of the U.S.-Japan Joint Technical Coordination Committee on PRESSS,* pp. 159-175, California, USA, November 18-20, 1992.

48. TS3233*, Building Code Requirements for Prestressed Concrete,* Turkish Standard Institute, 1979.

49. ACI T1.2-03, *Special Hybrid Moment Frames Composed of Discretely Jointed Precast and Post-Tensioned Concrete Members*, ACI, 2003.

50. ACI 445R-99, *Recent Approaches to Shear Design of Structural Concrete*, ACI-ASCE Committee 445, American Concrete Institute 2004.

51. Cheok, G. S., W. C. Stone and S. D. Nakaki, *Simplified Design Procedure for Hybrid Precast Concrete Connections*, *Report NISTIR 5765*, NIST, 1996.

52. Raynor, D. J., D. E. Lehman and J. F. Stanton, "Bond-Slip Response of Reinforcing Bars Grouted in Ducts", *ACI Structural Journal*, Vol. 99, No. 5, pp. 568-576, September-October 2002.

53. Park, R., "Evaluation of Ductility of Structures and Structural Assemblages from Laboratory Testing", *Bulletin of the New Zealand National Society for Earthquake Engineering,* Vol. 22, No. 3, pp. 155-166, September 1989.

54. Stanton, J., W. C. Stone and G. S. Cheok, "A Hybrid Reinforced Precast Frame for Seismic Regions", *PCI Journal*, Vol. 42, No. 2, pp. 20-32, March-April 1997.

55. Chopra, A. K., *Dynamic of Structures-Theory and Applications to Earthquake Engineering*, International Edition, Prentice Hall, New Jersey, 1995.

56. ACI 318-99, *Building Code Requirements for Structural Concrete*, ACI 318 Committee, American Concrete Institute, Chicago 1999.

57. TS500, *Requirements for Design and Construction of Reinforced Concrete Structures*, Turkish Standard Institute, 2000.

58. Cheok, G. S., W. C Stone and S. K. Kunnath, "Seismic Response of Precast Concrete Frames with Hybrid Connections", *ACI Structural Journal*, Vol. 95, No. 5, pp. 527-539, September-October 1998.

59. Christopoulos, C., A. Filiatrault and B. Folz, "Seismic Response of Self-centering Hysteretic SDOF Systems", *Earthquake Engineering and Structural Dynamics,* Vol. 31, No. 5, pp. 1131-1150, May 2002.

60. Christopoulos, C., A. Filiatrault, , C. M. Uang and B. Folz., "Posttensioned Energy Dissipating Connections for Moment-Resisting Steel Frames", *Journal of Structural Engineering, ASCE,* Vol. 128, No. 9, pp. 1111-1120, September 2002.

61. Christopoulos, C., S. Pampanin and M. J. N. Priestley, "Performance-Based Seismic Response of Frame Structures Including Residual Deformations", *Journal of Earthquake Engineering,* Vol. 7, No. 1, pp. 97-118, January 2003.

62. El-Sheikh, M., S. Pessiki, R. Sause and L.W. Lu, "Moment Rotation Behavior of Unbonded Post-Tensioned Precast Concrete Beam-Column Connections", *ACI Structural Journal*, Vol. 97, No. 1, pp. 122-131, January-February 2000.

63. El-Sheikh, M., R. Sause, S. Pessiki, and L.W. Lu, "Seismic Behavior and Design of Unbonded Post-Tensioned Precast Concrete Frames", *PCI Journal,* Vol. 44, No. 3, pp. 54-71, May-June 1999.

64. Kurama, Y., "Seismic Design of Unbonded Post-Tensioned Precast Concrete Walls with Supplemental Viscous Damping", *ACI Structural Journal,* Vol. 97, No. 4, pp. 648-658, July-August 2000.

65. Kurama, Y., "Simplified Seismic Design Approach for Friction-Damped Unbonded Post-Tensioned Precast Concrete Walls", *ACI Structural Journal,* Vol. 98, No. 5, pp. 617-716, September-October 2001.

66. Kurama, Y., R. Sause, S. Pessiki and L.W. Lu, "Lateral Load Behavior and Seismic Design of Unbonded Post-Tensioned Precast Concrete Walls", *ACI Structural Journal,* Vol. 96, No. 4, pp. 622-632, July-August 1999.

67. Pampanin, S., M. J. N. Priestley and S. Sritharan, "Analytical Modeling of the Seismic Behavior of Precast Concrete Frames Designed with Ductile Connections", *Journal of Earthquake Engineering,* Vol. 5, No. 3, pp. 329-367, July 2001.

68. Priestley, M. J. and J. R. Tao, "Seismic Response of Precast Prestressed Concrete Frames with Partially Debonded Tendons", *PCI Journal,* Vol. 38, No. 1, pp. 58-69, January-February 1993.

69. Ricles, J. M., R. Sause, M. M. Garlock and C. Zhao, "Post-tensioned Seismic Resistant Connections for Steel Frames", *Journal of Structural Engineering, ASCE,* Vol. 127, No. 2, pp. 113-121, February 2001.

70. Kunnath, S. K., A. M. Reinhorn and R. F. Lobo, *IDARC Version 3.0: A program for the Inelastic Damage Analysis of RC Structures", Technical Report NCEER-92-0022,* NCEER, State University of New York at Buffalo, August 1992.

71. Prakash, V., G. Powell and S. Campell., *DRAIN-2DX Program Description, Report No. UCB/SEMM-93/17&18,* University of California, Berkeley, December 1993.

72. Paulay, T. and M. J. N. Priestley, *Seismic Design of Reinforced Concrete and Masonry Buildings*, John Wiley and Sons Inc., New York, 1992.

73. Restrepo, J. I., *Seismic Behavior of Connections between Precast Elements*, Ph.D. Dissertation, University of Canterbury, Christchurch, New Zealand, 1993.

74. Akpınar, E., *Normal Dayanımlı Betonda Donatı Kenetlenme Özelliklerinin Karbon Elyaf Sargısı ile İyileştirilmesi,* M.S. Thesis, Kocaeli University, 2004.

75. Karaduman, C., *An Investigation on Anchorage Bond Properties of Reinforcement in High-Strength Concrete*, M.S. Thesis, Bogazici University, 1998.

76. Tezcan, J., *Anchorage Behavior of Reinforcement in High Strength Concrete under Load Reversals*, MS Thesis, Boğaziçi University, 1999.

77. Yalcinkaya, O*., Bond Fatigue Behavior of Reinforced High Strength Concrete under Cyclic Loading*, M.S. Thesis, Boğaziçi University, 2004.

78. Mander, J. B., M. J. N. Priestley and R. Park, "Theoretical Stress-Strain Model for Confined Concrete", *Journal of Structural Engineering, ASCE,* Vol. 114, No. 8, pp. 1804-1826, August 1988.

79. Takeda, T., M. Sozen, and N. N. Nielsen, "Reinforced Concrete Response to Simulated Earthquakes", *Journal of the Structural Division, ASCE,* Vol. 96, No. 12, pp. 2557-2573, December 1970.

80. Kawashima, K., "The 1996 Japanese Seismic Design Specifications of Highway Bridges and the Performance Based Design", *Proceedings, Seismic Design Methodologies for the Next Generation of Codes,* pp. 371-382, Balkema, Rotterdam, 1998 .